

CUTTING EDGE MICROGEOMETRY
MODELING & ELECTRO-EROSION HONING

**CUTTING EDGE MICROGEOMETRY
MODELING & ELECTRO-EROSION HONING**

By

NIMA ZARIF YUSSEFIAN, B.Sc., M.Sc.

A Thesis

Submitted to the School of Graduate Studies
in Partial Fulfillment of the Requirements
for the Degree
Doctor of Philosophy

McMaster University

© Copyright by Nima Zarif Yussefian, October 2012

DOCTOR OF PHILOSOPHY (2012)
(Mechanical Engineering)

MCMASTER UNIVERSITY
Hamilton, Ontario

TITLE: **Cutting Edge Microgeometry
Modeling & Electro-Erosion Honing**

AUTHOR: Nima Zarif Yussefian
B.Sc., M.Sc.

SUPERVISOR: Dr. Philip Koshy

NUMBER OF PAGES: xvii, 151

Abstract

This thesis presents the proof-of-concept of electro-erosion edge (EE) honing as a novel edge preparation process that is based on micro-shaping of the cutting edges of metal cutting tools by electro discharge machining (EDM). This process in its simplest form is first applied to straight edge high speed steel cutting tools which results in a four-fold enhancement in the lives of these tools as compared to the sharp unprepared ones. In the next step the EE-honing application is expanded to hone carbide tools of a complex geometry through the innovative idea of using foil counterfaces. Foil counterface ensures the uniform processing of the entire edge length irrespective of macro-geometric complexities such as curvilinear cutting edges and nose radii. By employing this technique, cutting tools of a complex geometry can be prepared with only 13% edge radius variation which is significantly lower than 40% variation reported for conventional edge preparation processes. ED-machining of cemented carbides necessitates the systematic identification of optimal process parameters to preserve process stability and surface integrity. It is shown that by the application of optimal EE-honing process parameters, EE-honed tools achieved the same life of conventionally prepared ones with the same radii.

The advent of advanced edge preparation techniques like EE-honing process has led to the emergence of engineered cutting edge microgeometries most of which cannot be represented by a single edge radius value. In this regard,

a novel idea of using parametric quadratic curves for comprehensive cutting edge characterization is presented in the next part of this thesis. The free-knot B-spline approximation enables the unique identification of cutting edge separation points from the clearance and rake faces. Subsequent to the edge identification, quadratic parametric polynomials are employed to characterize the cutting edge by four characterization parameters. These parameters are contour-based and easy to visualize. As the final part of the thesis, the EE-honing process is simulated numerically to gain a better insight into the process. Simulation can model the generation of symmetrical and asymmetrical edges and predict edge geometry with the maximum of 14% error.

Acknowledgements

For me PhD was a wonderful journey during which I got to know many amazing individuals. I would like to thank every single one of them for accompanying me on this four-year journey through science, academia and life.

I like to express my sincerest gratitude to Dr. Philip Koshy, my supervisor. When I look back and review the past four years beginning from the day of my interview for this position, I cannot imagine a supervisor being more supportive, caring and compassionate as he is. Dr. Koshy stood by me in every single step of this way and every hardship that lay ahead. No matter if it was on developing an idea, a scientific challenge or even a personal circumstance; I was always delighted with his sage advice, enlightening instruction and inspiring guidance. Our numerous discussions in his office, in coffee and lunch breaks (that he never allowed me to pay for) or during our bi-weekly group meetings paved the way for the timely completion and success of this thesis. Thank you very much.

I am extremely grateful to my parents for their selfless support and continuous encouragement during all these years. I was always blessed with their limitless care and endless affection. I owe a big thank you to my wife, Banafsheh, for her understanding and generous love. Without her on my side this period would never be as joyful. For these, I wish to dedicate this thesis to my lovely family.

I would like to express my special appreciations to Dr. Ng and Dr. Had-dara for honoring me by being a part of my PhD supervisory committee. I was indeed privileged to have such knowledgeable and supportive committee members. Also, I want to thank shop members; Ron, Joe, Jim, Terry, JP and Mark for their assistance, training and technical support during this project. Finally, I am thankful to all my invaluable friends who made my PhD studies more colorful.

List of Notations and Symbols

β	tool angle
γ_e	effective rake angle
Δr	distance of the edge apex to the virtual sharp edge
θ	angle between the axis of symmetry of the parabola and the wedge angle bisector
τ	duty factor
ϕ	angular shift of edge apex
A_r	reference crater area
$C(u)$	B-spline curve
d	crater depth
D	cutting edge data points
D_α	parameter for edge characterization on flank face
D_γ	parameter for edge characterization on rake face
f_a	vertical distance of edge apex to virtual sharp edge
h	chip thickness
i_e	pulse current
$m + 1$	number of knots
m_1	flank line slope
m_2	rake line slope
$N_{i,p}$	B-spline basis function

$n + 1$	number of control points
p	degree of the B-spline curve
P_i	B-spline control points
R	crater radius
r_β	edge radius
r_a	curvature radius of cutting edge apex
R_a	arithmetic average of absolute values for surface roughness
R_n	cutting tool nose radius
S	gap width
S_α	cutting edge start point on flank face from virtual sharp edge
S_γ	cutting edge start point on rake face from virtual sharp edge
S_a	edge apex horizontal position
S_f	cutting edge start point on flank face from wedge angle bisector
S_r	cutting edge start point on rake face from wedge angle bisector
t_i	pulse on-time
t_o	pulse off-time
u	curve parameter
U	working voltage
U_o	open circuit voltage
u_i	B-spline knot
V_c	volume of material removed from counterface
V_t	volume of material removed from tool electrode
V_w	volume of material removed from workpiece
w	crater width

Contents

Abstract	iii
Acknowledgements	v
List of Symbols	vii
List of Figures	xvi
List of Tables	xvii
1 Introduction and Literature Review	1
1.1 Cutting Edge Microgeometry	3
1.2 Importance of Cutting Edge Geometry	5
1.3 Edge Honing Processes	11
1.3.1 Conventional Edge Honing Processes	12
1.3.2 Modern Honing Processes	16
1.3.3 Summary of Preparation Methods	21
1.4 Cutting Edge Characterization	22
1.5 Electrical Discharge Machining (EDM)	24
1.6 Thesis Objectives and Outline	29
1.6.1 Thesis Objectives	29
1.6.2 Thesis Outline	30
1.6.3 Contributions to Articles	31

2	Cutting Edge Geometric Modeling	33
2.1	Cutting Edge Modeling	34
2.2	Edge Modeling by Optical Microscope	36
2.2.1	Focused Pixel Extraction Algorithm	38
2.2.2	Filtering, Surface Interpolation and Cross Sectioning	39
2.2.3	Advantages of Optical Measurement Method and Profile Validation	41
3	Electro-erosion edge honing of cutting tools	45
3.1	Introduction	46
3.2	Process concept	48
3.3	Experimental	50
3.4	Results and discussion	51
3.5	Conclusions	58
3.6	Acknowledgements	58
4	Application of foil electrodes for electro-erosion edge honing of complex-shaped carbide inserts	61
4.1	Introduction	62
4.2	Electro-erosion edge honing process	65
4.2.1	Application of a foil counterface	66
4.2.2	Choice of counterface material, polarity and pulse parameters	69
4.3	Experimental	74
4.4	Results and Discussion	76
4.4.1	Edge geometry	76
4.4.2	Surface integrity, tool life and processing time	80
4.5	Conclusions	85

5	Parametric characterization of the geometry of honed cutting edges	91
5.1	Introduction	92
5.2	Cutting edge identification	96
5.3	Cutting edge characterization	105
5.4	Conclusions	110
6	Numerical Simulation of Electro-Erosion Edge Honing	115
6.1	Introduction	115
6.2	Simulation Methodology	117
6.3	EE-honing Process Investigations	123
6.3.1	Electrode Wear at Sharp Edges	123
6.3.2	Effect of Wear Ratio	124
6.3.3	Effect of Foil Counterfaces	126
6.4	Experimental Verification	127
6.4.1	Required Data for the Simulation	127
6.4.2	Symmetric Edge Honing	129
6.4.3	Asymmetric Edge Preparation	131
6.5	Conclusions	133
7	Conclusions and Future Work	135
7.1	Conclusions	135
7.2	Future Work	138

List of Figures

1.1	A typical cutting tool insert.	3
1.2	Importance of cutting edge preparation [9].	4
1.3	Resolving the resultant force R into two components: ploughing force P and tool face force Q; adapted from [5].	5
1.4	Material separation point.	6
1.5	Forces vs. uncut chip thickness : (a) cutting (b) thrust [14].	7
1.6	Effect of tool-edge radius on in-depth RS11 profile [17].	8
1.7	Characterization of the asymmetrically honed cutting edge [21].	10
1.8	Effect of symmetrical and asymmetrical cutting edge geometries on material separation point [22].	10
1.9	(a) Nylon abrasive cutting edge preparation machine [23]. (b) Nylon abrasive filaments.	13
1.10	Effect of filament condition on the repeatability of brush honing [24].	13
1.11	Abrasive Jet Machining [27].	14
1.12	Tool wear for tools prepared by AJM and brush honing [9].	15
1.13	Abrasive Flow Machining.	16
1.14	Comparison of the flank wear development between a blasted and a AFM honed cutting edge of similar radii [18].	17
1.15	Influence of the cutting edge design on tool wear [31].	18

1.16	Enhanced drill life by means of MAM [34].	19
1.17	5-Axes brush honing [36].	20
1.18	Cutting edge characterization methods due to: (a) Denkena et al. [21], (b) Rodriguez [9], and (c & d) Wyen et al. [37].	23
1.19	Material removal of EDM	25
1.20	(a) Sink EDM process. (b) EDM machine used for experimental tests.	26
1.21	Shape change of edge portion of cylindrical copper electrode [44]	27
1.22	Concept of relative duty [46]	28
2.1	Optical edge measurement technique.	37
2.2	Filtering and sectioning the edge model	40
2.3	3D cutting edge model of the developed measurement methodology and two cutting edge profiles	41
2.4	Circular regression applied on a cross-section of the cutting edge model	42
2.5	Verification of the developed measurement technique by other conventional methods	43
3.1	Schematic representation of electro-erosion edge honing.	49
3.2	Effect of counterface material on edge geometry: (a) aluminum, (b) copper.	52
3.3	Simulated effect of wear ratio on edge geometry.	53
3.4	Micrographs of: (a) HSS and (b) cemented carbide ground (sharp) edges; (c) and (d) are the corresponding electro-erosion honed edges.	54
3.5	Profilometer traces of HSS edges showing their evolution.	55
3.6	Effect of gap voltage and flushing on edge radius.	56
3.7	Effect of edge preparation on tool life.	57

3.8	Box plot showing edge radius variability between edges.	58
4.1	Principle of electro-erosion edge honing.	66
4.2	Kinematic configurations of electro-erosion edge honing.	67
4.3	Example of a tool insert with a complex geometry.	68
4.4	A comparison of the application of thick and foil counterfaces.	68
4.5	Concept and calculation of threshold wear ratio.	70
4.6	Threshold wear ratio for a wedge angle of 90°	71
4.7	Effect of counterface material and polarity on edge geometry.	72
4.8	Effect of gap voltage on wear ratio (t_{on} 0.4 μ s, i_e 1.2 A).	74
4.9	Experimental configuration for electro-erosion honing.	75
4.10	(a) Electro-erosion honed edge of CCMT insert, (b) honing quality along a curved edge, and (c) edge chipping and flash on the unprepared edge (white arrows indicate the honed segment).	76
4.11	(a) Comparison of cutting edge profiles obtained by optical microscope, white light interferometer (WLI) and form tracer; (b) overlay of profile (broken white line) obtained using the microscope on a micrograph showing the section of the edge.	78
4.12	Variability in edge radius: (a) between inserts. (b) along the edge of a single insert.	79
4.13	A comparison of edges: (a) electro-erosion honed, (b) brush honed, and (c) ground.	80
4.14	Effect of pulse parameters on the integrity of cemented carbide surfaces.	82
4.15	(a) Taylor's tool life plots for electro-erosion honed and brush-honed inserts; (b) edge profiles of typical inserts used in tool life tests.	83
4.16	Edge radius and processing time as a function of foil thickness.	84

5.1	Edge characterization methods due to: (a) Denkena et al. [3], (b) Rodriguez [14], and (c & d) Wyen et al. [15].	94
5.2	Terminology of tool edge profile.	97
5.3	Effect of deemed edge boundary on edge radius r_β	97
5.4	Edge identification using a quadratic B-spline with three sections.	100
5.5	Cutting edge identification by free-knot B-spline approximation.	102
5.6	Identification of tool face margins in consideration of wedge angle β	104
5.7	Robustness of edge identification against point uncertainty. . .	105
5.8	Invariability of edge identification algorithm to tool face region considered.	106
5.9	Limitations of current edge characterization parameters. . . .	107
5.10	Proposed edge characterization parameters.	108
5.11	Characterization of: (a) symmetric, and (b) asymmetric edges.	109
6.1	Circular crater geometry in the direction of spark.	120
6.2	Simulated removal mechanism per spark.	121
6.3	Modeling of overlapping craters (a) Constrained by geometry (b) Constant removal per spark.	122
6.4	Discharge density along the electrode length.	124
6.5	Cutting edge geometry for (a) 0.15 (b) 0.4 (c) 5 wear ratios. .	125
6.6	(a) Simulated effect of wear ratio on edge geometry. (b) Effect of wear ratio on spark angular sweeping range	125
6.7	The effect of foil counterfaces.	126
6.8	SEM micrographs of spark craters on carbide surface.	128
6.9	Simulated and experimental edge radius values for different counterface thicknesses.	129
6.10	Effect of initial edge defects on final honed edge geometry. . .	130

6.11 Preparation of asymmetric cutting edge.	131
6.12 Asymmetric edge preparation for rotation angle of 20° for foil thickness of (a) 50 μm (b) 100 μm	132
6.13 Asymmetric cutting edge characterization parameters.	133

List of Tables

- 5.1 Cutting edge characterization parameters 110
- 6.2 Baseline EE-honing parameters 128
- 6.3 Asymmetric edge characterization parameters 133

Chapter 1

Introduction and Literature Review

The history of metal cutting may be traced back thousands of years to the middle east when ancient people shaped gold into primitive tools. But perhaps the beginning of modern metal cutting can be attributed to Time [1] and Treska [2] who made the first attempts to explain the mechanics of chip formation. From then on, the theory of metal cutting developed over the years. The metal cutting industry on the other hand was revolutionized in 1900 when Taylor presented his invention of high speed steel (HSS) as a tool material that replaced the long used carbon steels. In 1940 carbide tools brought about another turning point to the machining industry by enabling elevated speeds.

During this period of time, for almost a century the cutting edge was considered to be sharp. For instance, Merchant [3] assumed the cutting edge to be sharp in his widely accepted analytical model of orthogonal cutting. The extensive effect of cutting edge geometry (simply represented by an edge radius at that time) on the mechanics of machining was only realized in 1950-60, perhaps first documented in Japanese by Masuko [4] and later by Albrecht [5].

The enhancement of cutting tool life and performance subsequent to applying a small hone or chamfer on sharp cutting edges, a process that is called edge honing or edge preparation, quickly became a common practice in the machining community. It took only 10 years for honing techniques to become a winning factor for one tool manufacturer over a competitor in 70s [6].

Over the next years, driven by the demands of a highly competitive market, machining industry underwent constant advancements. Micromachining, high performance machining and high speed machining which came into existence in the past couple of decades are some of the responses to these demands. More advanced machine tools, robust structures, high-tech spindles, complex drives and controls have all been under constant development. The significance of the cutting edge, as the final link in this chain of high-tech machine tool components, cannot be overemphasized, since if it fails all other machine tool components will be rendered redundant. For this reason, cutting edge preparation and characterization techniques have gained special attention among the international machining research community in recent years. The emergence of novel edge preparation techniques in the past five years has led to the advent of tailored cutting edge microgeometry and techniques for advanced cutting edge characterization.

In this context, this PhD thesis presents the proof-of-concept of the electro erosion edge honing technique which is a novel cutting edge preparation process based on electrical discharge machining (EDM). It further presents a new methodology for parametric characterization of the cutting edge microgeometry.

This chapter briefly introduces the cutting edge microgeometry and edge preparation in section 1.1. The significant effect of cutting edge geometry on the mechanics of metal cutting process is detailed in section 1.2. With

the importance of cutting edge geometry established, further cutting edge related research are categorized into two groups: (i) research related to cutting edge preparation, and (ii) edge geometric characterization. Section 1.3 reviews conventional and novel edge preparation techniques. Section 1.4 details the latest advancements in cutting edge geometric characterization. Since the electro-erosion edge honing is based on electrical discharge machining (EDM), a brief introduction to EDM is also provided in section 1.5. Finally, section 1.6 presents the objectives and outline of the thesis.

1.1 Cutting Edge Microgeometry

Cutting tools come in thousands of different geometries specifically designed for particular applications. An indexable cutting tool consists of a tool holder and an insert. Specifically designed tool holders hold the inserts while it is the insert that performs the actual machining process. Depending on their application, cutting tool inserts might adopt different macrogeometric features such as chip breakers, nose radius (R_n) or curvilinear edges, Fig. 1.1.

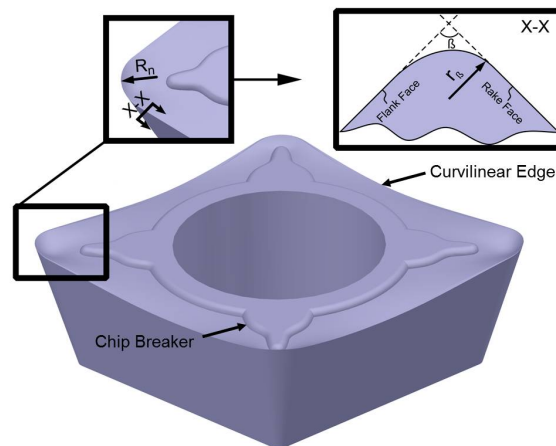


Figure 1.1: A typical cutting tool insert.

Regardless of various complexities an insert might have, the focus of this thesis is on the microgeometry relating to the cutting edge of the tool (section X-X in Fig. 1.1) which plays a major role by removing chips from the work-piece surface. Most of the early models of chip formation, such as the widely used Merchant's model [3], Lee and Shaffer's Model [7] and Oxley's model [8], considered this microgeometry to be perfectly sharp. Nevertheless, cutting edges have always a finite sharpness which through extensive experimental tests is shown to significantly affect the machining process. This is detailed in the next section.

Upon the realization of such importance, edge preparation techniques were developed for micro-shaping the sharp edges of cutting tools. Edge preparation removes initial edge defects, Fig. 1.2 (such as edge chipping, die flashes and burrs) from the sharp edges of cutting tools by replacing them with a smooth profile and thereby increases the tool life. Furthermore, edge preparation techniques are employed to fabricate engineered edge microgeometry for enhanced tool performance since machining responses exhibit optimum value with respect to cutting edge microgeometry.

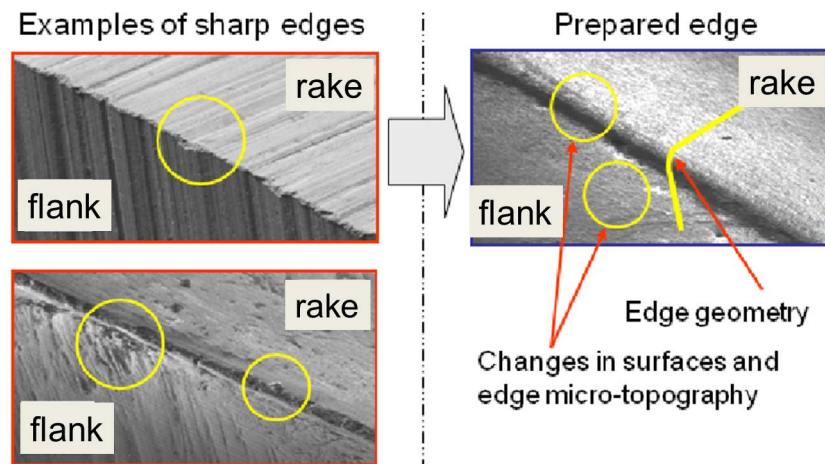


Figure 1.2: Importance of cutting edge preparation [9].

1.2 Importance of Cutting Edge Geometry

Cutting edge microgeometry affects many aspects of a machining operation like cutting force, surface quality, stress and temperature distribution on the tool, tool wear and tool life. Several researchers have investigated the influence of edge geometry on machining results. The research in this area can be divided to two major groups. In the first group cutting edge geometry is represented by an edge radius value (r_β in Fig. 1.1) assuming that the geometry of the cutting edge corresponds to a circular profile connecting the rake and clearance (flank) faces, a brief review of which follows.

The first study (atleast in the English literature) in this group is the work of Albrecht [5]. By considering the edge roundness, Fig. 1.3, Albrecht suggested that in addition to material shear which was known to be a major factor in the mechanics of chip formation, ploughing can be considered to be of significance as well.

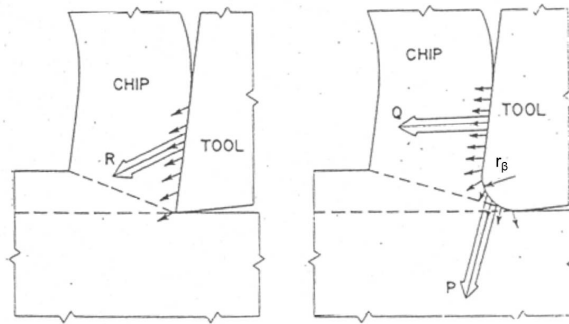


Figure 1.3: Resolving the resultant force R into two components: ploughing force P and tool face force Q; adapted from [5].

As the tool progresses in the cut, the small amount of material in front of the cutting edge flows with respect to the material separation point. Above

this point material is pressed into and becomes a part of chip. Below this point material is considered to flow into the workpiece forming the newly machined surface. This action is termed as ploughing. Albrecht showed that considering the ploughing effect enables the metal cutting theory to explain some of the not previously well-understood phenomena like chip curl and compressive residual stresses in the workpiece.

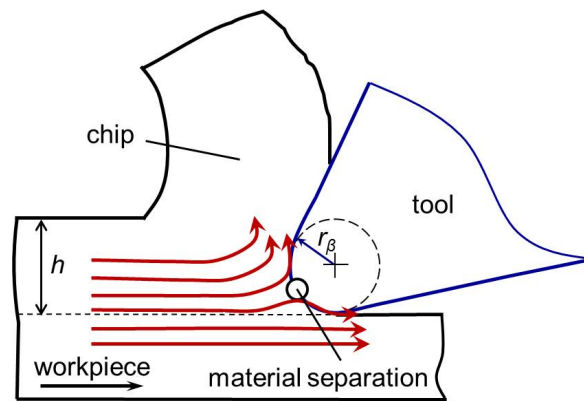


Figure 1.4: Material separation point.

Considering the geometry of the cutting edge provides the rationale to explain various machining responses, one of which is the size effect. Size effect is defined as the nonlinear increase of specific cutting energy, energy required to remove a unit volume of material, with decrease in undeformed chip thickness [10]. It is due to the size effect that classical chip formation models which ignore the finite edge geometry are only valid when the magnitude of edge radius is quite small ($r_\beta/h \ll 1$) compared to the uncut chip thickness (h). The effect of cutting edge microgeometry becomes particularly pronounced when $r_\beta/h \leq 1$ in processes such as finish hard turning or micro-machining. A small change in undeformed chip thickness significantly affects the machining process as the material removal mechanism changes from cutting to ploughing

and thereby affecting the tool life and the surface quality of workpiece [11]. Alternatively, a chip formation theory based on slip line model considering the effect of edge microgeometry has been proposed by Fang [12] which accounts for the size effect.

Through experimental cutting tests, Rech [13] and Schimmel et al. [14] have shown that by increasing the cutting edge radius the thrust force component elevates considerably but the cutting force is not significantly affected, Fig. 1.5. This is due to the increased ploughing while machining with tools with larger edge radius. Fang [15] obtained similar results using the analytical slip line chip formation model.

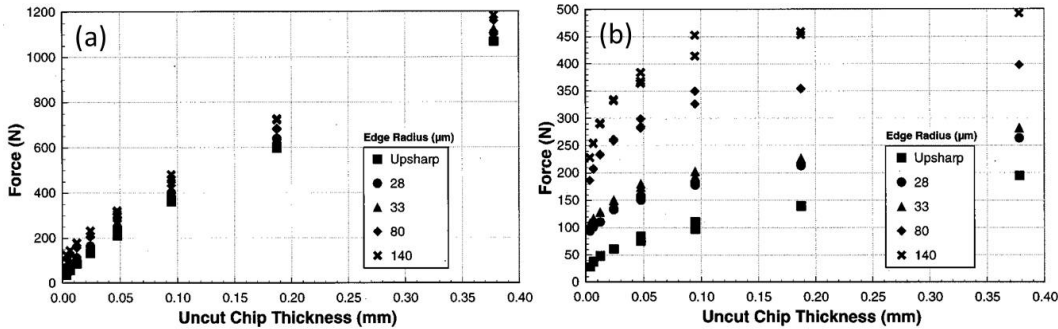


Figure 1.5: Forces vs. uncut chip thickness : (a) cutting (b) thrust [14].

While high speed machining of 44 HRC hardened INCONEL 718, Coelho et al. [16] studied the effect of edge honing on surface roughness and residual stresses. They reported the potential improvement in the surface roughness and an increase of the compressive residual stresses on the machined surface while machining with tools honed to 13 - 38 μm as compared to unprepared ones. Nasr et al. [17] also studied the effect of edge radius on residual stresses for orthogonal cutting AISI 316L steel by using a finite element model, Fig. 1.6.

By increasing the edge radius value, higher tensile residual stresses were induced in the near surface layer. This is due to the increase in workpiece temperature since more heat is generated when the contact area between the tool-tip and the workpiece increases. Larger tool-edge radius induced higher compressive residual stresses far from the surface and moved the location of their maximum magnitude deeper into the workpiece, Fig. 1.6. This is attributed to higher material plastic deformation and more material being ploughed into the newly machined surface [17].

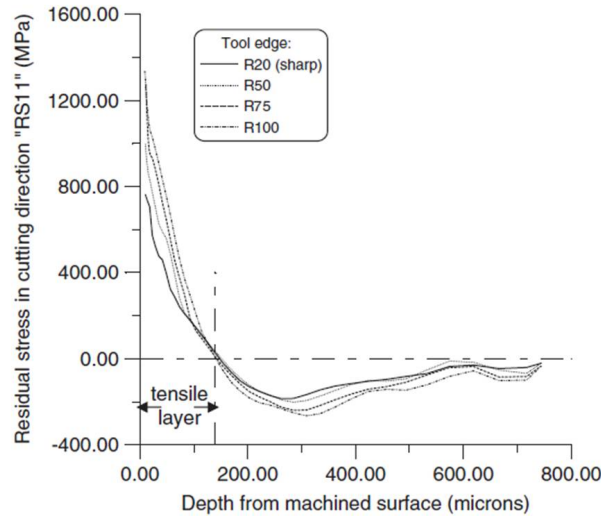


Figure 1.6: Effect of tool-edge radius on in-depth RS11 profile [17].

Bouzakis et al. [18] showed that an increase in the edge radius of coated cemented carbide inserts from $8 \mu\text{m}$ to $35 \mu\text{m}$ decreased the maximum mechanical stress in the cutting edge, in a milling application. This was found to lead to a delayed onset of coating fracture and a four-fold enhancement in tool life. Rech et al. [13] reported similar results by investigating the wear resistance of powder metallurgy high speed steel (PM-HSS) milling inserts. It was concluded that the best performance in the dry milling tests corresponded to

honed tools with a cutting edge radius of $10\ \mu\text{m}$ which increase the cutting tool life dramatically by a factor of 4-5 compared to ground tools. This small cutting edge radius prevents the PM-HSS tool from chipping of the substrate and from fatigue fracture of the coating in high speed dry milling [13]. They also developed a 2-D finite element model to study the stress distribution within the tool coating and substrate through which the optimal edge radius that allows the minimization of equivalent stress inside the coating was found to be $14\ \mu\text{m}$. While increasing the cutting edge radius, its optimum value can be related to the trade-off between the increased machining forces which results in higher mechanical stresses on the tool and the decreased stress concentration in the cutting edge that delays the onset of coating fracture.

By using a CCD camera, M'Saoubi and Chandrasekaran [19] investigated the influence of cutting edge microgeometry on cutting tool temperature. They reported that a higher radius (from 2 to $25\ \mu\text{m}$) induces an increase of around 15°C of the maximum cutting temperature on the rake face due to larger plastic deformation and more heat generation. Yen et al. [20] reported that the maximum tool temperature near the tool tip exhibits optimum value with respect to edge radius. This is attributed to the opposing effects of more heat generation and better heat dissipation due to the larger contact area when increasing edge radius.

In the past two or three years, with the advent of advanced edge preparation techniques, researchers have studied the cutting edge microgeometry in more details. Therefore, the second group of research, in addition to the roundness of the edge previously investigated, consider the effect of edge asymmetry on process behavior.

In order to differentiate asymmetric cutting edge microgeometries, Denkena et al. [21], employed S_α and S_γ parameters which are defined as the distance

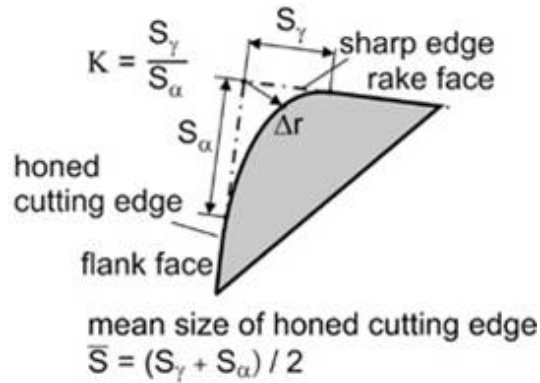


Figure 1.7: Characterization of the asymmetrically honed cutting edge [21].

between the virtual sharp edge to the cutting edge margins on flank and rake faces, respectively, Fig. 1.7. S_α was shown to directly influence the thermal load on the wedge of the cutting tool as a result of increased contact area and higher friction of the flank face with the workpiece.

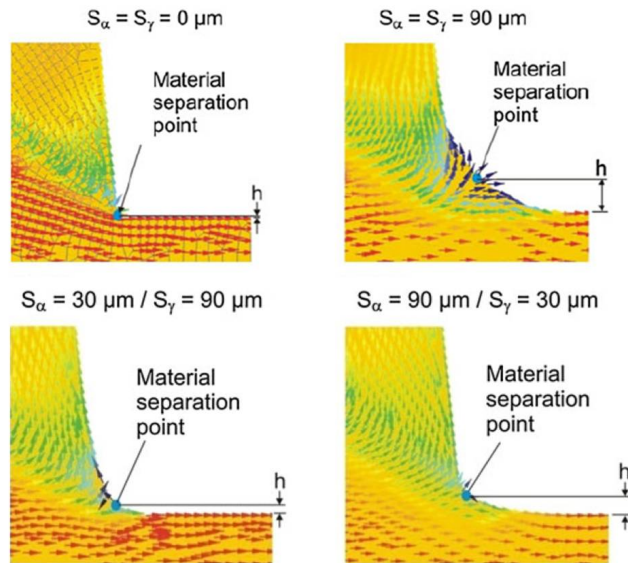


Figure 1.8: Effect of symmetrical and asymmetrical cutting edge geometries on material separation point [22].

In a later study, Denkena et al. [22] developed a finite element model to convey a more in-depth analysis of the effect of symmetrically and asymmetrically rounded cutting edge on the flow of material in the vicinity of the cutting edge. They were able to explain the changes in cutting force and tool thermal load by looking at the material separation point and the length of the effective cutting edge while changing the asymmetrical geometric parameters, Fig. 1.8. They concluded that the tool temperature and cutting force increase with increasing S_α and S_γ with the thrust force being dominantly influenced by S_α . By increasing S_α material separation point moves higher from the newly machined surfaces, thus more material needs to be ploughed into the workpiece surface, Fig. 1.8.

It is obvious from the reviewed research that the cutting edge geometry has a significant role in the mechanics of cutting and tool performance. Variations of edge geometry from one insert to another or along a single cutting edge will therefore lead to non-consistent machining results. This reveals the significance of developing a repeatable, cost-effective edge preparation techniques capable of consistently honing cutting edges for cutting tools of different materials and macrogeometries.

1.3 Edge Honing Processes

Upon the realization of the advantages of edge honing on the mechanics of machining, processes for microshaping the sharp edge of cutting tools were developed. These methods are called edge preparation methods. Edge preparation is a necessity in almost 100% of all hardmetal tooling [6]. Depending on the cutting tool application, edge preparations are applied in a variety of sizes and shapes. Proper edge preparation is important for tool performance since

it strengthens the tool and delays or eliminates edge chipping or breakage. As explained previously, it has a significant effect on cutting force, surface finish, residual stresses and tool wear rate. It also removes edge imperfections and prepares the edge for coating. This section reviews the conventional and novel edge preparation techniques.

1.3.1 Conventional Edge Honing Processes

In this section two of the common industrial edge preparation methods presently used to generate the edge radius are introduced. Both of these methods rely on material removal by abrasion.

Brush honing (Nylon Abrasive Filament Brushes)

The most common method for honing the cutting edges employs nylon abrasive filament brushes. In this method the inserts to be honed are passed through nylon brushes impregnated with abrasive grits. In some applications inserts also rotate around the machine table as they all revolve under the brushes. Brush honing edge preparation machines are manufactured in different configurations. Fig. 1.9a shows a brush honing setup. Similarly, the brush honing wheels are produced in different shapes and geometries (Fig. 1.9b). By varying the time, speed, depth of contact between the tool and the brush wheel and the direction of engagement, different edge geometries can be generated.

Shaffer [6] explained the characteristics and limitations of the brush honing process. He mentions that the most influential parameter on the quality of the finished part is the in-coming part condition as these parts might have initial die flash, edge chipping or damaged edges. Moreover, the variable honing characteristics of different cutting tool materials sometimes even within the same batches of inserts is another decisive limitation. Therefore, the edge

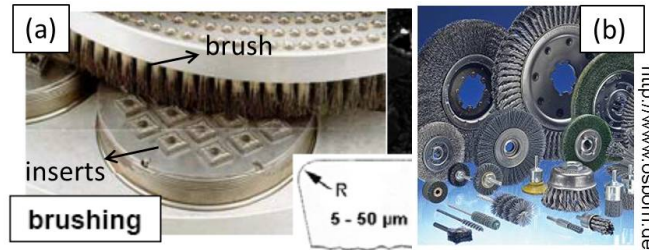


Figure 1.9: (a) Nylon abrasive cutting edge preparation machine [23]. (b) Nylon abrasive filaments.

honing process requires a delicate balance of operating parameters. This makes the machine setup time consuming and greatly dependent on operator skills.

Another limitation of the brush honing process is the constant change in the condition of filaments. Shaffer indicates this limitation as nylon smearing caused by incorrect setup and incorrect operating parameters [6]. Bassett et al. [24] investigated this phenomenon more closely by looking at the filament wear behavior. While preparing a batch of 80 inserts, it was shown that the edge radius variability of the brush honed inserts is highly dependent on filament conditions, Fig. 1.10. The brush honing process achieves its maximum repeatability in the middle of the filament life cycle in the stabilized process stage.

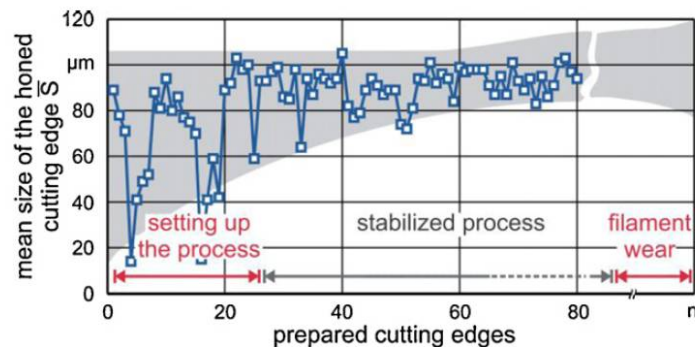


Figure 1.10: Effect of filament condition on the repeatability of brush honing [24].

By analyzing the geometry of edges prepared by this method, it was shown that edge radius variability could be as high as 40% along the same edge [25] and up to 35% from the measured value to the nominal edge radius [26].

Abrasive Jet Machining (AJM)

Abrasive jet machining (AJM), also called micro blasting, is a manufacturing process that utilizes a high-pressure air stream to propel small abrasive particles to impinge on the workpiece surface for material removal and shape generation. The removal occurs due to the erosive action of particles striking the workpiece surface, Fig. 1.11. AJM has limited material removal capability and is typically used as a finishing process [27]. The mechanical properties of the substrates will determine the type of treatment, i.e. particle hardness, velocity and duration of application [28]. The advantages of this method include [28]

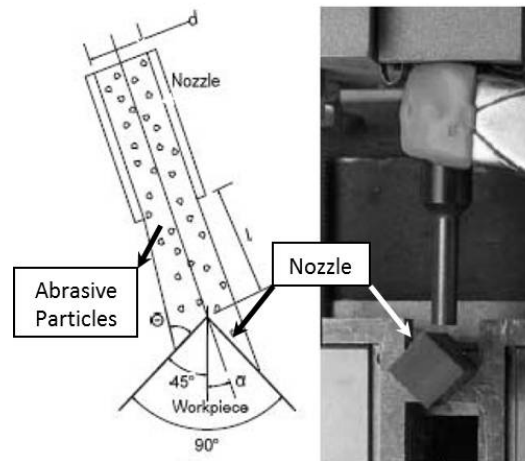


Figure 1.11: Abrasive Jet Machining [27].

increased fatigue life, change in residual stresses, and it being economical and easy to apply. The major limitation of this process is the low removal rate which limits its application to intermediate hone sizes (5 - 20 μm) [23]. Higher

radius values require longer processing times which cause collateral damage to the rake and flank [27]. Moreover, uniform profile generation requires the rotation of the edge (or nozzle) around three perpendicular directions in order to ensure uniform treatment of all the cutting edges and faces. There is also the risk of abrasive grains getting embedded into the substrate. These grains are usually non-conductive and may hence adversely affect the coating deposition process for PVD coatings [13].

Rodriguez [9] compared the life of the carbide cutting tools prepared by brush honing with abrasive jet machining for different edge radius values ($r_\beta = 7 - 26 \mu\text{m}$), Fig. 1.12. It was shown that for the entire edge radius range abrasive jet machined tools correspond to an increased flank wear. This is due to the collateral damage of abrasive jet to the cutting edge.

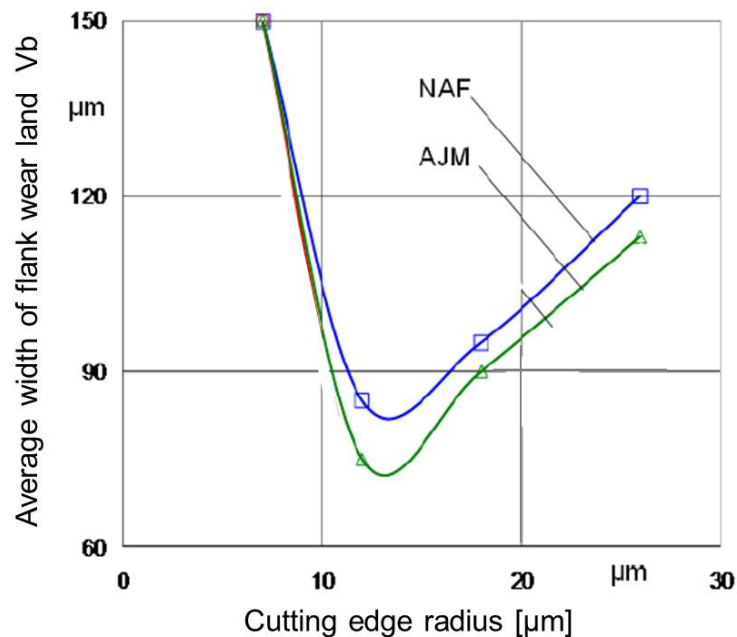


Figure 1.12: Tool wear for tools prepared by AJM and brush honing [9].

1.3.2 Modern Honing Processes

The limitations of brush honing and micro blasting as conventional edge preparation techniques along with the ever-increasing demand for high performance cutting tools have led to the emergence of novel edge preparation techniques in the past 5 years, a review of which follows.

Abrasive Flow Machining (AFM)

Abrasive Flow Machining (AFM) was developed in 1960s as a process to polish, debur and hone difficult to reach surfaces and edges by flowing an abrasive laden fluid over them. It uses two vertically opposed cylinders which extrude abrasive medium back and forth through the passage formed by the workpiece and the tooling. Abrasion occurs whenever the medium passes through the restrictive passage [29], Fig. 1.13.

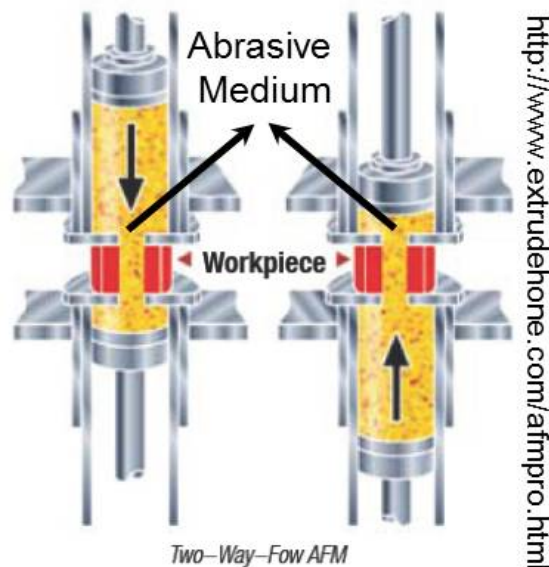


Figure 1.13: Abrasive Flow Machining.

The AFM process has been adapted to manufacture cutting edge radii by extruding an abrasive paste containing SiC or diamond grains around the cutting edge [13]. This process has the advantage of being more flexible to create a wide range of radii compared to micro sandblasting [13]. The novel AFM method is one of the common methods that some tool manufacturers use for edge radius generation. The rheological properties of the medium affect the abrasion process dramatically.

Bouzakis et al. [18] investigated the effect of cutting edge radius prepared by micro-sandblasting and AFM method on the wear behaviour of PVD coated cemented carbide inserts for the milling process. Comparing the two preparation methods resulted in the conclusion that AFM method produces tools with longer tool life than micro-blasting, Fig. 1.14. This was related to the removal of carbide grains on the outer surface by the sand jet. Rech [30] reported similar results for prepared gear hobs made of PM-HSS.

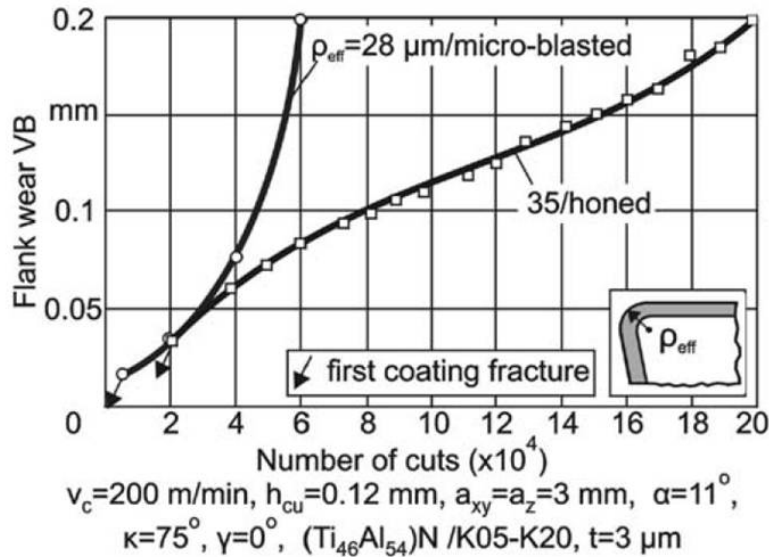


Figure 1.14: Comparison of the flank wear development between a blasted and a AFM honed cutting edge of similar radii [18].

Abrasive Waterjet Blasting

Biermann and Terwey [31] employed the abrasive waterjet blasting process to prepare different cutting edge designs of twist drills prior to coating. Pressurized water was mixed with the abrasive medium in a swirl chamber. Accelerated grains impact the cutting edge with high velocity and remove small amount of material. By varying the jet-feed speed, they were able to generate variable edge radius along the twist drill cutting edges based on which they prepared four different cutting edge designs, Fig. 1.15.

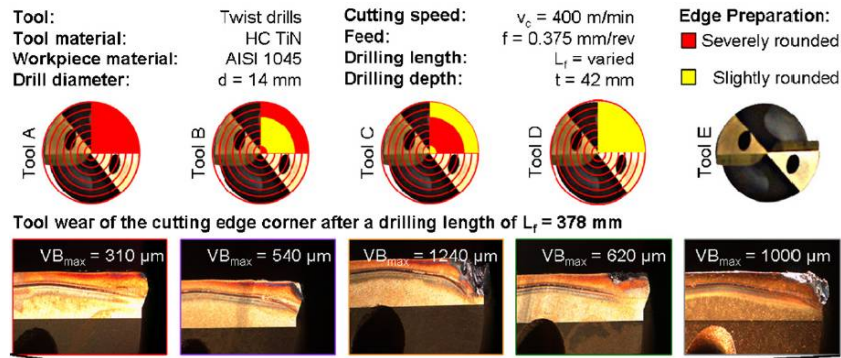


Figure 1.15: Influence of the cutting edge design on tool wear [31].

It was concluded that the size of the cutting edge rounding (especially at the corner) has a pronounced influence on tool wear and the quality of the borehole, as edges with higher rounding exhibited higher stability and decreased chipping. Better adhesion of the coating was claimed to be responsible for enhanced process performance.

Magnetic Abrasive Machining (MAM)

In the magnetic abrasive machining method, a magnetic field is used to generate cutting and polishing forces to treat the surface of a machined part. The magnetic field behaves as an elastic bond for the abrasive ferromagnetic

grains and allows more effective use of cutting edges; furthermore, it provides conditions for a small cutting force and a low surface temperature for finishing operations [32].

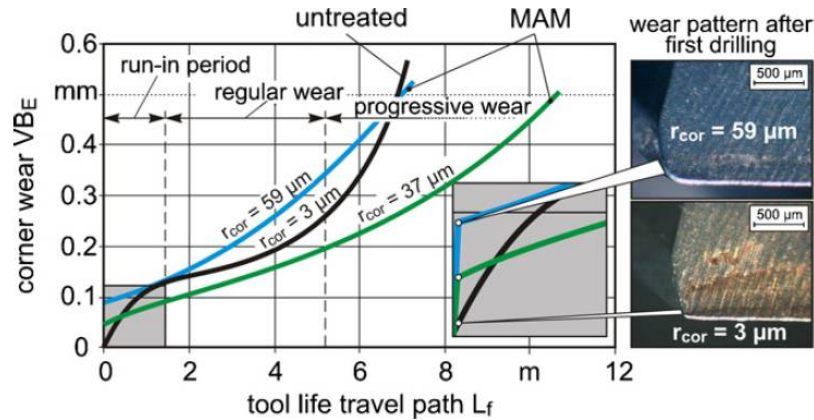


Figure 1.16: Enhanced drill life by means of MAM [34].

Cheung et al. [33] used the magnetic polishing method for edge preparation of HSS drills. Through improvement of the cutting edge condition, the process has shown to be beneficial in the enhancement of drill life as drills with edge radius ranging from 24 -27 μm achieved the maximum life when machining 30 HRC Bohler M238 plastic mould steel. By magnetic abrasive machining edge preparation of high speed steel drills, Karpuschewski et al. [34] enhanced the tool life by 80%. The prepared cutting tools exhibited optimum behaviour for edge radius of 25 - 35 μm , Fig. 1.16.

Edge Preparation by Marking Laser

Aurich et al. [35] developed the innovative application of marking laser for cutting edge preparation. Several tool material layers needed to be removed for generation of edge radii greater than 14 μm or an appropriate cutting edge roughness ($R_a < 1.5 \mu\text{m}$). One of the limitations of this method was the decreasing machining accuracy as the number of layers increases. This method

was shown to successfully increase the tool life by more than 50% as compared to sharp tools. However, it is unclear if the tools prepared by this method show the same or better functionality, when compared to brush-honed tools with the same radii. This is specifically important since laser machining is a thermal process and hence alters the substrate surface integrity.

5-Axes Brush Honing

Denkena et al. [36] have been able to address some of the disadvantages of conventional brush honing by introducing the simultaneous 5 axis brushing technique, Fig. 1.17.

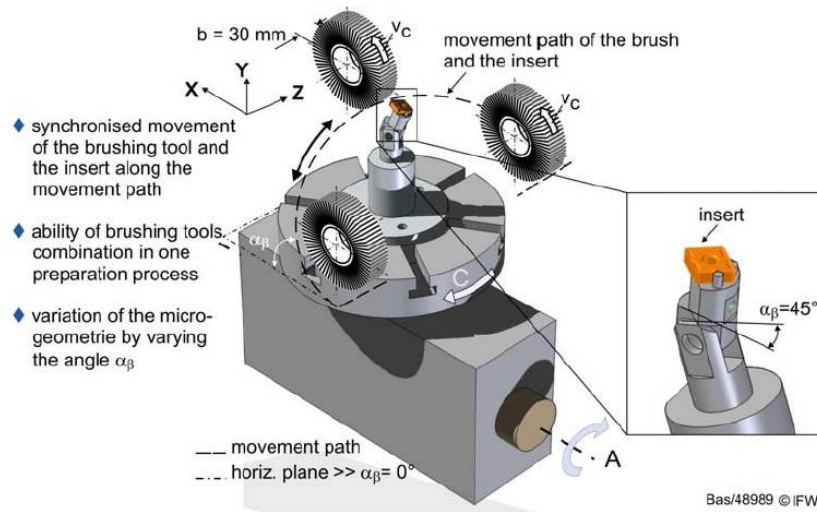


Figure 1.17: 5-Axes brush honing [36].

Consistent cutting edge microgeometry was achieved along the cutting edge even at the nose section. By taking advantage of 5-axis brushing wheel movement, they have also been able to generate asymmetric edge microgeometry along the cutting edge. This process appears to be promising though it will be complicated on complex edge macrogeometries having nose radius and curvilinear edges, since the machine should be programmed differently for various

cutting edge macrogeometries. The variable condition of abrasive filaments also remains to be a limitation for successive honing of several batches of inserts.

1.3.3 Summary of Preparation Methods

An introduction to available edge preparation techniques was presented in this section. Two conventional edge preparation techniques are brush honing and micro blasting, both relying on material removal by abrasive grits. However, inadequacy of the conventional edge preparation methods which is manifested in edge radius variations by as much as 40% [25] on one hand, and the fact that circular edge profile does not necessarily correspond to the most optimal edge geometry [21] on the other, has led to the development of a series of novel edge preparation techniques in the past few years. Magneto-abrasive cutting edge preparation [34], edge preparation by marking laser [35] and 5-axis brush honing [36] are some of these novel micro-geometry fabrication techniques, aiming to enhance the controllability of the edge preparation process. The motive behind their development is particularly pronounced when it comes to machining high value components. Despite the advantages that these methods offer, they have also some limitations. 5-Axes brush honing, AFM, MAM and abrasive water jet machining are abrasion based, hence their application is highly limited by the hardness of the material being prepared. Marking laser preparation is also limited for honing large size hones as several layers need to be removed. Furthermore, a major common confinement is the preparation of cutting edges of complex macrogeometries where intricate kinematic configurations are required for uniform treatment of all the cutting edge.

Keeping in mind the prominent role of edge microgeometry in machining operations, developing a repeatable, defect-free and low cost preparation method is the major motive of this thesis. The development of such a preparation method based on electro-discharge machining is detailed in Chapter 3.

1.4 Cutting Edge Characterization

Cutting edge geometry has a significant role on the mechanics of chip formation. It is known to considerably affect the cutting force, machined surface roughness, tool life and residual stresses. Accordingly, edge preparation techniques have been developed to secure consistent tool performance by replacing the initial sharp cutting edge with a tailored cutting edge profile.

Due to the lack of advanced measurement methods and effective edge preparation techniques, for years cutting edge geometry was represented by a single edge radius value assuming that the edge profile can be best described by a circular arc connecting the rake and flank faces. With the advent of engineered cutting edge microgeometries resulted from novel edge preparation techniques, however, cutting edge radius was not sufficient to represent these complex geometries. With a view to bridging this gap, several researchers have proposed novel edge characterization methods.

Denkena et al. [21] suggested four parameters to characterize the asymmetrically honed edge, Fig. 1.18a. Distance between the virtual sharp edge and edge separation points (points 1 and 2) on the rake (S_γ) and on the flank (S_α), Δr which is the apex distance to the virtual sharp edge and ϕ that describes the angular shift of the apex to the wedge angle bisector. However, this method lacks a robust approach for the determination of S_α and S_γ . These parameters are therefore based on ideal geometric shapes and are affected by

local form variations and measurement point uncertainties.

Rodrigues [9] has developed an edge characterization method in which the profile is approximated by a sixth-degree polynomial. Cutting edge was defined with respect to uncut chip thickness (points 1 and 2), Fig. 1.18b. Based on this polynomial, a series of geometric functions (i.e. effective rake and curvature function) and parameters were calculated for every point on the edge. This method is able to relate the machining behaviour to the shape of the cutting edge microgeometry, however it is incapable of providing a comprehensible description of the cutting edge geometry independent of machining conditions.

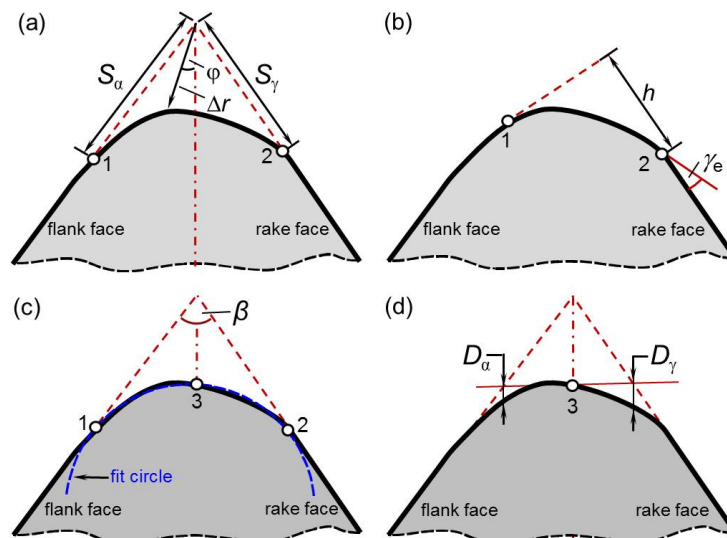


Figure 1.18: Cutting edge characterization methods due to: (a) Denkena et al. [21], (b) Rodriguez [9], and (c & d) Wyen et al. [37].

Wyen et al. [37], in an attempt to reduce the limitations inherent in Denkena's method, proposed a new set of edge characterization parameters. They indicated that if the cutting edge region is not properly identified, edge characterization is subject to significant uncertainty. Edge identification is a process that identifies points 1 and 2 in Fig.1.18a and thereby separates the

edge from the rake and flank faces. The application of an edge identification algorithm based on iterative circular fit prior to any edge characterization was therefore advised, Fig 1.18c. In order to make Denkena's parameters independent of cutting edge separation points (points 1 and 2), they suggested replacing S_γ and S_α with D_γ and D_α , respectively, Fig. 1.18d. This set of parameters, though independent of cutting edge separation points, is still dependent on the point uncertainty and local form errors of the cutting edge profile. As D_γ and D_α are point based parameters, they are sensitive to single point position variations.

Investigating more than 3000 cutting edge profiles during the course of this Ph.D research, revealed the lack of a comprehensive, contour-based, form error invariant and easy-to-understand set of edge characterization parameters. Chapter 5 presents the innovative application of free-knot B-spline approximation for contour-based cutting edge identification. The edge identification method is shown to be robust against local form errors and point uncertainties. Following the identification approach, a new set of edge characterization parameters using parametric quadratic polynomials is proposed. These parameters in addition to being able to effectively discriminate various edge micro-geometries, are easy to visualize and influential on process behavior.

1.5 Electrical Discharge Machining (EDM)

The cutting edge preparation technique that is developed in this PhD thesis is based on electrical discharge machining. Therefore, a brief introduction to EDM is presented in this section.

Fig. 1.19 shows the four stages of EDM process. In EDM, there is a micro-scale gap filled with a nonconductive dielectric fluid between the oppositely

polarized electrode and workpiece, Fig. 1.19a. Once a pulsed voltage (typically 50 V) great enough to ionize the dielectric fluid is applied [38], by overwhelming the electrical resistance of the dielectric fluid, a spark goes through and a plasma channel with high temperatures (in the range of 8000 K [39]) constitutes, Fig. 1.19b. As a result of a single spark, material melts and evaporates leaving a tiny spherical crater on the workpiece and electrode surface [40], Fig. 1.19c. The spark (electrical discharge) usually occurs at the shortest path between the workpiece and the electrode due to the smallest local dielectric resistance [41]. Once the pulsed voltage is removed, the plasma bubble collapses and debris particles will be flushed away by the dielectric fluid, Fig. 1.19d. Pulse voltage should be determined in a fashion to provide the most stable process. Higher pulse voltage leads to higher pulse energy and crater size. However reducing the pulse voltage results in reduced gap size leading to the higher possibility of short circuits and arcing [42].

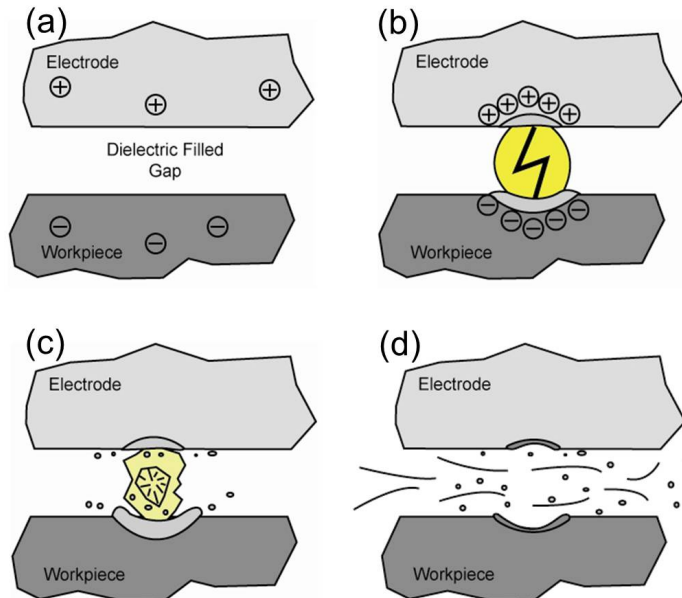


Figure 1.19: Material removal of EDM

The electrical discharges in the four stages explained above constitute the basic unit of material removal in EDM process. Crater dimension determines the workpiece surface roughness. Volumetric material removal per discharge is typically in the range of $10^{-6} - 10^{-4} \text{ mm}^3$ and material removal rate (MRR) is between 2 and 400 mm^3/min [43]. As mentioned, a small amount of material is also removed per spark from the tool electrode surface which causes electrode wear. The ratio of the volumetric amount of material removed from tool electrode (V_t) to that of workpiece (V_w) is called wear ratio (ν).

$$\nu = \frac{V_t}{V_w} \quad (1.1)$$

In a typical EDM process wear ratio is very small ($\nu < 0.05$) and therefore, as a result of hundreds of thousands of sparks per second (with spark duration typically being $10 \mu\text{s}$), workpiece will take the mirror shape of the tool electrode, Fig. 1.20a. This process is called sink EDM. The CNC sink EDM machine used for all the EDM experiments in this thesis is shown in Fig. 1.20b.

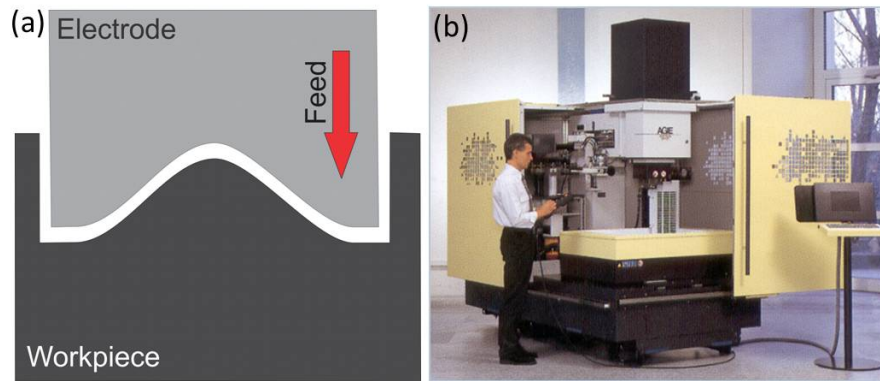


Figure 1.20: (a) Sink EDM process. (b) EDM machine used for experimental tests.

Although the electrode wear in EDM process is very negligible compared to workpiece material removal, in micro-machining and high precision EDM processes, it is indeed a major drawback. That is why in these applications several electrodes are used sequentially for roughing, semi-finishing and finishing cycles. Electrode wear is specially pronounced at the sharp corners of tool electrodes. Mohri et al. [44] measured the electrode wear for a cylindrical copper electrode with a diameter of 10 mm while machining carbon steel. The wear results are shown in Fig. 1.21. They reported that the initial electrode edge roundness of several micrometers enlarges to hundreds of micrometers after 106 mins of machining, Fig. 1.21.

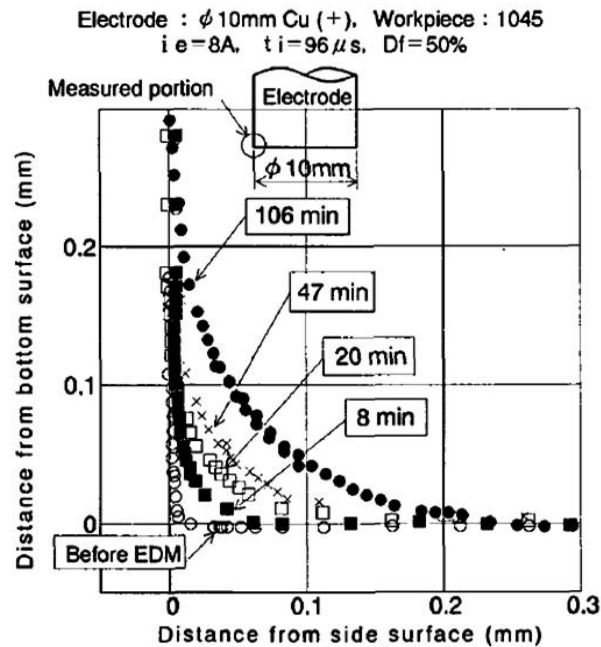


Figure 1.21: Shape change of edge portion of cylindrical copper electrode [44]

A geometric explanation for rapid degeneration of the electrode sharp corners during the sink EDM process can be deduced from considering a unit surface area of tool electrode facing the workpiece, Fig. 1.22. It can be seen that

the workpiece surface facing a unit electrode surface is larger at the edges [45] resulting in higher density of sparks and higher wear at the corners, Fig. 1.22. Crookall and Fereday [46] explained this phenomenon by introducing the concept of relative duty.

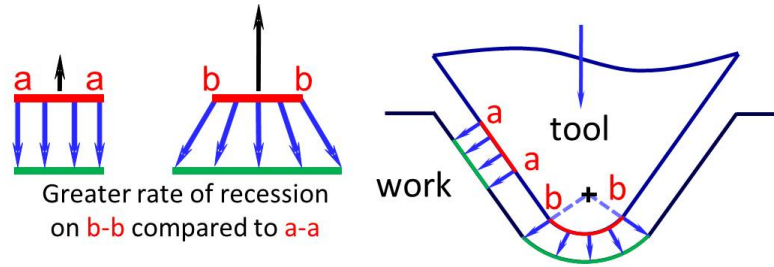


Figure 1.22: Concept of relative duty [46]

The key idea of the electro-erosion edge honing (EE-honing) is based on this drawback of sink EDM. Sharp unprepared cutting edges are used as tool electrodes. By taking advantage of localized electrode wear at sharp edges, sharp unprepared cutting edges can be honed as a result of the controlled EDM wear pattern while ED-machining of an appropriate counterface. This is elaborated in Chapter 3.

Prior to implementing the EE-honing process, there are a number of prospective advantages of using EDM for this application. There is no direct contact between the electrode and the workpiece in EDM, which eliminates mechanical stresses during machining [47]. EDM is known for its high repeatability, this can address the edge geometric variability of traditional preparation techniques. Materials of any hardness can be machined [48], as long as their electrical resistivity is lower than $100 \Omega\text{cm}$. The amount of material needs to be removed to hone a sharp edge is very minimal. Therefore, while keeping

the process time reasonably low, it is possible to hone the cutting edges by using conservative EDM parameters, which in turn make it possible to generate critical tooling surfaces with no functional detriment [49].

Electro-erosion edge honing process is elaborated in chapter 3. It is shown that by controlled wear pattern, it is possible to hone the sharp edges of straight edge HSS inserts using this idea. The application of EE-honing is then expanded to include carbide tools of complex macrogeometry in chapter 4.

1.6 Thesis Objectives and Outline

1.6.1 Thesis Objectives

The objectives of this thesis are two-fold. The first is to develop a reliable cutting edge preparation technique that can repeatedly and consistently generate fine geometries on the order of several micrometers on the sharp edge of a cutting tool after the grinding/compaction operation. This is to prevent catastrophic tool failure, and to enhance the life and reliability of the tool. This project entails the innovative application of electrical discharge machining (EDM) to generate this edge geometry, as opposed to conventional methods that rely on material removal by abrasion.

The second goal is to develop a robust, contour-based cutting edge characterization which is capable of identifying cutting edges of various forms and geometries. These parameters should be capable of representing symmetric and asymmetric cutting edge geometries. They should further be easy-to-visualize and at the same time influential on machining process behaviour.

1.6.2 Thesis Outline

Prior to the implementation of the electro-erosion edge honing idea, it was realized that a reliable edge measurement and modeling technique should be developed for subsequent investigations of the prepared edges. Chapter 2 explains the development of such method based on optical microscopy and compares the modeling results of this approach with other cutting edge modeling techniques including form tracer, white light interferometer and physical sectioning of the edge.

Chapter 3 is a reproduction of a paper published in the CIRP-Annals Manufacturing Technology in 2010. The key idea and methodology of electro-erosion edge honing is detailed in this chapter. EE-honing is a novel edge preparation process that is based on micro-shaping the cutting edges of metal cutting tools by electro discharge machining (EDM). This process has been applied to straight edge high speed steel (HSS) cutting tools and is shown to result in a manifold enhancement of tool life as compared to the sharp unprepared edges.

In chapter 4 the EE-honing application is expanded to hone complex geometry tools by an innovative idea of using foil counterfaces. Carbide tools are prepared considering that they are the most common metal cutting tool material. Electro-discharge machining of metal matrix composite carbides brought about lots of process stability and surface integrity challenges that required careful selection of the process parameters. The systematic approach of identifying effective EE-honing parameters is explained. Complex geometry cutting tools prepared by these parameters are then analyzed in terms of geometric consistency, surface integrity and tool life. This work is published in the Journal of Material Processing Technology in 2012.

The advent of advanced edge preparation techniques like EE-honing process

has led to the emergence of advanced cutting edge microgeometries. This however, developed a gap between the modern cutting edge geometries and cutting edge characterization techniques, since for more than 60 years cutting edge radius was used as the only parameter to represent the edge geometry assuming that the edge profile corresponds to a circular segment. In order to bridge this gap, a novel idea of using piecewise polynomial B-spline curves for cutting edge characterization is presented in chapter 5. The free-knot B-spline approximation enables the unique identification of the cutting edge separation points from the clearance and rake faces. Subsequent to edge identification, quadratic parametric polynomials are employed to characterize the cutting edge using four parameters. These parameters are contour-based, easy to visualize and influential on process behavior. This part of the thesis is also under review for publication.

As the final stage of the thesis, the EE-honing process is simulated numerically. The algorithm is first qualitatively verified by the predictions of several process behaviors. Finally, EE-honing simulation results for honing of cutting edges under increased processing were compared to experimentally generated hone sizes. It is shown that there is only a maximum error of 14% between the simulated and experimental results. These results documented in chapter 6, are to be shortly submitted for publication.

1.6.3 Contributions to Articles

Chapter 3, 4 and 5 of the thesis are reproductions of published or submitted articles in/to top journals of the manufacturing field. All the tests, measurements and computations are original research results and implemented in McMaster University.

The idea of the electro-erosion edge honing presented in chapter 3 is published in CIRP Annals, Manufacturing Technology. The primitive idea was developed previously by Dr. Koshy. Some preliminary tests on HSS inserts were conducted by a visiting student, Mr. Buchholz supervised by Prof. Klocke from Germany, both of whom are coauthors of the paper. In the second year of my PhD tenure, I performed the systematic development of the process through experimental tests, computations, measurements and simulations. All the presented results in this work are my research results (except for the tool life test for HSS tools which was previously done by Mr. Buchholz) developed under the supervision of Dr. Koshy. The paper was originally written by Dr. Koshy with my help on subsequent modifications. I prepared the figures and graphs out of the research results.

The EE-honing process was extended to prepare carbide tools with complex geometry. This work is presented in chapter 4 and is published in the Journal of Materials Processing Technology. I wrote the first draft of the paper and prepared all the figures and graphs after which they were modified in accordance with Dr. Koshy's instructions.

The innovative idea of using free knot B-splines for cutting edge identification and using quadratic parametric for edge characterization is presented in chapter 5. I generated the first paper draft, figures and results. The idea was originally mine and was further developed over numerous in-person meetings through elaborate discussions with Dr. Koshy looking at it from different perspectives. Results are documented in a paper that has been submitted to Precision Engineering.

Chapter 2

Cutting Edge Geometric Modeling

Cutting edge modeling provides the profile of the cutting edge cross section which can be used to evaluate the edge radius or its asymmetry. An effective edge modeling method should be capable of modeling edges of various sizes, microgeometries and textures with acceptable repeatability. Furthermore, it should be applicable to cutting tools with various macrogeometric complexities. It is also beneficial for a modeling technique to provide a surface model of a cutting edge so that edge geometric uniformity can be investigated without repositioning the edge for individual profile measurements. A reliable cutting edge modeling technique is required for investigating the geometry of the prepared edges prior to any attempt to develop a novel edge preparation process. In the context of this thesis, edge modeling technique facilitates the geometric evaluation of the cutting edges prepared by the developed method as compared to the ones prepared by conventional edge preparation processes.

In this chapter a brief review of the common cutting edge modeling methods is first presented. The cutting edge modeling technique that is developed based

on optical microscopy is then detailed.

2.1 Cutting Edge Modeling

Tactile or optical measurement methods are used for various metrology purposes. Some of these measurement methods are briefed in this section from the cutting edge measurement perspective.

Form tracers (Profilometers): Form tracers measure a contour of a specimen on which a stylus or a probe moves. A diamond stylus is used to trace the profile of the cutting edge. Typically, in order to fully characterize the tool, several traces are measured at the leading edge, nose and trailing edge. Although stylus form tracer have been a means of measurement for quite a long time, there are a number of limitations for this method:

- Form tracer provide a contour measurement of the surface. Consequently, for more in-depth analysis of the cutting edge like the variation of edge radius along the edge or tool wear analysis many contours need be measured.
- As the form tracer works on a contact based approach any deficiency in the measuring instrument necessitates calibration process or it will affect the accuracy of the results.
- The perpendicularity of the edge and the stylus path affects the measurement results since only a stylus path that is perfectly perpendicular to the edge will measure the true cross section.

Scanning Electron Microscope (SEM): SEMs are used to produce high resolution images from objects [50]. Edge radius measurement could be done in

destructive or non-destructive fashions using an SEM. In the non-destructive method the edge is oriented perpendicular to the electron beam. This method is obviously not precise since the measurement is strongly dependent on the specimen orientation.

The more precise method is the destructive one, where a cross section of an insert is examined under the SEM [51]. This method also suffers from a number of disadvantages. The most important one is that only one section of the cutting edge can be examined at a time. Moreover, cutting tools are hard materials. This makes the sample preparations (sectioning, mounting, grinding and polishing process), time and money consuming. In addition, since it is the edge of the specimen that is of interest, if edge retention strategies (use of edge retention powders, appropriate resin and sacrificial pieces) are not employed while preparing the samples, edge geometry will be altered due to edge rounding during grinding and polishing of the specimen.

White Light Interferometer: Basically developed for flat surface profile measurements, white light interferometers (WLI) are now widely used for edge profile measurements [25]. The most important disadvantage of this method is that obtaining interferometric fringes is limited, if not impossible, for sharp edges, since most of the incident lights scatter and cannot be observed by the objective lens. For the same reason the obtained three dimensional surface is of low resolution. This makes a more in-depth analysis like cutting edge geometric evaluation along the cutting edge almost impossible. The process is also strongly dependent on the specimen color and texture.

Atomic Force Microscope: AFM consists of a sharp probe at the end of a micro scale cantilever which collects data on a series of line scans across the part surface. A typical AFM cantilever has 400 μm length and 10 μm height and 10 nm tip radius [52]. This method is mostly used for measuring the

edge radius of micro machining tools (diamond tools), where a precise value of edge radius is vital. The slenderness and small ($<5 \mu\text{m}$) traveling range of the AFM cantilever is a limiting factor for measuring hard convex cutting edges confining its application to measurement of diamond tools.

Fringe Projection: Some researchers have reported the employment of fringe projection for cutting edge radius [35] and tool wear [53] measurements. In this method a pattern of equidistant stripes is projected on the object surface. This pattern is evaluated at a certain angle (e.g triangulation angle) on the basis of fluctuations in light intensity. Using the real distance of the projected stripes, the stripes distance registered from the position of observation and the triangulation angle the surface shape is reconstructed [54].

2.2 Edge Modeling by Optical Microscope

This section explains the method developed for edge radius measurement using an optical microscope and presents the experimental results. It should be noted that all the image processing, filtering and surface approximation algorithms are created by the author.

The Nikon AZ100 microscope consists of a lens with a very accurate focal point. Due to the accuracy of the focal point (small depth of field) points on the object surface which are slightly out of the focal plane will be out of focus and blurred in the images taken. Contrarily, the points on the focal plane of the lens will have the maximum sharpness. This helps to extract the points on the surface which lie on the focal plane of the lens. Since the focal distance of the camera lens is known, the depth of these points could be determined. However, the distance of the object surface to the lens is not of interest while the surface profile or the relative distance between the points on the object

surface is what is required.

Specimen surface can be modeled by taking a series of images which are uniformly z -spaced ($0.1\text{-}5\ \mu\text{m}$), Fig. 2.1. If the focused pixels on an image could be identified, the z -position of a pocket of in-focus pixels can be assigned with respect to the z -position of the image they belong to. This method could be employed to reconstruct the object surface. As can be seen in Fig. 2.1, at each z -depth there are a number of focused pixels. Those pixels are the ones corresponding to the points on the object surface which lie on the focal plane of the objective lens.

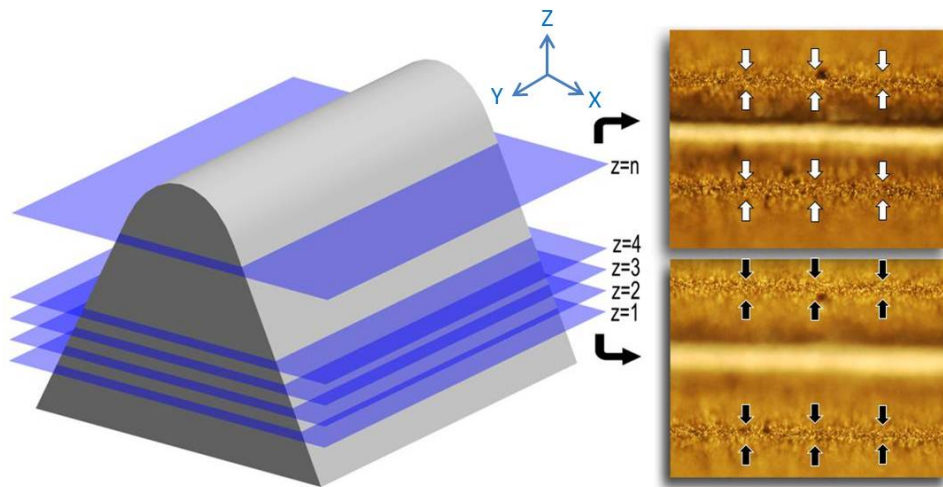


Figure 2.1: Optical edge measurement technique.

In each image, pixel size (typically in the range of 0.07 to $1\ \mu\text{m}/\text{px}$) is dependent on the image resolution (e.g. 960 by 1280) and the field of view (FOV) (e.g. $400 \times 600\ \mu\text{m}^2$). Field of view should be wide enough to cover the cutting edge and some of the flank and rake faces. It can be modified by changing the objective lens or its magnification. By moving the edge up (or the lens down) the points of maximum intensity (which are focused) are moving away from the center of image where the tip of the edge is located,

Fig. 2.1. This is due to the wedge shape of the cutting edge. The distance between successive images is known (on the order of 0.1-5 μm), therefore if the pixels of maximum intensity could be extracted the edge geometry can be reconstructed by processing a series of equidistant images. The image processing and edge modeling procedure is explained in the next sections.

2.2.1 Focused Pixel Extraction Algorithm

Each pixel on the image corresponds to a particular point on the object surface. The XY position of this point can be found by considering the pixel size and the position of the pixel in the image. Focused pixel extraction algorithm is designed to find the Z-position of this point by analyzing the pixel intensities of the image series.

For a particular point on the object the Z-position can be found by finding the image in which the corresponding pixel of that point is focused. Focused pixels are the ones having the maximum sharpness which means maximum intensity difference with their neighbouring pixels. Therefore, the intensity difference of a particular pixel compared to its neighboring pixels is computed at each image in the entire image series. The image in which this intensity difference is the maximum is the one in which that pixel has maximum sharpness and thereby defines the Z-position of the surface point corresponding to that pixel. Following the same procedure for all the pixels, the algorithm assigns the XYZ data to all the edge points, generating a point cloud data, as shown in Fig. 2.2a.

2.2.2 Filtering, Surface Interpolation and Cross Sectioning

As can be seen in Fig. 2.2a, the surface reconstruction is subjected to noise. To remove the noise, two types of filters have been designed and employed.

The noisy pixels of the sides of the edge model are not in our interest so a cut-off filter was first designed to identify and remove these regions. Starting from the two end sides, columns of data (in Y direction, Fig. 2.1) are examined for pixel intensity variations. If this intensity gradient per column is less than the average intensity gradient of the image consisting of all the focused pixels, that column of data will be removed.

There are also some points on the edge region which do not obey the continuous nature of the surface and should be filtered out Fig. 2.2a. Another filter has therefore been designed in MATLAB that works based on surface continuity and extracts the discontinuous pockets of points. The z-position of these points is replaced with the average z-position of the points surrounding them generating the filtered point cloud data, Fig. 2.2b.

Once the filtered point cloud data is obtained, it is approximated by a cubic B-spline surface [55], Fig. 2.2c. B-spline surfaces are the most flexible form of piecewise polynomial surfaces that will simplify the subsequent 3D edge processing and edge profile extraction. B-spline surface approximation algorithms have been employed to approximate a surface through the filtered point cloud data. In contrast to the surface interpolation where the surface is bound to pass through all the data points, B-spline approximation is an optimization algorithm that finds a surface which follows the data points with the minimum least square error [55]. B-spline approximation, therefore, not only provides the final edge surface model but it is also a filtering method in itself.

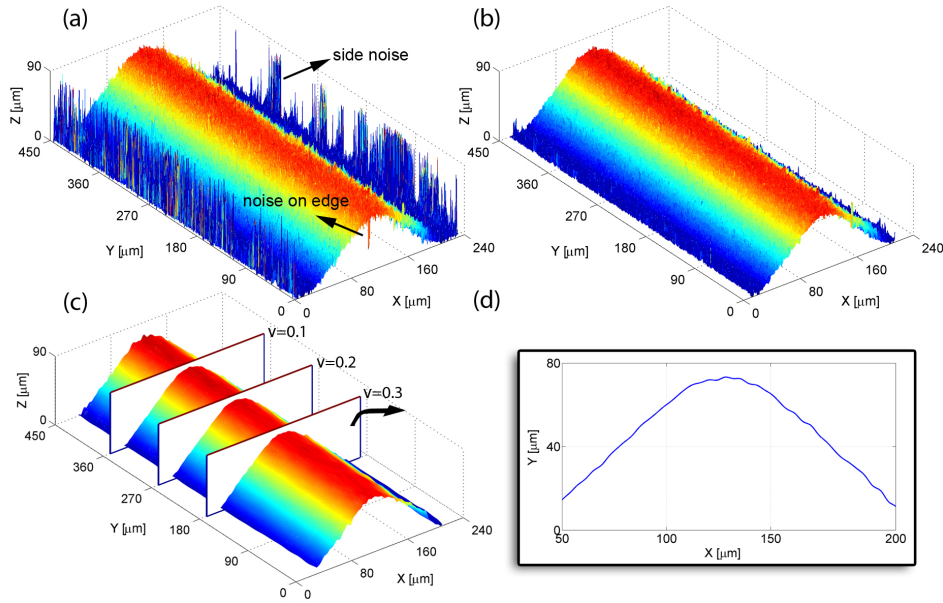


Figure 2.2: Filtering and sectioning the edge model

B-spline edge model provides the edge surface parametric equation $C(u, v)$ with u and v being the surface parameters in X and Y directions respectively. Using the B-spline surface properties, edge model can be rotated to be aligned to Y axis with minimal computations, Fig. 2.2c. Looking at different cross sections is also as easy as keeping one parameter (v) constant to pick the cross section location and changing the other, $C(u, v=\text{constant})$, Fig. 2.2d.

Fig. 2.3 depicts the 3D cutting edge model of a half worn cutting edge reconstructed by assigning the Z-position of the extracted focused pixels of the image series. Field of view was set to include both worn and unworn parts of the cutting edge. Cutting edge profiles corresponding to each part of the edge is illustrated.

The developed method facilitates the modeling of various cutting edge microgeometries. Having the profile of the cutting edge at different positions along the edge, enables the edge geometric evaluations of the prepared cutting

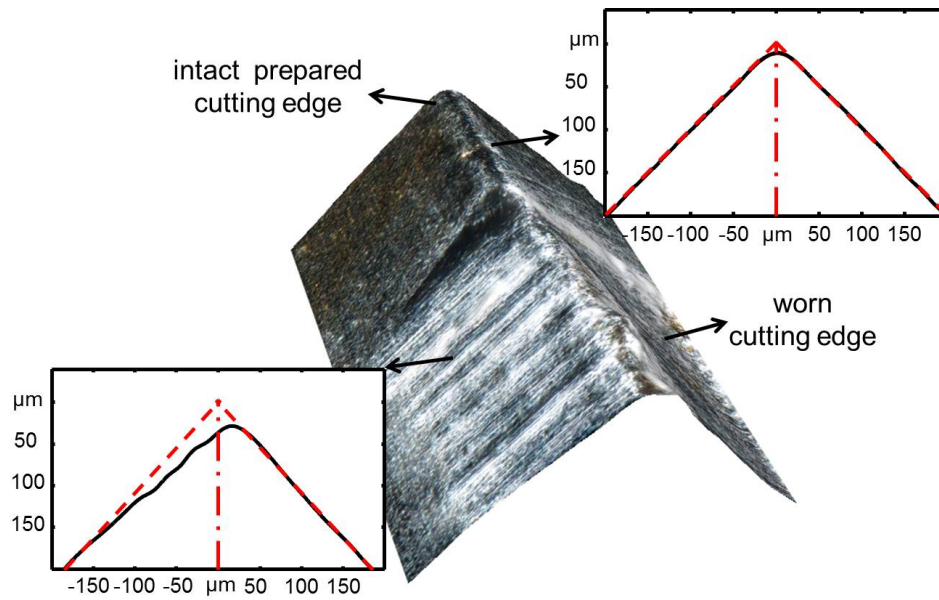


Figure 2.3: 3D cutting edge model of the developed measurement methodology and two cutting edge profiles

tools. If the edge profile is circular and symmetric, cutting edge radius is computed by circular regression [56] through all the points lying on the cutting edge, Fig. 2.4. Circular regression finds the circle that best fits a profile. The radius of such circle is the cutting edge radius. If it is asymmetric, it can be characterized by a comprehensive methodology for cutting edge characterization of various geometries in Chapter 5. If it is a worn edge, tool flank wear as well as other geometric features of a worn edge like built up edge can be analyzed.

2.2.3 Advantages of Optical Measurement Method and Profile Validation

The optical measurement method explained offers a number of advantages over other conventional measurement methods. The most important feature of

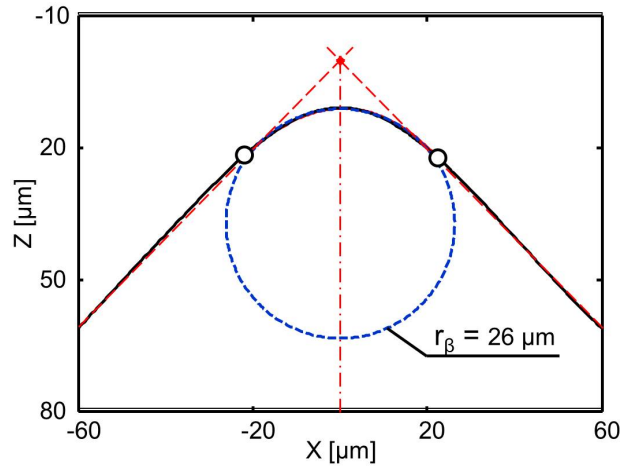


Figure 2.4: Circular regression applied on a cross-section of the cutting edge model

this technique is that it provides high resolution 3D model of the edge, enabling detailed edge studies, like cutting edge microgeometry, geometric uniformity along the cutting edge or tool wear. In contrast to the SEM method, it does not need any sample preparation. Edge orientation will not affect the measurement results. This is in contrast to SEM, profilometer and AFM methods. Even with white light interferometer, edge orientation has an unfavourable effect on fringe constitution. There are also microscopes with Z-resolutions as low as 10 nm facilitating finer edge measurements. The method can be used to investigate curvilinear edges and nose sections of a cutting edge with no limitation. It should only be noted that, uniform lighting is crucial for measurement by this method.

The uncertainty of the measurement method was computed against potential sources of uncertainty including lighting intensity, lighting angle, field of view, image taking gain, lens exposure and finally the image z-distance. A symmetrically honed cutting edge with a nominal edge radius of $50 \mu\text{m}$ was

measured repeatedly while varying these measurement parameters. Edge radius variation was computed to be less than 3 % ($1.5 \mu\text{m}$) which designates the high repeatability of the proposed approach.

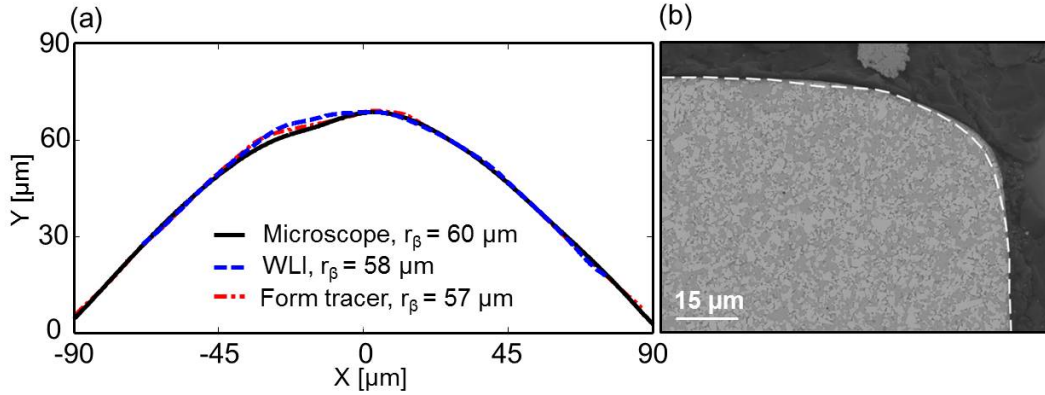


Figure 2.5: Verification of the developed measurement technique by other conventional methods

In addition, in order to verify the validity of optical measurement technique profiles of several commercial cutting edges were measured by optical microscope, profilometer and a white light interferometer. To ensure the measurement of a particular profile the middle part of the cutting edge was measured by all methods. Fig. 2.5a shows a profile of a symmetrically honed insert with a nominal edge radius of $60 \mu\text{m}$. There was only a maximum of 5% difference in edge radius value measured by optical method compared to those of form tracer and WLI.

For further verification a carbide insert was first modeled using the optical technique presented. Later the same edge was sectioned by EDM and carefully mounted with sacrificial pieces and edge retention powders in an epoxy resin to preserve the edge shape during the grinding and polishing process. The surface of the sample was later gold coated to provide the required conductivity for an SEM imaging. The maximum deviation of the asymmetric profiles shown

in Fig. 2.5b was measured to be less than $2 \mu m$.

The comparison of the profiles acquired by the methodology explained in this chapter with the profiles obtained with other measurement techniques verifies the accuracy of the developed edge modeling technique. The presented methodology is therefore used in this thesis for cutting edge geometric evaluations.

Chapter 3

Electro-erosion edge honing of cutting tools

This chapter is a copy of a paper published in CIRP Journal of Manufacturing Technology. It presents the key idea of the developed edge preparation technique. In this part of the research electro erosion edge honing is applied to symmetrically honed high speed steel (HSS) cutting tools. HSS is a steel alloy, rendering it the easiest tool material to be processed by EDM as compared to cemented carbide, CBN or PCD tool materials, all being metal matrix composites. Honing process is also applied to the simplest cutting tool macrogeometry at this stage of process implementation as cutting tools are straight edge SNE inserts with zero clearance angle. The electro-erosion edge honing process is shown to successfully create consistent edge geometry along a single cutting edge as well as between inserts. The life of the honed inserts is enhanced 400% compared to unprepared sharp ground tools.

Authors: N.Z. Yussefian, P. Koshy, S. Buchholz, F. Klocke

CIRP Annals – Manufacturing Technology 59, (2010), 215 - 218

Abstract

Sink EDM of fine features necessitates the application of several tool electrodes to sequentially generate the required geometry, due to the inevitable localized wear of the tool that rapidly rounds-off sharp edges. Be that as it may, this phenomenon can be exploited to hone sharp edges of electrically conducting cutting tools by sinking the cutting edge into an appropriate counterface material. This paper presents the proof-of-concept and operating characteristics of this innovative process. Robust edge geometry generation, and a significant improvement in the life of high speed steel tools consequent to such preparation of the cutting edge are demonstrated.

3.1 Introduction

Edge finishing is of critical importance in the function and performance of many engineering components: cutting tools in particular. Depending on the application, the edges of tools used in machining operations typically involve a chamfer and/or a hone, on the order of several μm . The meso-geometry of the cutting edge has a profound influence on the mechanics of chip formation, with important implications on the integrity of the generated surface. The primary motivations for edge preparation are however to enhance the edge strength towards precluding the incidence of catastrophic tool failure, to improve tool life and coatability, and to ensure consistent tool performance.

Bouzakis et al. [1] showed that an increase in the edge radius of coated cemented carbide inserts from 8 to 35 μm decreased the maximum mechanical stress in the cutting edge, in a milling application. This was found to translate favourably into a delayed onset of coating fracture and a four-fold enhancement

in tool life. Similar results were obtained by Rech et al. [2] in dry gear hobbing when using coated high speed steel (HSS) tools. Their work further indicated the existence of an optimum edge radius value that corresponds to the maximum tool life. Klocke and Kratz [3] demonstrated that it is feasible to forestall catastrophic failure of polycrystalline cubic boron nitride tools in hard turning applications, by a systematic variation of the edge geometry along the cutting edge profile. Karpuschewski et al. [4] recently reported that honing the cutting edges of HSS twist drills diminished the occurrence of edge chipping by a factor of three, while enhancing drill life by about 100%.

As attested to above, the significance of edge preparation in the performance of cutting tools in reference to diverse tool materials and machining processes cannot indeed be overemphasized. Accordingly, several edge preparation technologies have been developed [5], the most common of which are brush honing and micro-blasting. Brush honing involves material removal using a tool with synthetic bristles impregnated with abrasive grits, wherein the hone geometry is controlled essentially by the level of engagement of the cutting edge with the brush and the processing time. Micro-blasting entails the erosive effect of fine abrasive particles entrained in a pressurized air stream; alternatively, a viscous or granular media may be involved.

An issue with the aforementioned processes is the significant inherent variability [6] in the geometry of the generated hone, not just between cutting edges but also along the same edge. Further to problems with process control, mechanical edge preparation methods are somewhat limited in terms of their application to tool materials such as polycrystalline diamond on account of their extreme hardness. In this context, the research detailed in this paper presents the proof-of-principle of the novel application of electrical spark discharges for precision, non-contact edge preparation of cutting tools.

3.2 Process concept

It is a well-known issue in sink electrical discharge machining (EDM) that machining of intricate geometries with sharp features requires the application of several electrodes to successively confer the required geometry, due to deterioration of the tool shape, which generally manifests as rounding of sharp edges [7]. Be as it may a problem in EDM, this phenomenon can be exploited to generate controlled edge radii on cutting tools, by sinking the sharp cutting edge into an appropriate counterface material. This concept represents an innovative perspective that expands the application envelope and capability of EDM in the area of cutting tool manufacture. In light of the variability inherent to conventional edge finishing technologies, the general high level of precision associated with EDM processes would be advantageous in terms of generating consistent hone geometry, as demonstrated later. Furthermore, as the mechanism of material removal is melting and vaporization as opposed to abrasion, material removal is not influenced or limited by the hardness of the tool material; it just needs to possess the requisite electrical conductivity.

Systematic research into tool shape evolution in EDM was conducted by Crookall and Fereday [8] who invoked the concept of relative duty to elucidate the phenomenon of rapid shape degeneration of sharp corners. This notion considers that the macroscopic relative erosion rate observed between the tool and the work holds also at the micro-scale, across the spark gap. This implies that regions with a curvature in an electrode would entail a greater rate of recession, in comparison to linear segments. In addition to the geometric effect above, the accumulation of heat in the edge would further accentuate the effect of relative duty, especially in micro-EDM applications, when employing materials with poor thermal properties [9].

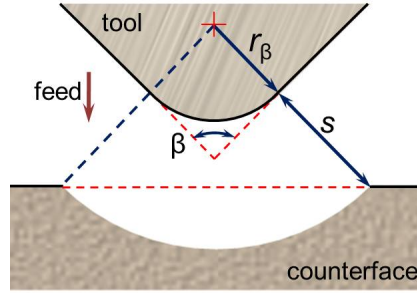


Figure 3.1: Schematic representation of electro-erosion edge honing.

Fig. 3.1 shows the schematic of an edge that was sharp (with a radius approaching zero) at the outset being sunk into an initially flat (referring to an infinite radius) counterface. This geometry corresponds to an extreme relative duty, and the sharp edge would hence degenerate virtually instantaneously; thereafter, the increase in curvature would progress at a rate consistent with the disparity in the relative duty between the electrodes. For unit thickness into the plane of Fig. 3.1, for the included angle $\beta = 90^\circ$, the volume of material V_t that has to be removed from the tool in order to generate a hone of radius r_β can be calculated as:

$$V_t = r_\beta^2 \left(1 - \frac{\pi}{4}\right) \quad (3.1)$$

For a given material removal rate, a higher included angle corresponds to a lower machining time to attain the same edge radius [8]. Neglecting the roughness of the surface, for nominal in-feed of the tool into the counterface, the volume V_c of material that is to be removed from the counterface to generate a honed edge of radius r_β is determined by the working gap width s , such that a radius $(r_\beta + s)$ is generated on the counterface, and is given by:

$$V_c = (r_\beta + s)^2 \left(\frac{\pi}{4} - \frac{1}{2}\right) \quad (3.2)$$

When using sink EDM to generate edge hones, there are several possibilities in terms of kinematic motions between the tool edge and the counterface. For

instance, asymmetric hones (e.g. waterfall hones) can be generated by tilting the edge relative to the feed axis in the plane of Fig. 3.1. The edge can be inclined also along the cutting edge (into the plane of Fig. 3.1) to induce a variation in edge radius, appropriate for machining applications wherein the uncut chip thickness varies along the cutting edge.

3.3 Experimental

As a first work, the kinematic employed in the present work refers to symmetric sinking of the tool edge on to a flat counterface as shown in Fig. 3.1. The objectives of the experimental work were to: (i) prove the concept of using electrical spark discharges for honing the edges of cutting inserts, (ii) investigate the shape evolution of the cutting edge geometry with reference to counterface material, machining time and pulse parameters, (iii) assess the effectiveness of edge hones generated using spark discharges by conducting tool life tests, and (iv) quantify the variability in edge geometry both along and between edges.

An important component of this work was the measurement of the cutting edge radius, which was accomplished using a confocal microscope. Cubic non-uniform rational B-spline (NURBS) surface models were fit to the point cloud data obtained using the confocal microscope, with 30x30 control points, chord length parameterization and knot vector. This measurement technique was verified by a tactile form tracer and a white light interferometer. The uncertainty in edge radius measurement was estimated to be less than 1 μm .

Experiments primarily involved finish-ground, uncoated AISI T-15 grade HSS inserts of specification SNEA 320 (included angle $\beta = 90^\circ$, edge length 10 mm) with sharp edges; limited results relate to C-2 grade uncoated cemented

carbide. Edges were electro-erosion honed using a solid state power supply, in an oil-based dielectric fluid, with no external flushing, at constant servo sensitivity. The baseline process parameters were: positive polarity on aluminum counterface, open circuit voltage $U_o = 100$ V, working voltage $U = 80$ V, on-time $t_i = 0.6$ μ s, duty factor $\tau = 0.5$, peak current $i_e = 1.8$ A, and machining *time* = 80 s, unless stated otherwise. These parameters were selected on the basis of extensive preliminary experiments, for the electro-erosion honing cycle time to be comparable to conventional processes, when employing conservative pulse parameters that relate to the micro-EDM regime, in the interest of maintaining the integrity of the functional surface generated.

3.4 Results and discussion

Figs. 3.2a and 2b show NURBS representations of HSS cutting edges along with aluminum and copper counterfaces, respectively, with the gap between them expanded for clarity. The corresponding wear ratios ν (ratio of the volumetric material removal from the cutting edge to that from the counterface) were calculated to be 0.5 and 7.5. While the edge prepared using the aluminium counterface is rounded (machining time 120 s, edge radius 40 μ m), use of a copper counterface results in an edge that entails a flat land. The figure highlights the critical influence of the counterface material and hence the wear ratio on the meso-geometry generated on the cutting edge, and the flexibility the process offers in terms of generating both hones and chamfers.

When a sharp edge is sunk into a counterface, for uniform debris distribution in gap space, successive spark discharges can be considered to occur at locations that relate to the closest distance between them, which results in

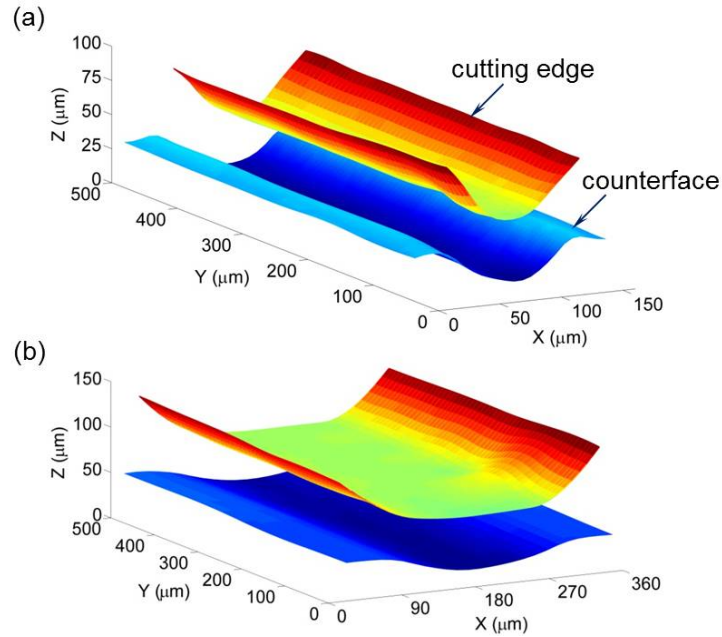


Figure 3.2: Effect of counterface material on edge geometry: (a) aluminum, (b) copper.

the shifting of the discharge location in the working gap. For a tool and counterface shown in Fig. 3.1, the generation of the rounded edge geometry can be visualised as the outcome of the intrinsic radial movement of the discharge location in the annular working gap of width s , about the center of the arc generated in the tool. It is interesting to note that such radial excursion of the discharge location obviates the need for any elaborate relative kinematics between the tool and the counterface to generate the rounded edge.

To realise such a radial movement of the discharge location, it is essential that a minimum volume of material, as determined by the instantaneous edge radius r_β and gap width s is removed from the counterface, which does correspond to a threshold wear ratio. For limited in-feed of the cutting edge into the counterface as portrayed in Fig. 3.1, an approximate limiting wear ratio can be calculated by way of eqns. 3.1 and 3.2. For wear ratios higher than the

limiting value, a chamfer rather than a hone will be generated. For parameters corresponding to Fig. 3.2a ($r_\beta = 40 \mu\text{m}$, $s = 15 \mu\text{m}$) the limiting wear ratio as given by eqns. 3.1 and 3.2 works out to 0.4, which explains the generation of the chamfer rather than a hone when a copper counterface (wear ratio of 7.5) is used (Fig. 3.2b). Lower wear ratios, on the other hand, lead to significant in-feed of the cutting edge into the counterface.

In addition to the simple model above, a numerical geometric simulation [10] was accomplished in the present work to understand shape generation in the spark erosion edge preparation process, by systematically varying the wear ratio over a wide range. Typical simulated tool edge profiles for different wear ratios are shown in Fig. 3.3, for a gap width of $15 \mu\text{m}$. The shape of the simulated profiles clearly indicates the progressive graduation of the edge shape from a hone to a chamfer, with an increase in the wear ratio. The profiles shown for wear ratios of 0.5 and 7.5 can further be seen to concur qualitatively with the shape of the profiles shown in Figs. 3.2a and 2b, respectively, which refer to these ratios experimentally. Results presented henceforth refer to the application of an aluminum counterface.

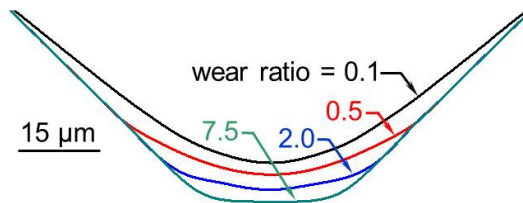


Figure 3.3: Simulated effect of wear ratio on edge geometry.

Figs. 3.4a and 4c are scanning electron micrographs of unprepared (ground) and electro-erosion honed HSS cutting edges. A topography that is characteristic of EDM surfaces can be seen along the cutting edge in Fig. 3.4c. Figs. 3.4b and 4d refer to cemented carbide edges; the honed surface on the carbide edge

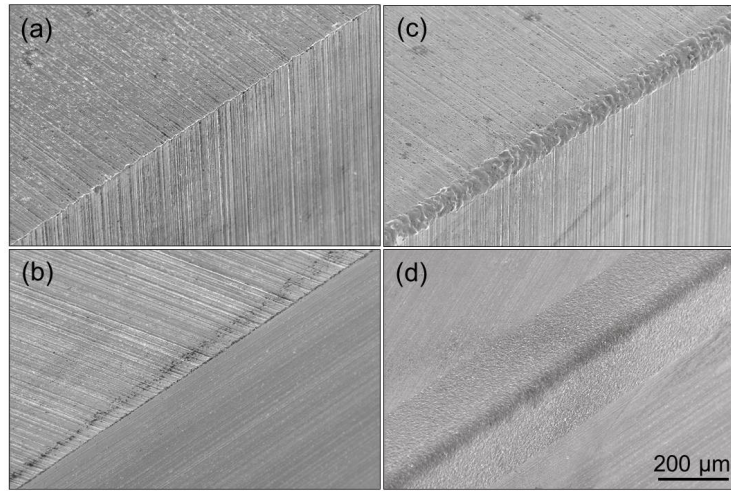


Figure 3.4: Micrographs of: (a) HSS and (b) cemented carbide ground (sharp) edges; (c) and (d) are the corresponding electro-erosion honed edges.

can be seen to be smoother, in comparison to the corresponding HSS edge. Micro-chipping along the cutting edge was present in both unprepared HSS and carbide inserts. It can be observed that while the hone is localized along the edge in the case of the HSS insert (Fig. 3.4c), the EDM surface extends appreciably further into the rake and clearance faces in the case of the carbide insert (Fig. 3.4d). This is due to the very low wear ratio (~ 0.01) pertaining, which results in substantial in-feed of the carbide edge into the aluminum counterface. It may be noted that the extraneous material removal on the lateral faces of the tool due to the incursion of the spark discharges away from the tool edge can be observed also on the simulated edge profiles in Fig. 3.3, for the relatively low wear ratio of 0.1.

Fig. 3.5 shows primary traces of typical HSS cutting edges obtained using a profilometer with a stylus of tip radius $5 \mu\text{m}$, at various machining times to indicate the evolution of the edge geometry. Micro-chipping seen on the unprepared edge sustained from the preceding grinding operation essentially limits the minimum edge radius that can be generated at this section of the

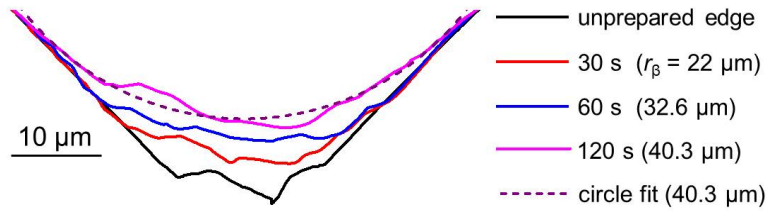


Figure 3.5: Profilometer traces of HSS edges showing their evolution.

edge. The geometry of honed edges was found to be best approximated as circular arcs [8], the radii of which were estimated by circular regression. The figure shows the fit circle for one of the profiles; the maximum absolute radial deviation of the actual shape with respect to the corresponding fit circles for the profiles shown was less than 5% of the edge radius. It is evident from the figure that the rate of increase in the edge radius diminishes with time, which is consistent with the progressive reduction in relative duty. It is instructive to note that the cycle times for electro-erosion honing are comparable to conventional edge preparation processes, and that the relatively low material removal rate of sink EDM is largely inconsequential in this process, as the volume of material that is to be removed from the ground edge to generate the hone is minimal.

The mechanisms of material removal and energy transfer in micro-EDM (pulse energy $< 100\mu\text{J}$) are currently not well understood [9]. As indicated before, the pulse energy in the present work ($85\mu\text{J}$) was determined in consideration of the removal rate and the surface integrity. Experiments with tool positive polarity related to a higher rate of hone radius generation, in line with the favorable energy distribution at the anode; however, this resulted in significant edge hone variability along the cutting edge, and hence a tool negative polarity was adopted. The effect of working voltage and flushing were

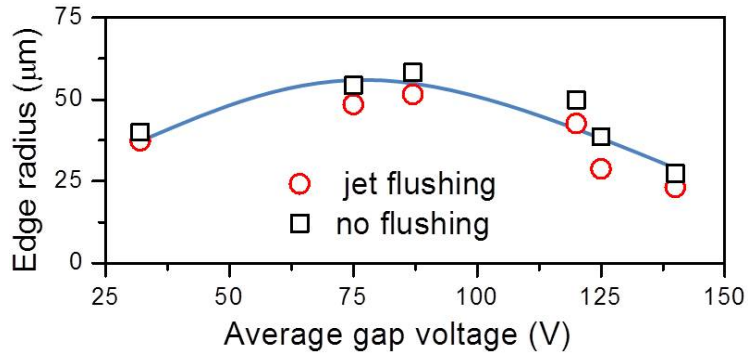


Figure 3.6: Effect of gap voltage and flushing on edge radius.

investigated (Fig. 3.6) at an open circuit voltage of 150 V. The optimum working voltage is a consequence of the reduction in the actual pulse energy due to an increase in the ignition time delay associated with larger gap widths at higher gap voltages. External jet flushing somewhat reduced the radius values conceivably due to induced discharge instability.

The efficacy of electro-erosion honed HSS edges was evaluated in terms of tool life when cutting annealed AISI 1045 steel, which was assessed using a variable speed test [11] in a facing operation (0.15 mm feed, 0.5 mm depth of cut), for a tool life criterion of 300 μm maximum flank wear. Fig. 3.7 shows the Taylor's tool life plots, which exemplifies a manifold enhancement in tool life, which is on an order similar to that realized elsewhere [1-4], through conventional edge honing processes. It is intriguing that the rather low volume of material removal involved in electro-erosion honing allows for the use of conservative spark energy levels, with no adverse affect on the cycle time. The tool life results affirm the observation in [12] that finish-EDM processes can be engaged to generate critical tooling surfaces with no functional detriment.

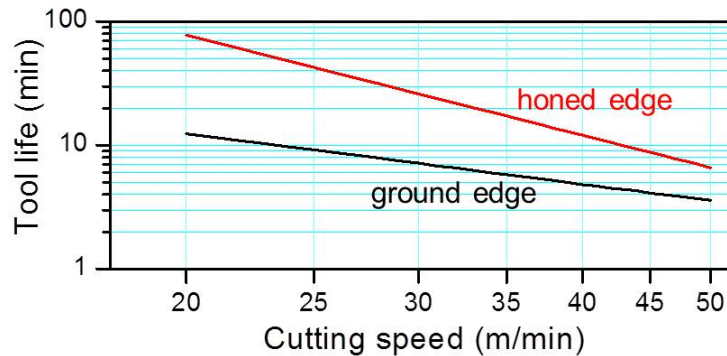


Figure 3.7: Effect of edge preparation on tool life.

As alluded to previously, an issue with conventional edge honing technologies is the variability in the edge geometry. Schimmel et al. [6] characterized the edge geometry of commercially procured inserts and reported that the measured radii deviated from the specified nominal value by as much as 43%, along the same cutting edge as well as between inserts. In fact, such significant variability is indicative of the reason that most manufacturers specify hones in rather wide ranges of radius values. In order to characterize the variability in electro-erosion honing, 140 edge radius measurements were taken along a single HSS edge over a length of 10 mm, which indicated the mean and standard deviation to be $32.1 \mu\text{m}$ and just $1.6 \mu\text{m}$, respectively. It should be noted that the parallelism of the tool edge with respect to the counterface (into the plane of Fig. 3.1) is critical in terms of the edge radius repeatability along the edge. The variability between edges was also assessed, the results of which are presented in Fig. 3.8 as a standard Box plot (box and whisker refer to the 25/75 and 1/99 percentiles, respectively), which substantiates the relatively good repeatability of the electro-erosion edge honing process, which is to be expected of controlled EDM processes.

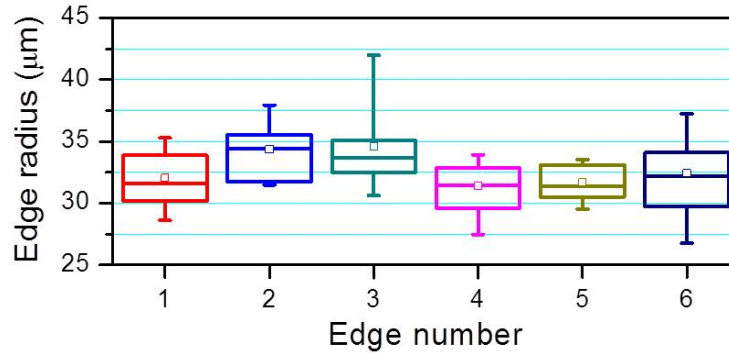


Figure 3.8: Box plot showing edge radius variability between edges.

3.5 Conclusions

The proof-of-concept of the novel process of using electrical spark discharges for the edge preparation of cutting tools in generating both hones as well as chamfers has been established. The counterface material (and hence the wear ratio) has been identified to be critical in terms of the edge geometry. Edge hones generated using electrical discharges have been shown to correspond to a manifold increase in tool life, in comparison to ground edges. The variability in the geometry of edges generated has been found to be minimal, when compared to values reported for conventionally prepared edges, for both along a single cutting edge as well as between edges. Further work will focus on electro-erosion honing of composite tool materials, particularly polycrystalline diamond that has an electrically non-conducting phase.

3.6 Acknowledgements

This work was funded by the AUTO21 Canadian Network of Centers of Excellence and the C4 Consortium of Ontario.

References

- [1] Bouzakis KD, et al, (2002) Effect of the Cutting Edge Radius and Its Manufacturing Procedure on the Milling Performance of PVD Coated Cemented Carbide Inserts. *CIRP Annals* 51(1):61-64.
- [2] Rech J, et al, (2005) Influence of Cutting Edge Radius on the Wear Resistance of PM-HSS Milling Inserts. *Wear* 259:1168-1176.
- [3] Klocke F, Kratz H (2005) Advanced Tool Edge Geometry for High Precision Hard Turning. *CIRP Annals* 54(1):47-50.
- [4] Karpuschewski B, Byelyayev O, Maiboroda VS (2009) Magneto-abrasive Machining for the Mechanical Preparation of High-Speed Steel Twist Drills. *CIRP Annals* 58(1):295-298.
- [5] Gillespie LK (1999) *Deburring and Edge Finishing Handbook*. Society of Manufacturing Engineers, Dearborn.
- [6] Schimmel RJ, Manjunathiah J, Endres WJ (2000) Edge Radius Variability and Force Measurement Considerations. *Journal of Manufacturing Science and Engineering* 122:590-593.
- [7] Mohri N, Suzuki M, Furuya M, Saito N (1995) Electrode Wear Process in Electrical Discharge Machining. *CIRP Annals* 44(1):165-168.
- [8] Crookall JR, Fereday RJ (1973) An Experimental Determination of the Degeneration of Tool-Electrode Shape in Electro-Discharge Machining. *Microtecnic* 17:197-200.
- [9] Tsai YY, Masuzawa T (2004) An Index to Evaluate the Wear Resistance of the Electrode in Micro-EDM. *Journal of Materials Processing Technology* 149:304-309.
- [10] Kunieda M, Kowaguchi W, Takita T (1999) Reverse Simulation of Die-sinking EDM. *CIRP Annals* 48(1):115-118.

[11] Armarego EJA, Brown RH (1969) *The Machining of Metals*. Prentice Hall, Englewood Cliffs.

[12] Yen YC, Jain A, Altan T (2004) A Finite Element Analysis of Orthogonal Machining Using Different Tool Edge Geometries. *Journal of Materials Processing Technology* 146:72-81.

[13] Lauwers B, Kruth JP, Eeraerts W (2005) Wear Behavior and Tool Life of Wire EDM-ed and Ground Carbide Punches. *CIRP Annals* 54(1):163-166.

Chapter 4

Application of foil electrodes for electro-erosion edge honing of complex-shaped carbide inserts

This chapter is a reproduction of a paper published in the Journal of Materials Processing Technology. Electro-erosion edge honing process was applied to straight edge HSS inserts in the previous chapter. In this chapter the application envelope of electro-erosion edge honing is expanded to prepare carbide cutting tools being the most common cutting tool material. EE-honing is also modified to be able to prepare complex geometry tools by using the idea of foil counterfaces.

Authors: N.Z. Yussefian, P. Koshy

Journal of Materials Processing Technology (2012)

<http://dx.doi.org/10.1016/j.jmatprotec.2012.09.022>

Date of Submission : 1 March 2012

Abstract

Electro-erosion honing is a novel process that exploits the undesirable but inevitable phenomenon of localized electrode wear in sink electrical discharge machining that rapidly rounds off sharp edges, for the edge honing of cutting tools. The process essentially entails the sinking of a sharp edge of a cutting tool into a counterface of an appropriate material to generate the round edge geometry. This paper proposes the innovative application of a foil counterface, with a view to expanding the capability of this process in the honing of tools with such geometric features as nose radii and curved edges. Such a configuration involves no particular alignment requirements, and facilitates the simultaneous processing of a batch of inserts. In consideration of their industrial significance, the process is evaluated in the honing of cemented carbide inserts. The novel process is demonstrated to address the limitation of the conventional brush honing process in being capable of generating consistent edge geometry, while delivering comparable tool life.

4.1 Introduction

The critical importance of the cutting edge in machining can be appreciated by considering the fact that all components that comprise the machining system, however sophisticated they may be, would be rendered entirely ineffective, should the cutting edge cease to perform as intended. With a view to ensuring consistent tool performance, cutting edges are commonly prepared to correspond to an approximately round shape, of a radius of several tens of micrometers. In addition to this process enhancing edge strength towards

precluding catastrophic tool failure, extending tool life and improving coatability, it exerts a considerable influence on the mechanics of chip formation, with consequent implications on the integrity of the generated surface. Accordingly, techniques for the characterization as well as the preparation of the cutting edge are assuming great importance of late, especially in the machining of high-value components.

Brush honing and micro-blasting are two common techniques that are currently used for edge honing. The former relies on the abrasive action of fine grits dispersed in a brush, and the latter the erosive effect of grits transported in a pressurized air stream. The major issue with these techniques is the significant variability in the geometry of the generated edge (Denkena et al., 2010), which is manifest not just between inserts, but also along the edges of the same insert. For instance, the edge radius variability could be as high as 40% along the same edge (Endres and Kountanya, 2002) and up to 35% off the nominal value (Schimmel et al., 2000) which is the reason that manufacturers find it expedient to specify edge hones in classes that span a rather wide range of radius values. Recent work by Bassett et al. (2012) documented the transient nature of the brush honing process arising from the condition of the filaments in the brush. In their work, brush honing of 80 inserts to a target edge radius of $30 \pm 5 \mu\text{m}$ in the stable region corresponded to a standard deviation of 12%; however, only about 75% of the honed inserts were found to be within the specified limits, which underscored the need for appropriately adapting and optimizing the process.

Machining performance measures such as tool life and residual stresses in the machined surface exhibit optimal values with respect to edge radius, and hence a high variability in edge geometry is not acceptable, in the interest of securing a robust process output. Furthermore, tool performance can be

enhanced by a systematic variation in the edge geometry along the edge in applications such as hard cutting (Klocke and Kratz, 2005), and hence a capability for controlled fabrication of precise edge hones is desirable. In addition to the process control aspect above, conventional edge preparation techniques are also limited when preparing tools fabricated from materials of an extreme hardness such as polycrystalline diamond. These issues have led to the conception of alternative approaches to edge preparation, a brief review of which follows.

In consideration of the acute edge geometry variability inherent to conventional brush honing, Denkena et al. (2008) proposed the application of 5-axes brush honing technology for fabricating tailored tools of a controlled geometry along the edge. Karpuscheski et al. (2009) demonstrated a magneto-abrasive method that is reportedly capable of robust edge honing. The process was shown to enhance the stability of the cutting edges of high speed steel drills, which translated into improved wear behavior that yielded a two-fold increase in drill life. Aurich et al. (2011) recently reported on the use of a low-cost marking laser for the edge honing of cemented carbide inserts. In this process, layers of tool material in the cutting edge are sequentially ablated over several passes to fabricate hones of a specified radius. This method was shown to enhance tool life by more than 50% as compared to ground tools with sharp edges.

Yussefian et al. (2010) presented the proof-of-concept of a novel process called electro-erosion edge honing that employs electrical discharge machining (EDM) for the edge preparation of electrically conducting tools. The process was demonstrated to be capable of enhancing the life of high speed steel tools by as much as 4 times as that of ground edges, and of generating edges with less than 10% variability, which is minimal compared to conventional processes.

The present paper builds on the concept above, and proposes the innovative application of foil electrodes as a means of expanding the application envelope of electro-erosion edge honing towards the preparation of tools with a complex macro-geometry, such as those with nose radii and curved edges. In light of their industrial relevance, the process is evaluated in the honing of cemented carbide inserts, with reference to the variability in edge geometry, surface quality, tool life and processing time. The essential features of the electro-erosion edge honing process are presented in the next section, so as to lead into presenting the new developments.

4.2 Electro-erosion edge honing process

The electro-erosion edge honing process exploits the well-known issue of inevitable localized electrode wear in sink EDM (Crookall and Fereday, 1973) that rapidly and selectively rounds-off sharp edges (Fig. 4.1). The process represents an innovative approach in the extension of sink EDM into the domain of tool manufacture, noting that the limitations inherent to EDM are of little consequence in this case.

Firstly, the relatively low material removal rate of EDM is not of any detriment, as the volume of material that is to be removed to generate the edge hone is very minimal. The time required for the preparation of an edge is accordingly on the order of just several seconds, which is comparable to conventional processes. The low removal volume further allows for very conservative EDM parameters, which ensures that the integrity of the generated edge that is critical to its performance is not compromised. The excellent repeatability of controlled EDM processes is indeed an advantage in the generation of precise

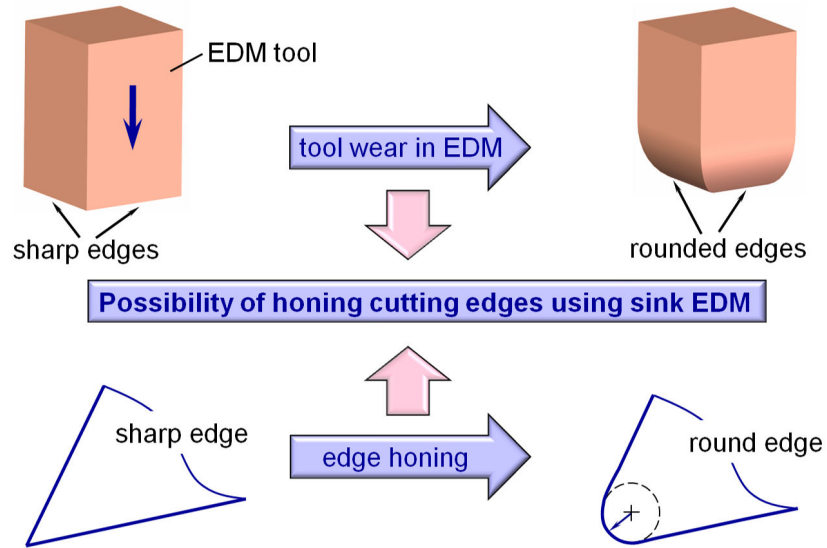


Figure 4.1: Principle of electro-erosion edge honing.

edge hones, which as indicated previously, is currently an issue with conventional edge preparation processes. Lastly, as EDM is a thermal process, it is not limited by the hardness of the tool material, which would enable the processing of even ultra-hard materials like polycrystalline diamond, provided the binder is metallic to render the composite to be of the requisite electrical conductivity.

4.2.1 Application of a foil counterface

The implementation of electro-erosion honing in its simplest form (Yussefian et al., 2010) entails the symmetric sinking of the cutting edge into a flat and thick counterface (Fig. 4.2a) under servo control in the presence of a dielectric fluid, so as to induce wear at the edge to generate a rounded shape.

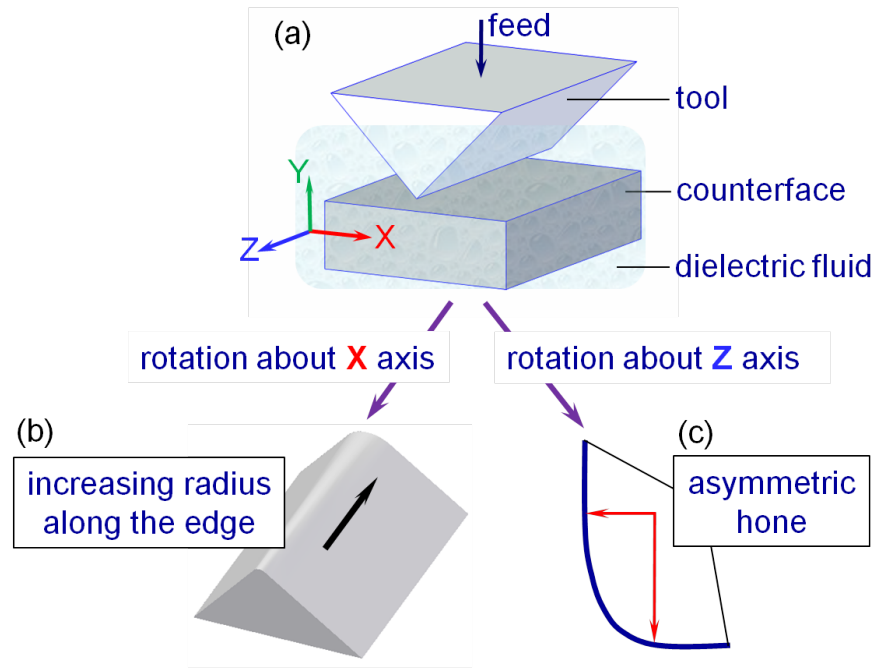


Figure 4.2: Kinematic configurations of electro-erosion edge honing.

A variant of this kinematic involves the rotation of the edge about the X-axis (Fig. 4.2b) that corresponds to the generation of a variable edge radius along its length. Similarly, a rotation of the edge about the Z-axis (Fig. 4.2c) would result in an asymmetric hone, such as a waterfall hone. In spite of these prospects, alignment of the tool about the said axes is crucial, if the objective is to generate a symmetric hone that is uniform along the edge.

Furthermore, while the configuration shown in Fig. 4.2a is adequate for the preparation of inserts of a simple geometry such as SNEA-type with straight edges and a flat rake face, it is limited in the preparation of complex-shaped ones such as CCMT-type (Fig. 4.3), the geometry of which involves such features as a pronounced tool nose and curved cutting edges. When inserts such as of the latter type are sunk into the counterface, geometric variations along the profile of the cutting edge would manifest systematic trends in the edge

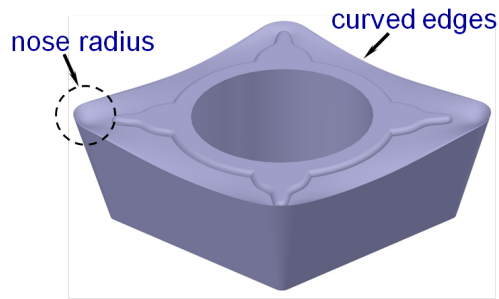


Figure 4.3: Example of a tool insert with a complex geometry.

radius (Fig. 4.4a), consistent with the differences in the processing time associated with individual segments that comprise the edge. One approach to solving this issue is to conceive a counterface of a shape that is complementary to the geometry of the edge profile; however, this is not an ideal solution, considering the additional effort associated with fabricating the counterface specific to the particular insert at hand, and having to precisely align it relative to the insert prior to the honing process.

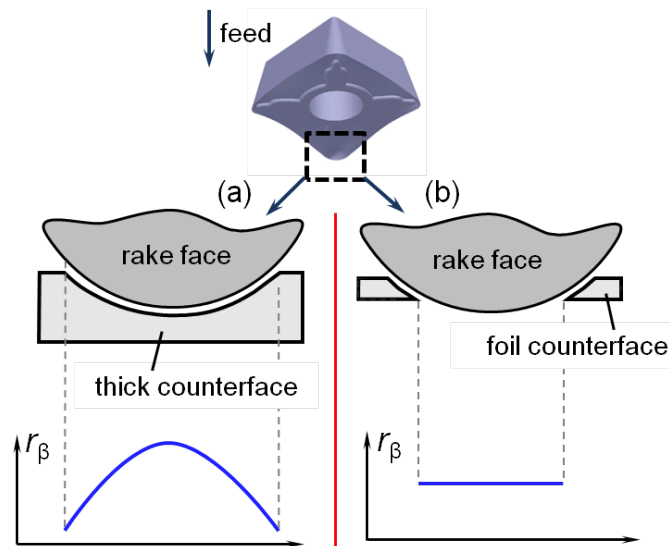


Figure 4.4: A comparison of the application of thick and foil counterfaces.

To this end, this paper presents a simple and elegant solution that employs a foil electrode as the counterface. In this case, the tool is sunk into and through the foil counterface under servo control (Fig. 4.4b), such that thermal erosion of the material from the tool leading to the generation of the hone is limited by the thickness of the foil. This ensures a uniform hone radius along the edge irrespective of the geometry of the tool profile. As the edge radius is controlled by the machining time, for a set of specified pulse parameters, edge hones of different radii can be generated by simply varying the thickness of the foil. Such a configuration further obviates the need for any alignment of the tool with respect to the counterface, and enables the simultaneous preparation of a batch of inserts, both of which are of much significance in insert manufacture.

4.2.2 Choice of counterface material, polarity and pulse parameters

In the electro-erosion edge honing process, the wear ratio ν that refers to the relative volume of material removed from the tool to that from the counterface, controls the meso-geometry of the edge in terms of it being a hone or a chamfer (Yussefian et al., 2010). An intriguing aspect of this process is that the rounded shape is generated by the radial excursion of the electrical discharges in the machining gap, which obviates the need for any elaborate relative motion between the tool and the counterface. The threshold wear ratio ν_t that corresponds to the generation of a circular edge can be obtained by considering a section of the tool and the counterface in the XY-plane in Fig. 4.2, as shown in Fig. 4.5. For an unit thickness of the tool, the volume of

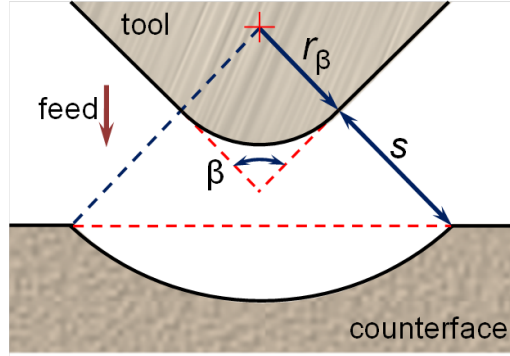


Figure 4.5: Concept and calculation of threshold wear ratio.

material removed from the tool V_t is given by:

$$V_t = r_\beta^2 \left[\cot \left(\frac{\beta}{2} \right) - \left(\frac{\pi - \beta}{2} \right) \right] \quad (4.1)$$

where r_β is the edge radius and β is the wedge angle of the tool. Similarly, the volume of material removed from the counterface is calculated as:

$$V_c = (r_\beta + s)^2 \left[\left(\frac{\pi - \beta}{2} \right) - \sin \left(\frac{\beta}{2} \right) \cos \left(\frac{\beta}{2} \right) \right] \quad (4.2)$$

where s is the inter-electrode gap width. The equations above enable the threshold wear ratio ν_t to be calculated as (V_t/V_c) . For typical values of edge radius and gap width on the order of $40 \mu\text{m}$ and $15 \mu\text{m}$, respectively, this simple geometric model specifies the target wear ratio that corresponds to a rounded edge to be around 0.4 (Fig. 4.6).

Measurement of wear ratios referring to several counterface materials under both polarities indicated a negatively polarized aluminum counterface to correspond to a wear ratio of 0.4 when machining cemented carbide. The sectional as well as three-dimensional views of an edge generated experimentally under this combination does indeed correspond to a well-rounded edge, as shown in Fig. 4.7a. Relative to this ideal case, Figs. 4.7b–7d depict the effect of the counterface material and the polarity in terms of the wear ratio

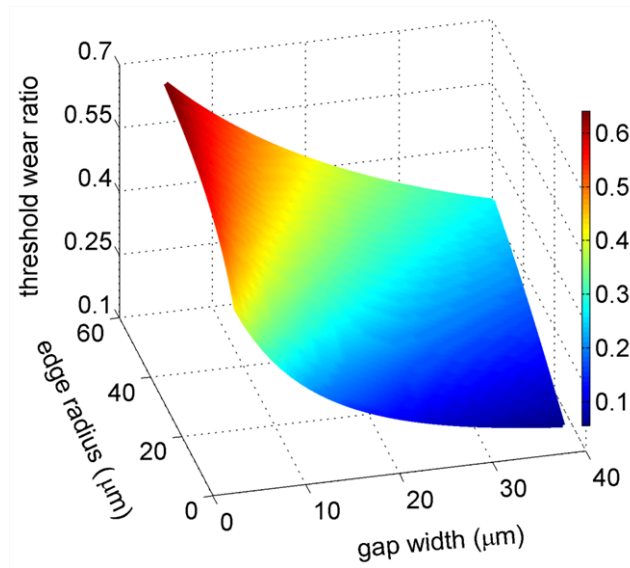


Figure 4.6: Threshold wear ratio for a wedge angle of 90° .

and the corresponding edge geometries. When using an aluminum counterface in positive polarity, the wear ratio reduces by an order of magnitude to 0.04, which refers to inadequate edge honing (Fig. 4.7b), on account of not enough material being removed off the tool.

Wear ratios much higher than the threshold value, on the other hand, result in the generation of a chamfer rather than a hone, as the discharges tend to traverse a linear rather than a radial path in the machining gap. This is precisely what was observed when using a copper counterface under negative polarity (Fig. 4.7c), for which the wear ratio was measured to be 5.0. Wear ratios smaller than the threshold refer to excessive in-feed of the tool into the counterface, which brings about an undesired incurrence of material removal on the rake and clearance faces, as opposed to localized removal just at the cutting edge. This situation was observed when using a copper counterface under positive polarity (Fig. 4.7d), which corresponded to a wear ratio of 0.15. A comparison of the four cases above clearly signifies the critical importance

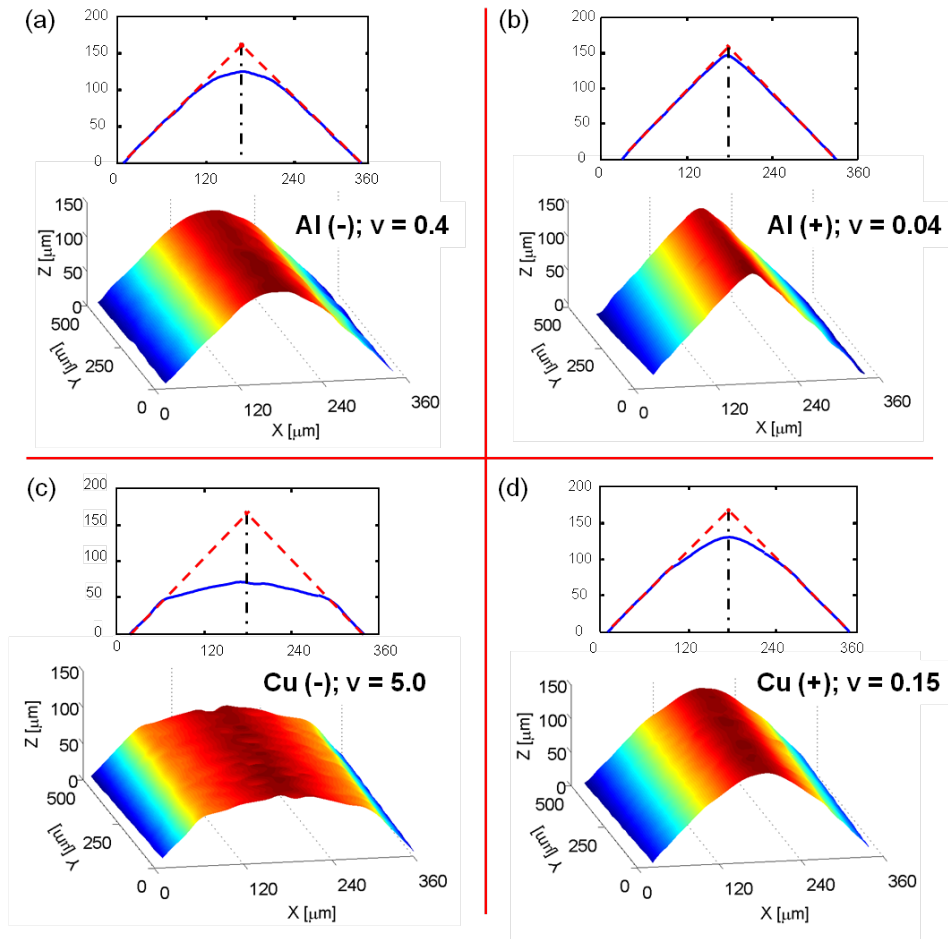


Figure 4.7: Effect of counterface material and polarity on edge geometry.

of the right combination of counterface material and polarity; a negatively polarized aluminum counterface that generates the desired honed was hence used in this work.

An appropriate selection of pulse parameters for the electro-erosion honing of cemented carbide tools needs to entail due consideration of the potential deleterious thermal effects (Jahan et al., 2011) on the performance of the generated surface, while maintaining the processing times to be comparable with those of conventional techniques. Previous work by Juhr et al. (2004) on

spark erosion of cemented carbides has identified the pulse on-time to be the dominant parameter that controls surface damage, with the recommendation that it be less than $0.5 \mu\text{s}$ for minimal strength degradation. Furthermore, the transverse rupture strength of cemented carbide machined by EDM has been reported (Lin et al., 2008) to exhibit a decreasing trend with respect to pulse current. A pulse on-time t_i of $0.4 \mu\text{s}$ and a pulse current i_e of 1.2 A , which happened to be the lowest possible values on the machine tool available in our laboratory, were hence used in the present work. The corresponding processing time will be shown later to be on the same order as that of the brush honing process.

As the boiling point of cobalt and the melting point of tungsten carbide are virtually the same, during EDM of tungsten carbide composite cemented by cobalt, tungsten carbide grains tend to get physically dislodged as individual units, once the cobalt binder around it is selectively removed. The implication of this occurrence is that the gap voltage (which controls the gap width) and the pulse off-time ought to be high enough to facilitate effective evacuation of the carbide grains off the machining gap, but for which the stability of the process will be affected adversely. Experiments conducted to investigate the effect of the average gap voltage on wear ratio revealed a rather weak sensitivity relative to the effects of counterface material and polarity, further indicating that the desired wear ratio of 0.4 referred to an average gap voltage of 50 V (Fig. 4.8). The process was further observed to be the most stable when the gap voltage was set at 50 V . A pulse off-time t_o of $1.12 \mu\text{s}$ (that refers to a duty factor of $\sim 35\%$) and a gap voltage of 50 V were hence selected, in consideration of the fact that higher values would affect the processing time and the surface integrity, respectively.

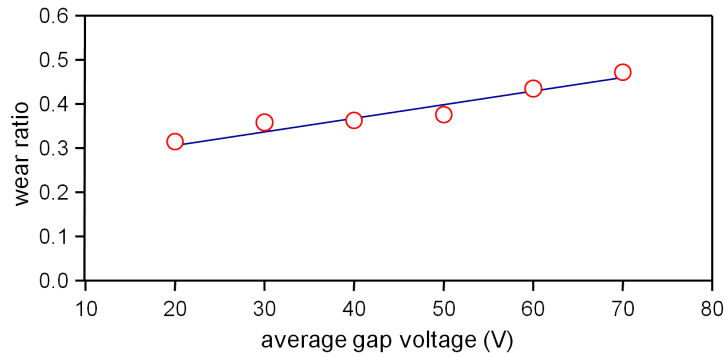


Figure 4.8: Effect of gap voltage on wear ratio (t_{on} $0.4 \mu s$, i_e $1.2 A$).

In terms of process design, the counterface material and polarity are chosen with reference to the wear ratio that corresponds to the desired edge geometry, and the pulse energy is limited in the interests of maintaining an appropriate surface integrity. Determination of the gap voltage and pulse off-time involve due consideration of process stability and processing time, and the edge radius is controlled by the thickness of the foil counterface.

4.3 Experimental

The objectives of the experimental work were two-fold: (i) to evaluate the capability of the electro-erosion honing process using a foil counterface in generating consistent edge geometry along nose radii and curved edges, and (ii) to quantify the tool life of cemented carbide inserts honed using this process, with a view to comparing them against those of brush-honed inserts of a similar edge radius. To this end, experiments involved uncoated pressed and sintered carbide inserts of CCMT geometry (see Fig. 4.3) and uncoated ground inserts of SNEA geometry, respectively.

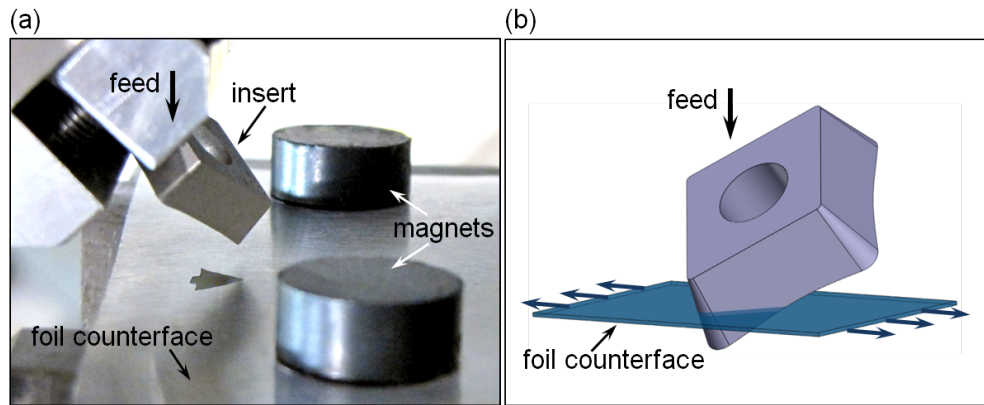


Figure 4.9: Experimental configuration for electro-erosion honing.

Experiments were conducted on a ram type EDM machine tool, in an oil-based dielectric under conditions of no external flushing, at a constant servo gain. Aluminum foil counterfaces of thickness ranging from 25–100 μm were used to generate edges with edge radius values in the range of about 30–50 μm . A photograph and a schematic of the experimental set-up are shown in Fig. 4.9a and 4.9b, respectively. The foil counterface was held taut using magnets to counteract their inherent compliance. An imprint from the edge honing operation can be seen on the counterface in Fig. 4.9a. The baseline machining parameters corresponded to values presented in the previous section as per the rationale indicated therein. To place the effect of the pulse parameters in perspective, experiments referring to a higher pulse on-time and gap voltage were also conducted. Some prepared edges were sectioned and polished to examine the geometry and integrity of the edge, and some were subject to accelerated tool life tests using a scheme outlined by Armarego and Brown (1969).

4.4 Results and Discussion

4.4.1 Edge geometry

Fig. 4.10a shows a micrograph of an electro-erosion honed edge of a pressed and sintered CCMT insert shown in Fig. 4.3. The excellent edge quality along the curved profile as seen in the inset in Fig. 4.10b is physical evidence to the efficacy of a foil electrode in being able to uniformly hone curved edges. Fig. 4.10c presents a comparison of the quality of the cutting edge between the honed and the unprepared sections of the edge. The segment of the edge left intentionally unprepared can be seen to sustain edge chipping as well as residual flash from the insert compaction process prior to sintering, at the location where the honing is terminated. Examination of the honed segment indicates electro-erosion honing to have effectively purged such detrimental features from the edge, which is a mechanism by which the honing process enhances both tool performance and reliability.

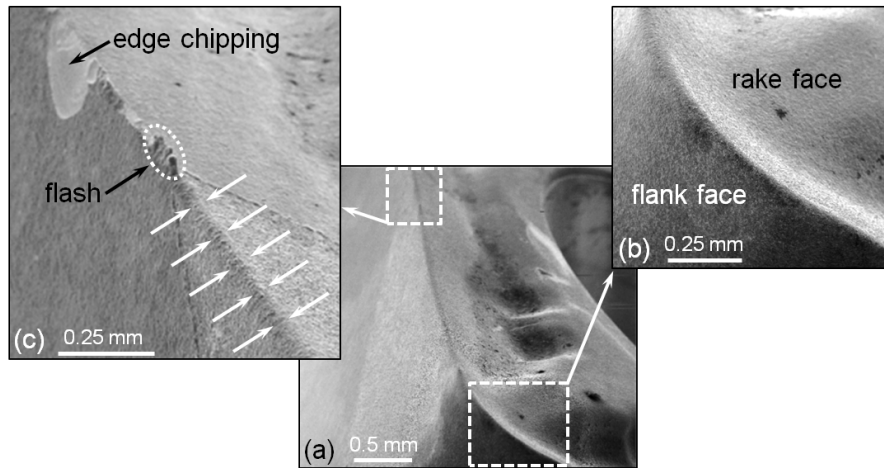


Figure 4.10: (a) Electro-erosion honed edge of CCMT insert, (b) honing quality along a curved edge, and (c) edge chipping and flash on the unprepared edge (white arrows indicate the honed segment).

Various geometric parameters have of late been proposed for the characterization of cutting edges (Wyen et al., 2012); in the present work, edge geometry was however quantified in terms of the edge radius considering that the honed edges were symmetric. Cutting edge measurements were conducted by processing the image data acquired using an optical microscope equipped with an automated stage to acquire a series of uniformly spaced images in the vertical direction. For the 30–50 μm range of edge radius values encountered in the present work, the field of view of the microscope was kept constant to be $450 \times 600 \mu\text{m}^2$ which corresponded to a XY (horizontal plane) resolution of 0.47 μm . The Z (vertical) resolution of the automatic stage was set to 1 μm . A B-spline surface was approximated through the point cloud data obtained using the microscope to reconstruct the cutting edge. This surface was then sectioned at 20 equally-spaced positions along the edge length of 450 μm to characterize the cutting edge using the cutting edge radius parameter r_β computed using circular regression. The uncertainty of this optical measurement method was investigated in consideration of variables such as the field of view, Z step height and lighting intensity. For a symmetrical cutting edge with an edge radius of 50 μm , this exercise indicated the measurement uncertainty to be 1.5 μm .

With a view to validating the optical measurement technique, Fig. 4.11a illustrates a comparison of symmetric edge profiles obtained using the optical microscope, white light interferometer (WLI) and form tracer, for an edge with a nominal edge radius r_β of 60 μm . The maximum deviation between the edge radius values measured using these devices was found to be 5%. Fig. 4.11b compares the profiles of a sharper asymmetric edge obtained using the optical microscope with that from subsequent physical sectioning and polishing of the edge at the same location. In this instance, the maximum deviation between

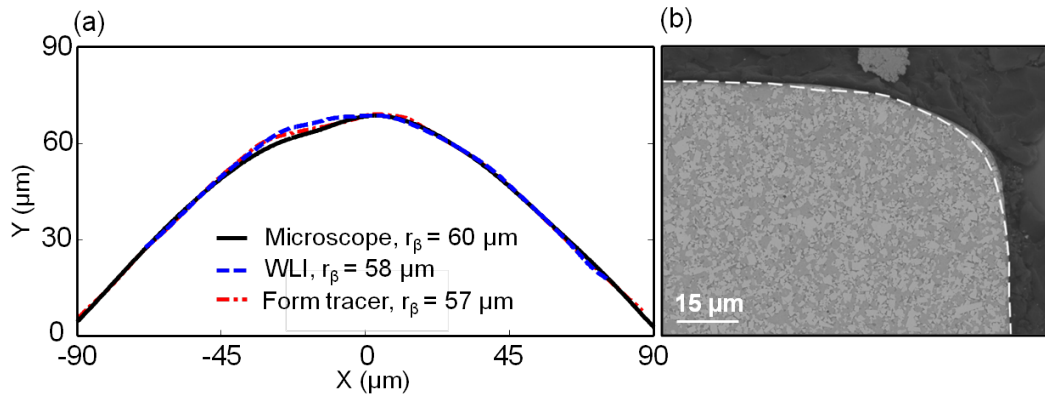


Figure 4.11: (a) Comparison of cutting edge profiles obtained by optical microscope, white light interferometer (WLI) and form tracer; (b) overlay of profile (broken white line) obtained using the microscope on a micrograph showing the section of the edge.

the two profiles was measured to be $2 \mu\text{m}$.

Fig. 4.12a displays the distribution of the edge radius measured using the said optical technique among 5 inserts that were chosen randomly, in the form of a Box plot. By convention, the boxes refer to the 25/75 percentile and the whiskers to the range. Each box contains 60 measurements along the cutting edge, corresponding to 20 edge measurements each taken $20 \mu\text{m}$ apart along the leading and trailing segments of the edge, as well as the tool nose region.

While the variability in the as-pressed and sintered inserts was 20%, electro-erosion honing reduced this to 13%, which is significantly smaller than the 35–40% measured on commercially retailed inserts (Endres and Kountanya, 2002; Schimmel et al., 2000). Such a process response attests to and is a consequence of the excellent repeatability of controlled EDM processes. Fig. 4.12b depicts the distribution of the edge radius along a single edge, at and on either side of the tool nose, which provides a quantitative measure of the consistency in edge geometry. The mean edge radius of the pressed and sintered CCMT insert was $12 \mu\text{m}$ with a 19% variation along the edge. Electro-erosion honing

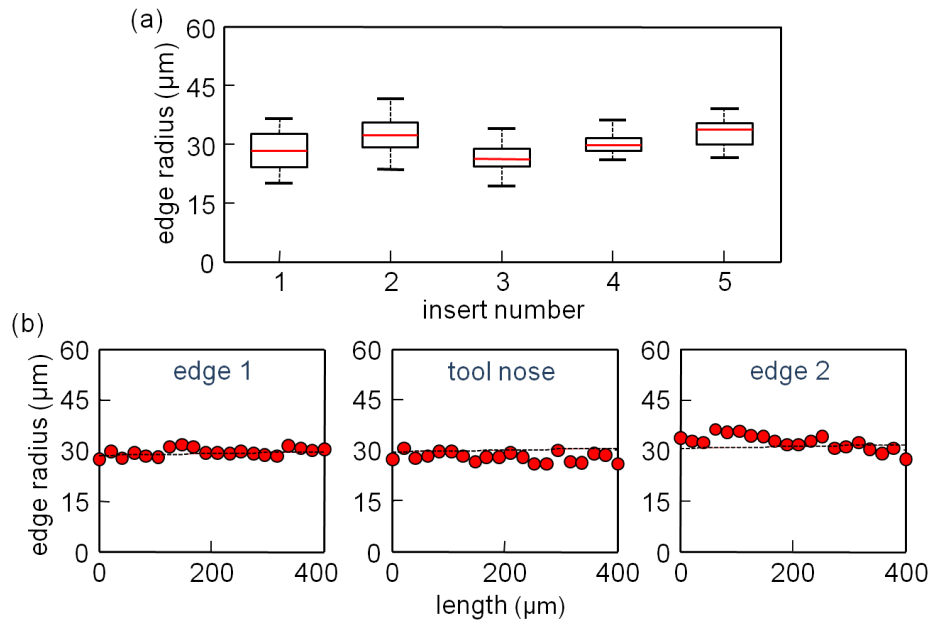


Figure 4.12: Variability in edge radius: (a) between inserts. (b) along the edge of a single insert.

of the insert to a target nominal edge radius of $30 \mu\text{m}$ reduced the variability along the edge to 13%.

Fig. 4.13a depicts the geometry, topography and cross-section of an electro-erosion honed insert. To place this in perspective, corresponding views of a brush honed insert (Fig.4.13b) and a ground insert (Fig.4.13c) are also provided. The prepared edges refer to a nominal edge radius of $40 \mu\text{m}$. The cross-sectional view of the electro-erosion honed insert confirms the efficacy of the proposed process in generating a symmetric, rounded edge. The surface roughness of the electro-erosion honed edge was measured to be $0.2 \mu\text{m } Ra$, which is similar in scale to the brush honed inserts ($0.14 \mu\text{m } Ra$). Aspects of a comparison of the performance of brush honed and electro-erosion honed inserts is discussed next.

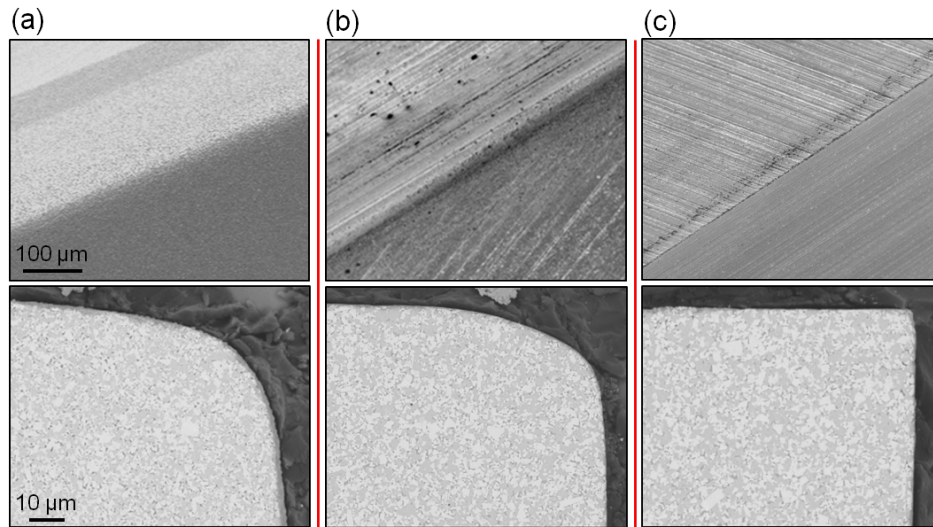


Figure 4.13: A comparison of edges: (a) electro-erosion honed, (b) brush honed, and (c) ground.

4.4.2 Surface integrity, tool life and processing time

In general, electrical discharge machined surfaces entail issues relating to recast material, micro-cracks and tensile residual stresses, as a consequence of the mechanism of material removal being primarily thermal in nature. In cemented carbides, this translates into a degradation in the flexural strength (Casas et al., 2006) and the tribological response (Bonny et al., 2009). In this light, the key to productive EDM of cemented carbides is the careful selection of machining parameter combinations and/or the adoption of strategies such as the application of successively finer machining regimes, in order to minimize the adverse effects without incurring an undue penalty on the machining rate. For instance, with the application of appropriate machining parameters, cemented carbide punches machined using wire-EDM have been shown (Lauwers et al., 2005) to be comparable to those that were finished by grinding, in terms

of wear behavior and tool life.

In the context above, the baseline EDM parameters in this work related to a pulse on-time t_i of $0.4 \mu\text{s}$, a discharge current i_e of 1.2 A , and a gap voltage U of 50 V , as detailed in section 4.2. With a view to placing these parameters in perspective, experiments were also conducted using a more aggressive set of parameters, which referred to an on-time t_i of $13 \mu\text{s}$ and a gap voltage U of 110 V , other conditions remaining the same. The latter set of parameters were derived from a complementary study involving a Taguchi design of experiments approach to minimize the deviation of the generated profile from that of an ideal circle. An evaluation of the corresponding surface integrity and tool life characteristics are presented in the following.

A comparison of the topography of the surface generated using the baseline set of parameters (Fig. 4.14a) with that of the more severe set (Fig. 4.14b) denotes the latter to correspond to a darker hue, conceivably due to the migration of carbon from the decomposition of the hydrocarbon dielectric during the honing process. These surfaces were of roughness $0.20 \mu\text{m } Ra$ and $0.23 \mu\text{m } Ra$, respectively. Closer examination of the surfaces (Figs. 4.14c and 14d) indicates the baseline parameters to correspond to a significantly reduced incidence of surface micro-cracking, in terms of both the number of cracks and their length. Similarly, the cross-sectional view (section X-X) referring to the baseline set (Fig. 4.14e) shows the surface to be relatively free of selective binder depletion and recast material, as compared to the latter (section Y-Y, Fig. 4.14f). A detailed investigation of the cross-section of the surface referring to the baseline set of parameters (Fig. 4.14g) provided further evidence towards the absence of recast material and cobalt depletion, while revealing sparsely dispersed micro-cracks, the depths of which were on the order of just $1 \mu\text{m}$; this is in stark contrast to the cross-section corresponding to the higher

pulse energy (Fig. 4.14h).

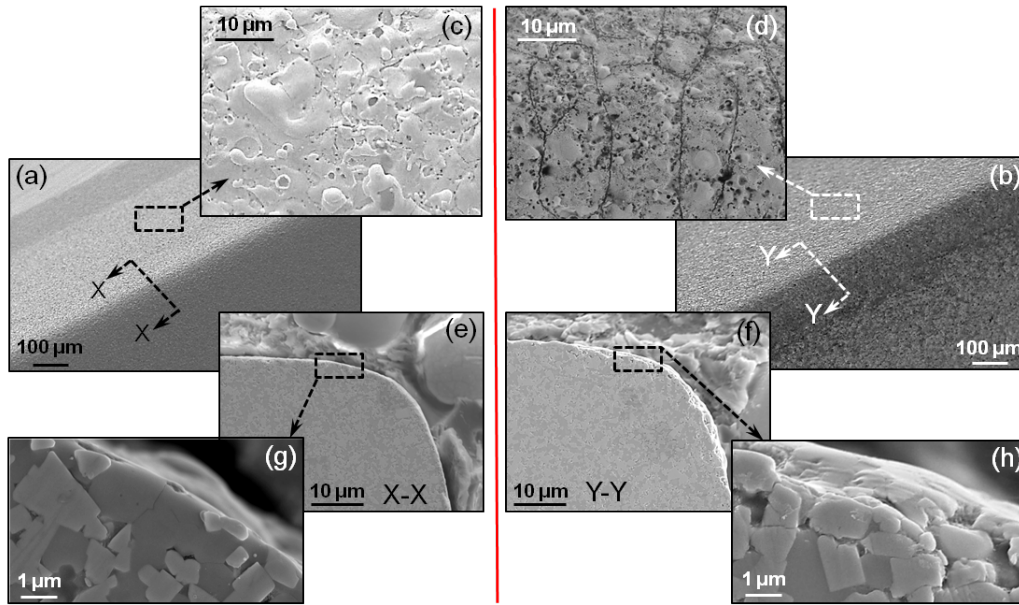


Figure 4.14: Effect of pulse parameters on the integrity of cemented carbide surfaces.

An interesting consequence of the application of EDM for edge honing is that the corresponding characteristic surface topography that entails a positive skewness may be deemed to be beneficial in the anchoring of a tool coating. It is also intriguing to note that a coating can concomitantly enhance the strength (Casas et al., 2004) and the tribological performance (Casas et al., 2008) of EDM-ed surfaces.

Considering that one of the primary motivations for edge honing is to obtain robust and enhanced tool performance in the first place, it is of interest to examine how the differences in surface integrity above translate into variations in tool life. It is further essential to benchmark the performance of electro-erosion edge honed tools against that of brush honed tools. A comparison of such tool life characteristics obtained using variable speed accelerated tests

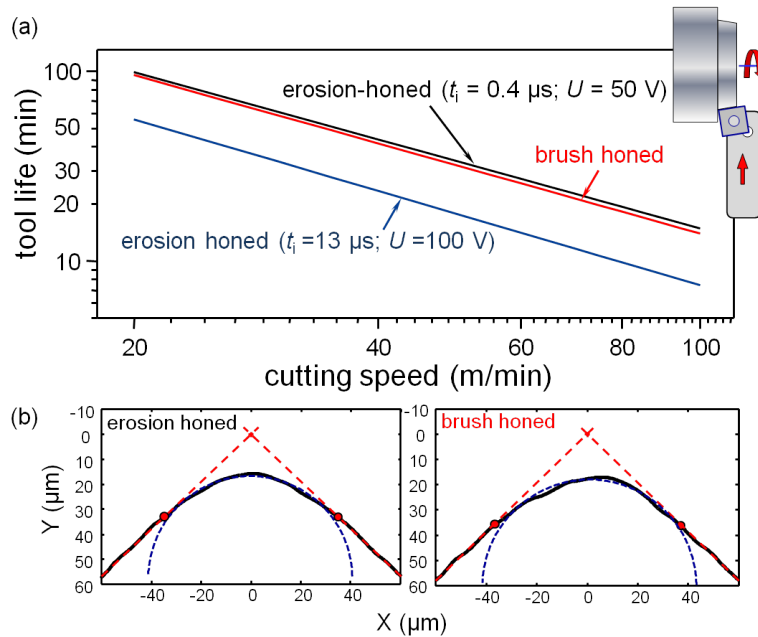


Figure 4.15: (a) Taylor's tool life plots for electro-erosion honed and brush-honed inserts; (b) edge profiles of typical inserts used in tool life tests.

(Armarego and Brown, 1969) performed in a facing operation is presented in Fig. 4.15a. These tests referred to a feed of 0.1 mm and a depth of cut of 1.0 mm, for a tool life criterion of $300 \mu\text{m}$ flank wear, on AISI 4140 steel workpieces of 40 HRC hardness. The tools used were uncoated SNEA grade C5 carbide from the same batch, and of a nominal edge radius of $40 \mu\text{m}$. Typical edge profiles are shown in Fig. 4.15b.

The tool life plots indicate the electro-erosion edge honed tools using the conservative baseline pulse parameters to correspond to a tool life that is virtually identical to that of brush honed tools. It is further evident that the surface generated using the relatively aggressive pulse parameters that refers to a seven-fold increase in pulse energy corresponds to a three-fold reduction in tool life, which is to be expected considering that such features as micro-cracks and selective cobalt erosion (see Fig. 4.14) depletes the surface strength

and undermines the tribological response. This trend is in line with the results obtained by Bonny et al. (2009) who report the successive execution of gradually finer EDM regimes to result in the enhanced wear performance of WC-Co, as evaluated in pin-on-flat tribological tests.

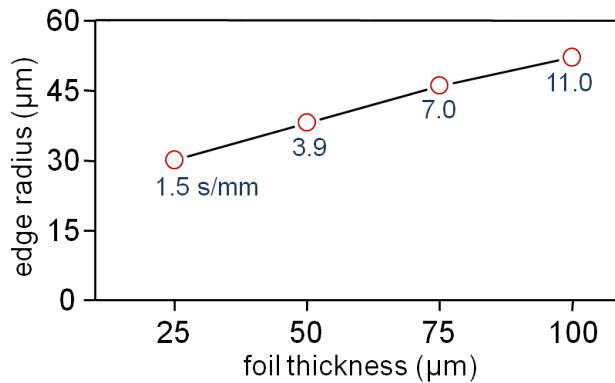


Figure 4.16: Edge radius and processing time as a function of foil thickness.

Notwithstanding the capability of electro-erosion edge honing process in generating consistent edge geometry as demonstrated in this paper, an important factor that is crucial in the industrial acceptance of such a novel technology is the processing time. Fig. 4.16 presents edge radius and the processing time for honing an unit length of a cemented carbide edge of a wedge angle of 90° as a function of counterface thickness. The processing times indicated are comparable to that of brush honing, which at the present time is largely the standard process in industry. It may be noted that the electro-erosion honing process using foil electrodes is amenable to the simultaneous honing of a large number of inserts, with no strict requirement for any intricate alignment. It is also possible to configure the process so as to selectively hone certain edge segments of an insert with a view to reducing the cycle time.

It may be inferred from the information presented in this paper that the

fabrication of a cutting edge of an appropriate geometry (e.g. honed) and surface integrity in a reasonable cycle time constrains the electro-erosion honing process to a rather restricted envelope of operating parameters. It would however be of interest to investigate possibilities for further minimizing processing time and maximizing tool life, through such avenues as a progressive decrease in the pulse energy during the course of honing an edge. The use of a dielectric fluid mixed with nano-powders (Jahan et al., 2010) that aid in dispersing the pulse energy towards improving surface quality without affecting the removal rate may also be considered. Additional strategies to process optimization may involve such approaches as pulse shaping (Juhr et al., 2004), physical vapor deposited coatings (Casas et al., 2004), and the application of secondary processes such as thermal annealing (Casas et al., 2006) and finish micro-blasting (Qu et al., 2005).

4.5 Conclusions

The primary focus of the work reported in this paper was on expanding the capability of the innovative electro-erosion edge honing process in the preparation of uncoated cemented carbide inserts with such geometric features as nose radii and curved edges. Specifically, the work introduced the application of a foil counterface, which facilitates the simultaneous processing of a batch of complex-shaped inserts, with no particular alignment requirements, which has significant positive implications in insert manufacture.

The use of aluminum as the counterface material in negative polarity was identified to generate rounded edge hones in cemented carbide tools, consistent with the insights gained from a simple model developed for the threshold wear ratio. Characterization of the meso-geometry of cutting edges generated in

this process has shown it to correspond to less than 15% variability in edge radius, which is significantly less, as compared to values that are as high as 40% reported for brush honed inserts. This renders the process to be quite attractive in the manufacture of tools used in the precision machining of high-value components.

In the current state of development, electro-erosion honing is shown to be comparable to brush honing in terms of tool life and processing time. This novel process warrants further research as it offers significant scope for further reduction in cycle time while concurrently enhancing tool performance. Considering that electro-erosion honing is a thermal process that is not limited by tool hardness, the process further offers prospects in the edge preparation of ultra-hard polycrystalline diamond tools that currently pose problems when using conventional processes.

Acknowledgments

This work was funded by the AUTO21 Network Centers of Excellence and the C4 Consortium of Ontario. Authors gratefully acknowledge the technical and in-kind contributions of Dr. R. M'Saoubi of Seco Tools.

References

- [Armarego and Brown(1969)] Armarego, E.J.A., Brown, R.H., 1969. The Machining of Metals. Prentice Hall, Englewood Cliffs.
- [Aurich et al.(2011)] Aurich, J.C., Zimmermann, M., Leitz, L., 2011. The preparation of cutting edges using a marking laser. *Production Engineering* 5, 17–24.
- [Bassett et al.(2012)] Bassett, E., Köhler, J., Denkena, B., 2012. On the honed cutting edge and its side effects during orthogonal turning operations of AISI1045 with coated WC-Co inserts. *CIRP Journal of Manufacturing Science and Technology* 5, 108–126
- [Bonny et al.(2009)] Bonny, K. et al., 2009. Influence of electrical discharge machining on the reciprocating sliding friction and wear response of WC-Co cemented carbides. *International Journal of Refractory Metals & Hard Materials* 27, 350–359.
- [Casas et al.(2004)] Casas B. et al., 2004. Mechanical strength improvement of electrical discharge machined cemented carbides through PVD (TiN, TiAlN) coatings. *Thin Solid Films* 447–448, 258–263.

- [Casas et al.(2006)] Casas, B., Torres, Y., Llanes, L., 2006. Fracture and fatigue behavior of electrical discharge machined cemented carbides. *International Journal of Refractory Metals & Hard Materials* 24, 162–167.
- [Casas et al.(2008)] Casas, B., Wiklund, U., Hogmark, S., Llanes, L., 2008. Adhesion and abrasive wear resistance of TiN deposited on electrical discharge machined WC-Co cemented carbides. *Wear* 265, 490–496.
- [Crookall and Fereday(1973)] Crookall, J.R., Fereday, R.J., 1973. An experimental determination of the degeneration of tool electrode shape in electro-discharge machining. *Microtecnic* 17, 197–200.
- [Denkena et al.(2008)] Denkena, B., Leon-Garcia, L., Bassett, E., 2008. Preparation of designed cutting edge microgeometries by simultaneous 5-axes brushing, In: *Proceedings of 3rd Int. Conf. on Manufacturing Engineering*, Greece, pp. 117–123.
- [Denkena et al.(2010)] Denkena, B. et al. 2010. Cutting edge preparation by means of abrasive brushing. *Key Engineering Materials* 438, 1–7.
- [Endres and Kountanya(2002)] Endres, W.J., Kountanya, R.K., 2002. The effects of corner radius and edge radius on tool flank wear. *Journal of Manufacturing Processes* 4, 89–96.
- [Jahan et al.(2010)] Jahan, M.P., Rahman, R., Wong, Y.S., 2010. Modeling and experimental investigation on the effect of nanopowder mixed dielectrics in fine-finish micro-EDM of tungsten carbide. *Journal of Engineering Manufacture* 224, 1725–1739.
- [Jahan et al.(2011)] Jahan, M.P., Rahman, M., Wong, Y.S., 2011. A review on the conventional and micro-electrodischarge machining of tungsten

- carbide. *International Journal of Machine Tools and Manufacture* 51, 837–858.
- [Juhr et al.(2004)] Juhr, H., Schulze, H.P., Wollenberg, G., Kunanz, K., 2004. Improved cemented carbide properties after wire-EDM by pulse shaping. *Journal of Materials Processing Technology* 149, 178–183.
- [Karpuscheski et al.(2009)] Karpuschewski, B., Byelyayev, O., Maiboroda, V.S., 2009. Magneto-abrasive machining for the mechanical preparation of high-speed steel twist drills. *CIRP Annals* 58, 295–298.
- [Klocke and Kratz(2005)] Klocke, F., Kratz, H., 2005. Advanced tool edge geometry for precision hard turning. *CIRP Annals* 54, 47–50.
- [Lauwers et al.(2005)] Lauwers, B., Kruth, J.P., Eeraerts, W., 2005. Wear behaviour and tool life of wire-EDM-ed and ground carbide punches. *CIRP Annals* 54, 163–166.
- [Lin et al.(2008)] Lin, Y.C., Hwang, L.R., Cheng, C.H., Su, P.L., 2008. Effects of electrical discharge energy on machining performance and bending strength of cemented tungsten carbides. *Journal of Materials Processing Technology* 206, 491–499.
- [Qu et al.(2005)] Qu, J., Shih, A.J., Scattergood, R.O., Luo, J., 2005. Abrasive micro-blasting to improve surface integrity of electrical discharge machined WC-Co composite. *Journal of Materials Processing Technology* 166, 440–448.
- [Schimmel et al.(2000)] Schimmel, R.J., Manjunathaiah, J., Endres, W.J., 2000. Edge radius variability and force measurement considerations. *Journal of Manufacturing Science and Engineering* 122, 590–594.

[Wyen et al.(2012)] Wyen, C.F., Knapp, W., Wegner, K., 2012. A new method for the characterization of rounded cutting edges. International Journal of Advanced Manufacturing Technology, Article in Press DOI: 10.1007/s00170-011-3555-4.

[Yussefian et al.(2010)] Yussefian, N.Z., Koshy, P., Buchholz, S., Klocke, F., 2010. Electro-erosion edge honing of cutting tools. CIRP Annals 59, 215–218.

Chapter 5

Parametric characterization of the geometry of honed cutting edges

This chapter is a copy of the paper submitted for publication. Edge preparation and characterization for symmetrically and circularly honed tools were presented in the previous chapters. This chapter presents a novel methodology for characterization of asymmetric cutting edge microgeometries that is based on parametric quadratics.

Authors : N.Z. Yussefian, P. Koshy

Submitted to : Precision Engineering

Date of Submission : 28 April 2012

Abstract

Development of methodologies for the geometric characterization of cutting edges is of significant current interest, in light of the profound influence that the edge geometry wields on virtually every machining response, and the evolving capability for generating tailored edges. This paper proposes the parametric modeling of the tool edge geometry through the application of free-knot B-splines that comprise three piecewise segments corresponding to the cutting edge profile and the two tool faces. The transition points that demarcate the cutting edge from the tool faces are objectively and robustly identified by the adaptive placement of the knots that minimizes the residual error from fitting the B-spline to the tool profile data. On identification of the cutting edge, the edge profile is modeled by parametric quadratics to yield four geometrically-relevant, contour-based parameters that characterize both symmetric and asymmetric honed edges.

5.1 Introduction

The role of the meso-geometry of the cutting edge on the mechanics of chip formation was first documented by Albrecht [1] in 1960. It has however taken several decades since, for this important aspect to be accorded its due consideration. The geometry of the edge has now been demonstrated to affect practically every machining response including: forces [2], temperature distribution [3], tool life [4], surface finish [5] and residual stress [6], in addition to wielding a controlling influence on process stability [7]. Consequently, there is much interest of late amongst the machining research community on the generation and characterization of the cutting edge.

Conventional edge preparation techniques such as brush honing and micro-blasting correspond to significant variability in edge geometry, not just between edges but also along the profile of the same edge [8]. This is of particular detriment in the machining of high-value components in terms of robust tool performance. Avenues to addressing this issue have involved process developments such as 5-axis brush honing [9], and the conception of novel processes that entail magneto-abrasive [10], laser [11] and electro erosion [12] techniques. Further to the variability arising from the process itself, it is intriguing to note that the lack of a standard characterization methodology is also a factor contributing to variability, as identified in a round-robin investigation [13].

In terms of edge characterization, it has thus far been expedient in most instances to specify the geometry of honed edges by a simple edge radius parameter. This inherently assumes the edge profile that bridges the rake and flank faces to conform to a sector of a circle. This need not however be the case, and indeed tool performance may be enhanced when the cutting edge is appropriately asymmetric [3]. Given the critical influence of edge geometric attributes on process responses, and the evolving capability of aforementioned novel processes in the generation of tailored cutting edges, it is imperative to develop methodologies for the comprehensive geometric characterization of the cutting edge.

Denkena et al. [3] proposed that the edge geometry be characterized with reference to the virtual tool tip derived from the linear extension of flank and rake faces (Fig. 5.1a). Any asymmetry in the edge geometry is signified by the ratio of distances S_α and S_γ from the tool tip to points 1 and 2, from where the edge profile diverges away from the flank and rake faces, respectively. The degree of edge flattening is specified by parameter Δr which is the distance from the virtual tool tip to the apex of the edge profile, and parameter φ locates

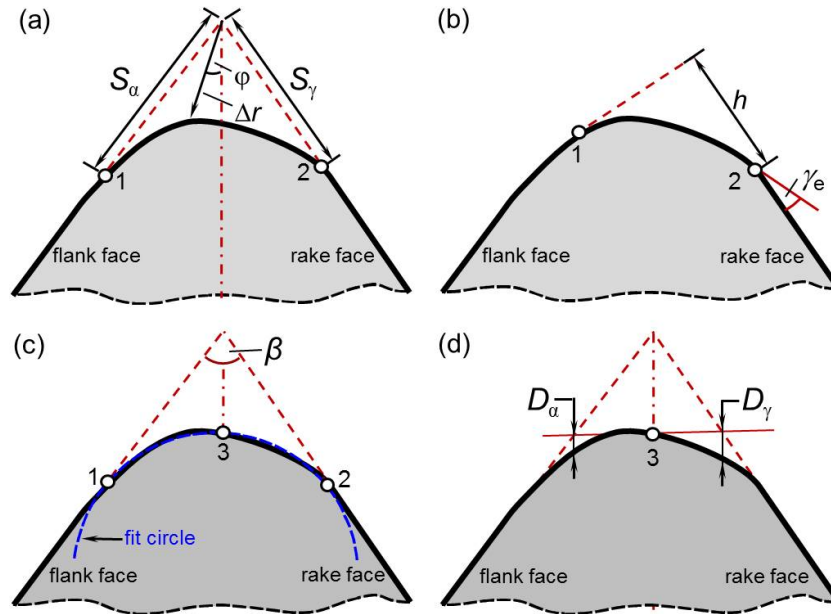


Figure 5.1: Edge characterization methods due to: (a) Denkena et al. [3], (b) Rodriguez [14], and (c & d) Wyen et al. [15].

the tool apex relative to the tool faces. Such a characterization is simple and facilitates easy visualization of the edge; however, the said parameters are evaluated based on just three points on the edge profile, which are not adequate to uniquely characterize the edge geometry. Furthermore, ref. [3] did not specify a method to objectively determine the transition points 1 and 2 wherefrom the edge profile deviates off the tool faces.

Rodriguez [14] attempted to address the issue above by defining the transition points 1 and 2 in terms of the intersection of the edge profile (Fig. 5.1b) with the uncut chip thickness h , with the orientation of the edge specified with respect to the effective rake angle γ_e . This renders the edge geometric parameters to be dependent on the cutting conditions rather than be intrinsic to the cutting edge. Rodriguez further approximated the edge profile by a sixth-degree polynomial, with the unfavorable implication [15] that the error

between the edge profile and the interpolating polynomial of such high order could be unacceptably high, due to oscillation effects known as Runge's phenomenon in numerical analysis.

Wyen et al. [15] recently proposed a method for identifying the transition points that delineate the meso-geometry of the cutting edge from the flank and rake faces of the tool. The first step in this iterative method involves least squares fitting of straight lines to represent the tool faces over a domain that spans a certain preset distance from the apex of the edge profile. These lines are extended to locate the virtual tool tip to enable the computation of the point of intersection of the edge profile and the bisector of the wedge angle β (point 3 in Fig. 5.1c). A circle is then constructed such that it passes through point 3 and is tangential to the said straight lines representing the tool faces. Points 1 and 2 at which this circle intersects the straight lines are considered first approximations for the transition points, which constitute the updated upper limit for the subsequent least squares fitting of the tool faces. The steps above are iterated to refine the location of the transition points.

As the edge is approximated as a circle in this method, any deviations from the ideal such as the edge being asymmetric adversely affects edge identification. In consideration of this, Wyen et al. [15] proposed that the fit be reconsidered should the value of the coefficient of determination R^2 be less than a predefined value, say 90%. They further proposed that any cutting edge asymmetry be denoted by the ratio of distances D_α and D_γ measured from a line passing through point 3 and perpendicular to the wedge angle bisector, to the edge profile, as shown in Fig. 5.1d. This is different from the proposal in [3] in terms of the direction in which these distances are measured.

The review of the relevant literature above clearly indicates that a novel approach is required for the identification and characterization of the cutting

edge, given that published methods refer to ideal geometric shapes and to discrete points on the edge profile. In this context, Section 2 of this paper proposes the application of parametric B-splines for the contour-based identification of the transition points that demarcate the cutting edge from the tool faces. Being piecewise polynomials, B-splines are a logical choice for such identification, as the flank/rake faces and the edge profile that constitute the cutting edge are themselves piecewise in nature. The robustness of such an identification method is investigated in light of several potential sources of uncertainties. Following edge identification, the characterization of the cutting edge profile using parametric quadratics is proposed in Section 5.3. Four contour-based parameters are derived to uniquely quantify the geometry of an edge, which are exemplified in terms of their application to both symmetric and asymmetric honed edges.

5.2 Cutting edge identification

As the meso-geometry of a tool edge profile comprises two tool faces that flank the cutting edge (Fig. 5.2), unambiguous identification of the transition points that separate the edge from the tool faces is the first step that should precede edge characterization. The critical importance of this is illustrated in Fig. 5.3, wherein it is shown that the same symmetrically honed edge could correspond to significantly different edge radius (r_β) values, depending on where the color-coded sets of transition points are deemed to be located. The uncertainty imposed by the boundaries of the cutting edge domain necessitates an edge identification method capable of uniquely and objectively demarcating the cutting edge from the rake and flank faces.

The key idea in the proposed contour-based edge identification method is

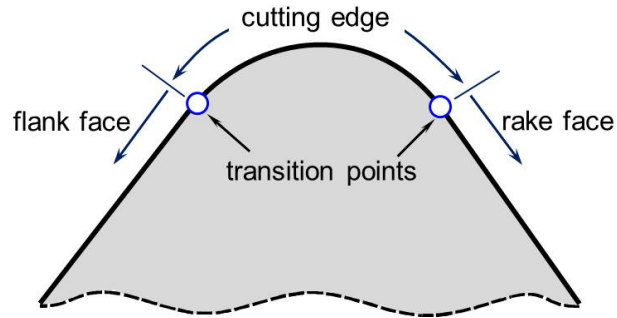


Figure 5.2: Terminology of tool edge profile.

that the edge geometry may be modeled by three piecewise segments to represent the flank/rake faces and the cutting edge, with zero and first geometric continuity at the joining points. Multi-degree splines are most suited to this end, with the first and third sections corresponding to flank and rake faces constrained to be linear, while assuming higher orders for the curvilinear cutting edge in between. As the approximation algorithms for such curves are somewhat complex, a simpler alternative is to employ a single-degree piecewise curve, wherein the first and third segments are geometrically constrained to conform to the linear shape of the tool faces. The profile of the cutting edge is usually free of any change in the direction of curvature, and hence a second degree curve should suffice for modeling it.

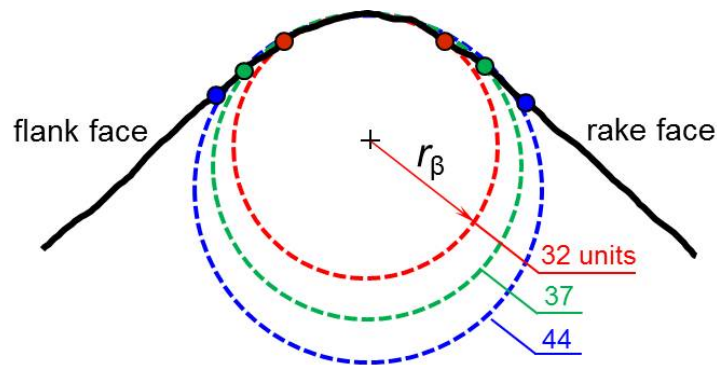


Figure 5.3: Effect of deemed edge boundary on edge radius r_β .

In terms of cutting edge identification, the joining points of the spline sections assume great importance as they correspond to the transition points that demarcate the cutting edge from the tool faces at either ends. With this in view, an appropriate family of spline curves would be the one that enables the curve fitting process to be optimized with respect to the points that connect the three segments. A family of curves that offers this feature are piecewise parametric polynomials called B-splines [16], which are defined as:

$$\mathbf{C}(u) = \sum_{i=0}^n N_{i,p}(u) \mathbf{P}_i \quad (5.1)$$

where $u \in [0, 1]$, and \mathbf{P}_i are $n + 1$ control points that represent the polyline form of the curve in a way that the actual curve always lies completely in their convex hull. $N_{i,p}(u)$ are B-spline basis functions of degree p computed recursively as:

$$N_{i,0}(u) = \begin{cases} 1 & \text{if } u_i \leq u \leq u_{i+1} \\ 0 & \text{otherwise} \end{cases} \quad (5.2)$$

$$N_{i,p}(u) = \frac{u - u_i}{u_{i+p} - u_i} N_{i,p-1}(u) + \frac{u_{i+p+1} - u}{u_{i+p+1} - u_{i+1}} N_{i+1,p-1}(u)$$

Eqn. (5.1) can be expressed as:

$$\mathbf{C} = \mathbf{N}\mathbf{P} \quad (5.3)$$

where \mathbf{N} and \mathbf{P} are matrices of basis function coefficients and control points, respectively.

Basis functions facilitate the piecewise nature of B-spline curves by making use of parametric values called knots (u_i). Each u_i is one of $(m + 1)$ B-spline knots from the knot vector $[u_0, u_1, \dots, u_m]$ and corresponds to a parameter at which one polynomial section ends and another begins. In other words, knots

may be considered as division points that subdivide the curve into segments with $(p - 1)$ continuity at the joining points. For B-spline curves, the knot vector is usually on the $[0, 1]$ interval, with the $(p + 1)$ first and last knots being identical, as in:

$$\begin{aligned} [u_0 = u_1 = \dots = u_p = 0, u_{p+2}, \dots, u_{m-p-1}, u_{m-p} = u_{m-p+1} \\ = \dots = u_{m-1} = u_m = 1] \end{aligned} \quad (5.4)$$

The number of knots $(m + 1)$, the degree of the B-spline curve p and the number of control points $(n + 1)$ are related as:

$$m = p + n + 1 \quad (5.5)$$

The proposed method uses a quadratic B-spline to model the cutting edge. For a second degree B-spline to constitute three polynomial sections that correspond to the flank/rake faces on the cutting edge, the knot vector should have three spans and will be of the form $[0, 0, 0, u_1, u_2, 1, 1, 1]$. Based on this knot vector, the second degree basis function matrix N can be computed from eqn. (5.2) to be:

$$\begin{bmatrix} \frac{(u_1-u)^2}{u_1^2} & -\frac{u^2}{u_1^2} + \frac{2u}{u_1} - \frac{u^2}{u_1 u_2} & \frac{u^2}{u_1 u_2} & 0 & 0 \\ 0 & \frac{(u_2-u)^2}{u_2(u_2-u_1)} & \frac{(u^2-u_2)u_1-u^2+2uu_2-u_2u^2-u_2u^2}{u_2(u_2-u_1)(1-u_1)} & \frac{(u-u_1)^2}{(1-u_1)(u_2-u_1)} & 0 \\ 0 & 0 & \frac{(1-u^2)}{(1-u_1)(1-u_2)} & \frac{(1-u^2)(u-u_1)}{(1-u_1)(1-u_2)} + \frac{(1-u)(u-u_2)}{(1-u_2)} & \frac{(u-u_2)^2}{(1-u_2)^2} \end{bmatrix} \quad (5.6)$$

For a second degree polynomial ($p = 2$) with eight knots ($m + 1 = 8$), five control points ($n + 1 = 5$) are required to uniquely define the curve, as per eqn. 5.5. Knowing u_1, u_2 and five control points, the desired B-spline curve $C(u)$ is fully defined using eqn. (5.3) and eqn. (5.6), and the cutting edge will be subdivided into three quadratic profiles joining smoothly at u_1 and u_2 , as shown in Fig. 5.4. The equation for each individual section of the cutting edge

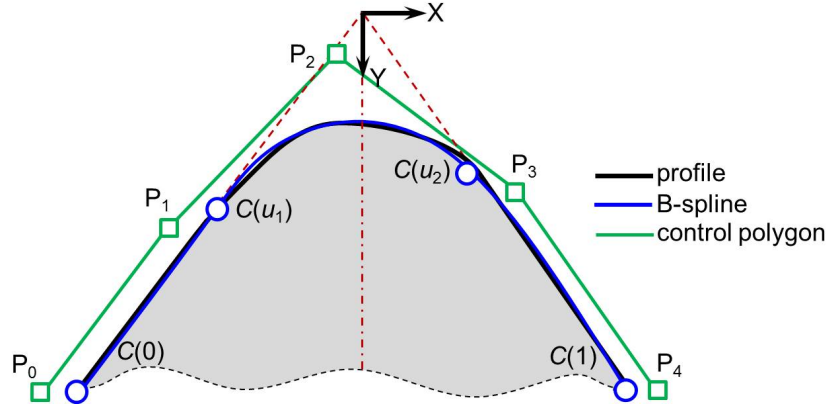


Figure 5.4: Edge identification using a quadratic B-spline with three sections.

profile can be derived from the corresponding row of the N matrix multiplied by the control points matrix P .

The profile of a tool edge can be acquired by techniques such as profilometry, white light interferometry and confocal microscopy. With the profile data points $\mathbf{D} = [D_1, \dots, D_q]$ in place, the edge identification algorithm reduces to the determination of u_1 and u_2 . However, before proceeding with such fitting computations, a set of parameters $t = [t_1, \dots, t_q]$ should initially be assigned to the data points so that $C(t_i) \approx D_i$ holds subsequent to fitting, a process known as parametrization. Among the different methods available for parametrization, the method used in this research refers to uniformly spaced parameters:

$$t_i = \frac{i-1}{q}; \quad i = 1 : q \quad (5.7)$$

The algorithm for finding the cutting edge profile is then equivalent to the minimization of the least square B-spline curve fitting function:

$$L = \sum_{i=1}^q |C(t_i) - D_i|^2 \quad (5.8)$$

The unknowns are five control points ($n + 1 = 5$), u_1 and u_2 . If the values of u_1 and u_2 are predetermined (as in uniformly spaced knot generation, e.g.

$u_1 = 1/3$ and $u_2 = 2/3$), the problem simplifies to a fixed knot B-spline approximation, and eqn. (5.8) will reduce to a linear least square problem that can be solved by simple linear algebraic formulations. However, with u_1 and u_2 unknown, the fit is allowed to modify the boundaries of sections for the best-fit three-segment quadratic polynomial. This is a key point in that the transition points that demarcate the cutting edge from the tool faces are objectively and robustly identified by the adaptive placement of the knots that minimizes the residual error from fitting the B-spline to the tool profile data. This type of B-spline curve fitting is categorized as free-knot B-spline approximation, and as a result eqn. (5.8) will be a nonlinear least squares problem, which can be solved by iterative numerical methods like Gauss-Newton [17].

To render the first and third segments corresponding to flank and rake faces to conform to the geometry of the tool faces, the approximation procedure is further coupled with two geometric constraints:

$$\begin{aligned}\frac{dC_y}{dC_x}(0) &= m_1 \\ \frac{dC_y}{dC_x}(1) &= m_2\end{aligned}\tag{5.9}$$

where m_1 and m_2 are the slopes of the lines representing the flank and rake faces.

In the context of the background above, the steps to cutting edge identification are enumerated below and accordingly illustrated in Fig. 5.5, with the virtual tool tip as the origin of the coordinate system.

1. Having the profile data points (\mathbf{D}_0), two horizontal margins that best include the linear sections on rake and flank faces are given as inputs. Based on linear regression of the points contained between these margins, the rake and flank lines, and the origin of the coordinate system are constituted.

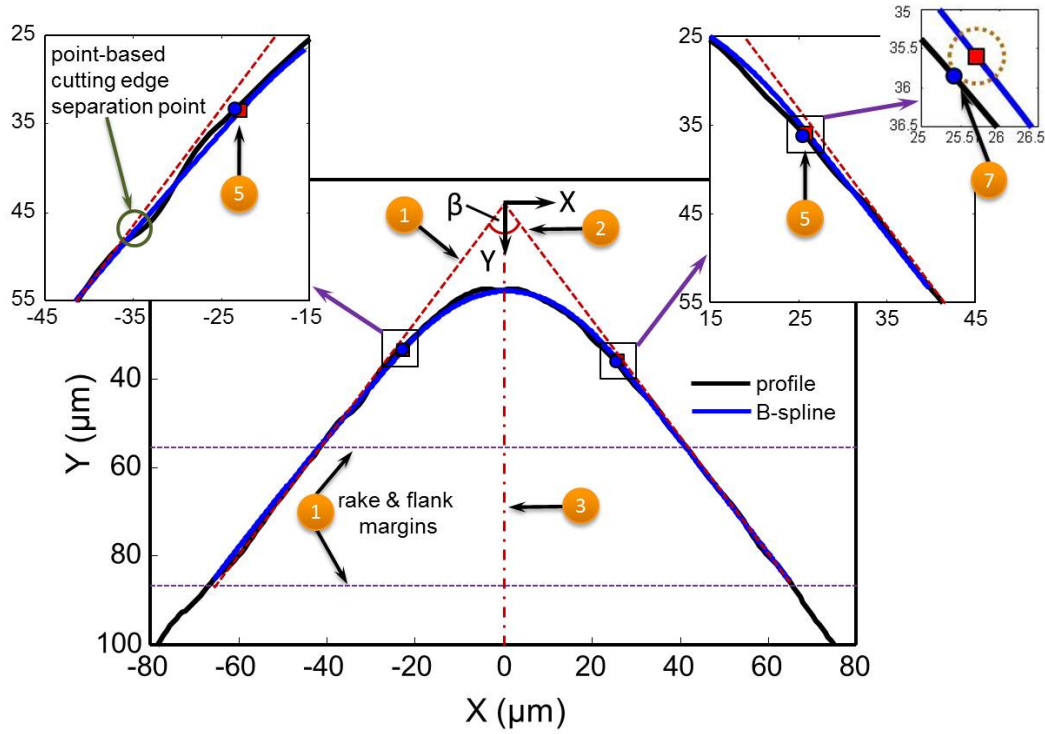


Figure 5.5: Cutting edge identification by free-knot B-spline approximation.

2. Using these rake and flank lines, the wedge angle β is computed. If the computed wedge angle is not within a predefined margin (say $\pm 5\%$) of the nominal value, step one is repeated with two updated horizontal marginal lines.
3. Profile data points are then rotated (**D**) such that the wedge angle bisector coincides with the Y axis, for which the rake and flank line slopes (m_1 and m_2) will be equal but with opposite signs.
4. Profile data points are then parameterized using eqn. (5.7).
5. Eqn. (5.8) is solved for profile points (**D**) starting from the lower marginal line using Gauss-Newton [17] method, with eqn. (5.9) as constraints. The

resultant u_1 and u_2 will provide the first guess for the transition points, with the cutting edge bounded between $C(u_1)$ and $C(u_2)$.

6. If the closest distance of $C(u_1)$ (or $C(u_2)$) to flank (or rake) line is more than a threshold value (say 3% of $|C(u_2) - C(u_1)|$), u_1 (or u_2) will be decreased (or increased) until this condition is met.
7. The closest points on the actual profile (**D**) to $C(u_1)$ and $C(u_2)$ will be the start and end points of the edge region.

The algorithm above is applicable to all edge geometries; however, if the cutting edge profile contains an abrupt slope change between the sections that the quadratic polynomial cannot closely follow, the precise identification of the cutting edge is affected. One example of such abrupt geometric change is a T-land (chamfer) edge geometry for which all three tool sections are linear. It is suggested that first degree B-splines rather than quadratics be used in such an instance. All other steps remain unaffected.

Point-based cutting edge identification methods which consider the edge boundaries to be defined by the points from where the edge profile separates off the rake and flank lines are quite sensitive to minor form errors and profile irregularities. This issue is addressed by the proposed contour-based method, as illustrated in the inset on the left of Fig. 5.5, wherein the transition point can be seen to be not affected by variations in the form of the tool profile.

The proposed algorithm is intended to minimize the influence of potential sources of uncertainty in cutting edge identification. This algorithm is based on the fact that rake and flank geometries can be rendered as two lines. Inappropriate consideration of the tool macro-geometry comprising the rake and flank faces might result in improper cutting edge identification. As shown in Fig. 5.6, points lying between horizontal margins 1 and 2 contain the actual

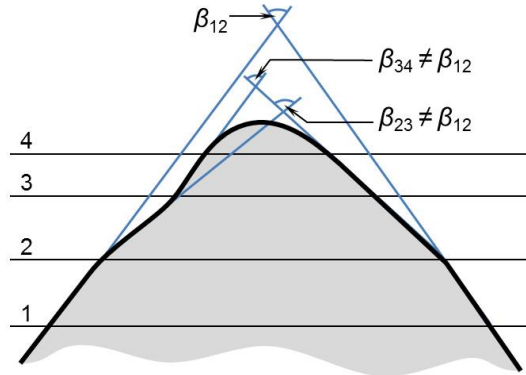


Figure 5.6: Identification of tool face margins in consideration of wedge angle β .

macro-geometry of the cutting tool, referring to the nominal wedge angle β_{12} . Erroneous consideration of points between margins 2 and 3, or 3 and 4, results in entirely different flank and rake lines that respectively refer to wedge angles β_{23} and β_{34} that are different from the nominal value. The comparison of the computed tool wedge angle with the nominal value in the second step of the identification algorithm precludes such misinterpretations. Step 6, though rarely required, is added to ensure that the edge is properly determined.

Fig. 5.7 depicts three edge profiles with a point uncertainty of $1 \mu\text{m}$ to demonstrate the robustness of the edge identification method against such. The variability in the location of the edge identification points is less than $2 \mu\text{m}$, which highlights the superiority of a contour-based approach. One of the sources of uncertainties in the identification of the cutting edge refers to the distance from the tool tip over which rake/flank faces are being considered for modeling. While unreasonably too big or too small values of this distance will lead to inaccurate edge identification, any algorithm should yet be as invariable as possible to this factor. Fig. 5.8 illustrates the robustness of the proposed edge identification method against the marginal distance (lower

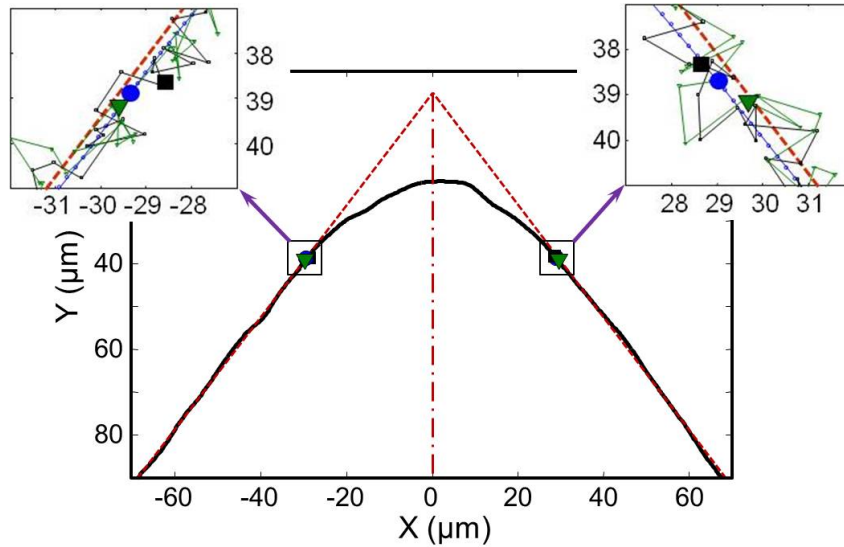


Figure 5.7: Robustness of edge identification against point uncertainty.

margin in Fig. 5.5) by taking advantage of free-knot B-spline approximation. Intentional translation of the lower marginal line from $80 \mu\text{m}$ up to $170 \mu\text{m}$ can be seen to induce a variability of less than $2 \mu\text{m}$ in the identification of the cutting edge boundaries.

5.3 Cutting edge characterization

As reviewed in section 5.1, methods currently used to characterize edge geometry refer to parameters that are evaluated based on discrete points on the edge profile. Fig. 5.9 illustrates issues arising from such an approach. Fig. 5.9a shows two edges that would refer to different machining responses to correspond to identical S_α and S_γ parameters used in ref. [3]; similarly, Fig. 5.9b illustrates the limitation of parameters D_α and D_γ proposed in ref. [15] in being able to effectively distinguish the edges, as the two entirely different profiles correspond to identical parameters.

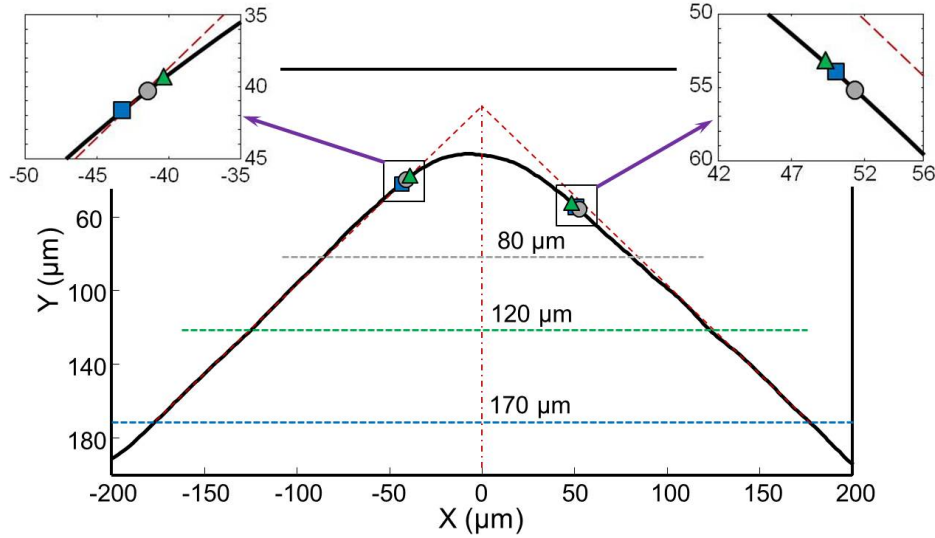


Figure 5.8: Invariability of edge identification algorithm to tool face region considered.

To characterize an edge by a comprehensive set of contour-based parameters, it may be modeled by a geometric curve that can be adequately fit to various edge geometries. To this end, it is proposed herein that parametric quadratic curves be fit to the edge profile:

$$\begin{aligned} x(u) &= a_2u^2 + a_1u + a_0 \\ y(u) &= b_2u^2 + b_1u + b_0 \end{aligned} \quad (5.10)$$

Parametric quadratic curves are simple polynomials for which standard fitting algorithms are commonly available, one of which is the B-spline approximation.

In reference to the coordinate system shown in Fig. 5.10, the cutting edge is modeled by fitting a second degree parametric curve with $u \in [0, 1]$ to the spatial coordinates of the cutting edge. The quadratic equations of the edge may be obtained directly from the parametric equations of the second segment of the tool geometry, which refers to the cutting edge profile obtained during

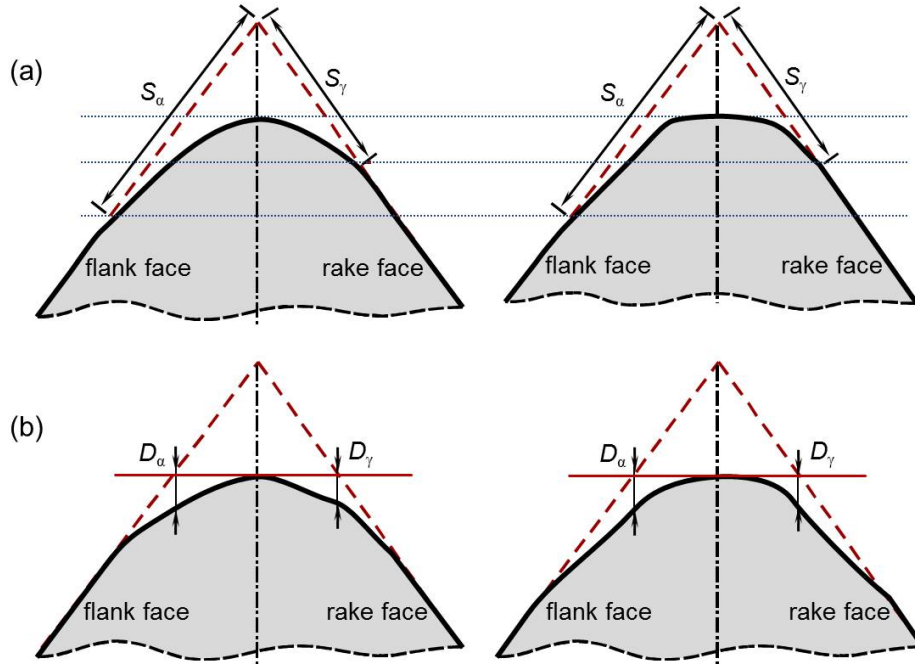


Figure 5.9: Limitations of current edge characterization parameters.

the edge identification process (as presented in section 2). This requires re-parametrization from $[u_1, u_2]$ to $[0, 1]$ by replacing u with $[(u - u_1)/(u_2 - u_1)]$. Alternatively, an additional single span approximation may be accomplished with a fixed knot ($u_i = [0, 0, 0, 1, 1, 1]$) B-spline using linear algebraic algorithms. The fit of the B-spline to the cutting edge profile may be evaluated in terms of goodness-of-fit measures such as the coefficient of determination R^2 , as suggested in ref. [15].

In the interest of rendering the edge characterization parameters to comprehensible and easy to visualize, the six constants in eqn. (5.10) need be viewed in light of parameters that are of physical relevance. It can be shown that the implicit form of a parametric quadratic curve is a parabola [18] with the general form:

$$Ax^2 + Bxy + Cy^2 + Dx + Ey + F = 0 \quad (5.11)$$

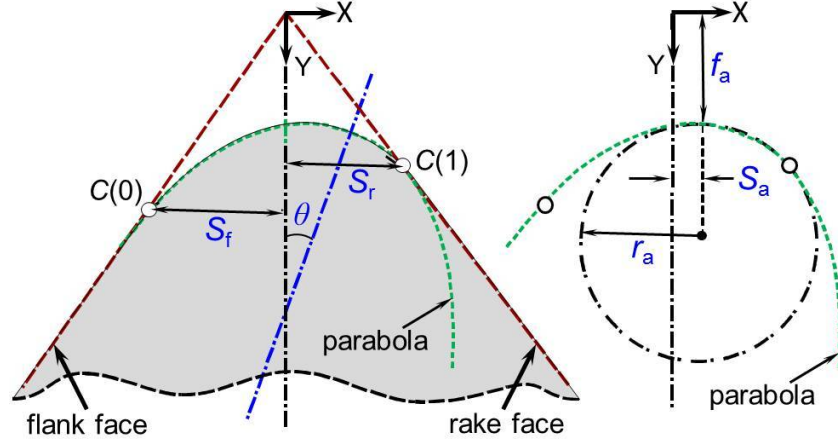


Figure 5.10: Proposed edge characterization parameters.

subject to $B^2 = 4AC$. Accordingly, the minimum number of parameters to construct the edge is four, since parabolas have four degrees of freedom in the two-dimensional plane. However, to designate the cutting edge margins, two of these parameters have to correspond to the two points referring to the start and end points of the cutting edge profile. If these points are assumed to lie on the rake and flank lines within a set tolerance, the cutting edge profile can be fully defined using four parameters, considering that for the given tool wedge angle β , $x(0) = -y(0) \tan(\beta/2)$ and $x(1) = y(1) \tan(\beta/2)$. Fig. 5.10 depicts these four characterization parameters to comprise two form parameters and two edge marginal parameters. If $u_a = (-b_1/2b_2)$ refers to the apex of the cutting edge, the two form parameters are:

1. $S_a = x(u_a) = a_2(-b_1/2b_2)^2 + a_1(-b_1/2b_2) + a_0$, a measure of profile asymmetry, and
2. $r_a = [(a_1b_2 - a_2b_1)^2/(2b_2^3)]$, the radius of curvature of the apex.

The two edge marginal parameters:

3. $S_f = a_0$

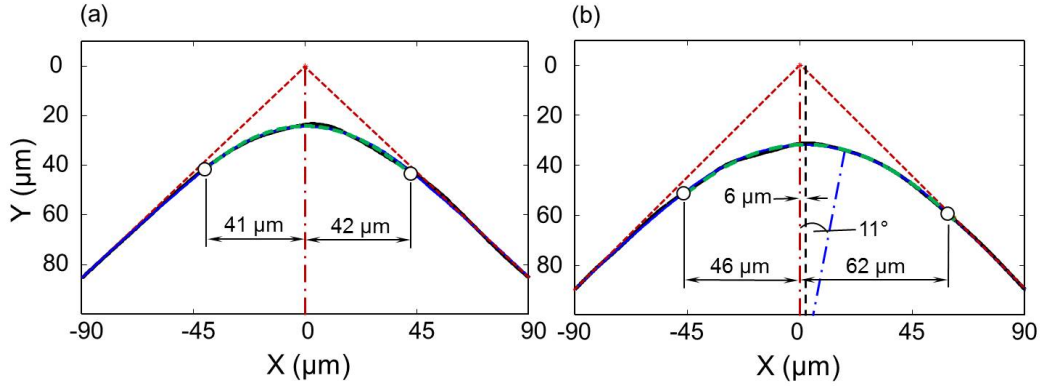


Figure 5.11: Characterization of: (a) symmetric, and (b) asymmetric edges.

$$4. S_r = a_2 + a_1 + a_0$$

define the region that the edge profile extends to, with respect to the flank and rake faces, respectively. If the assumption of the start and end points of the edge profile being on the flank and rake lines is relaxed, the following two additional parameters (see Fig. 5.10) are required to fully define the cutting edge:

5. $f_a = y(u_a) = (-b_1^2/4b_2) + b_0$, a measure of cutting edge flatness, and
6. $\theta = (1/2)\tan^{-1}[(-2a_2b_2)/(b_2^2 - a_2^2)]$, the angle between the axis of symmetry of the parabola and the wedge angle bisector.

The four parameters S_a , r_a , S_f and S_r can represent both symmetric and asymmetric edge profiles. S_f and S_r define the margins of the cutting edge profile and cannot therefore represent any asymmetry in the form of the edge profile. Form asymmetry is well brought out by parameter S_a that designates the location of the edge apex. Parameter r_a denotes the roundness of the edge profile.

Fig. 5.11 illustrates the fit of a B-spline to a symmetric edge and an asymmetric edge, the coefficient of determination R^2 for both of which exceeded

98%. For the symmetric profile (Fig. 5.11a), the cutting edge marginal parameters S_f and S_r are essentially the same (see Table 1). The symmetry of the edge is also denoted by the S_a and θ parameters being close to zero. If the cutting edge refers to an arc of a circle, $r_a \approx r_\beta$. For this profile, r_β was measured using circular regression over the points on the cutting edge profile to be $53 \mu\text{m}$. For the asymmetrically honed insert shown in Fig. 5.11b, edge asymmetry is clearly signified in the disparity between S_f and S_r values, and the parameters S_a and θ assuming non-zero values that are larger relative to those corresponding to the symmetric edge.

Table 5.1: Cutting edge characterization parameters

Parameter	$S_a(\mu\text{m})$	$r_a(\mu\text{m})$	$S_f(\mu\text{m})$	$S_r(\mu\text{m})$	$f_a(\mu\text{m})$	$\theta(^{\circ})$
Symmetric edge	0	50	41	42	25	-2
Asymmetric edge	6	65	46	62	33	11

It may be noted that the proposed characterization parameters enable the calculation of the parametric quadratic coefficients of eqn. (5.10), which serves to reconstruct the edge profile for further numerical analyses such as finite element modeling of cutting.

5.4 Conclusions

A parametric approach to the identification and characterization of the meso-geometry of honed cutting edges has been presented. Considering that the profile of a honed cutting edge transitions smoothly into the rake and clearance faces that flank the edge, unambiguous identification of the transition points that delimit the cutting edge from the tool faces has been demonstrated to be a critically important step that ought to precede edge characterization.

Accordingly, parametric modeling of the tool edge geometry through B-splines that are presently standard modeling tools in CAD/CAM applications has been proposed.

The B-splines considered comprise three piecewise segments corresponding to the cutting edge profile and the two tool faces. The transition points that demarcate the cutting edge from the tool faces are objectively identified by the adaptive placement of the knots that minimizes the residual error referring to fitting of the B-spline to the tool profile data. This methodology has been evaluated to be robust against point uncertainty and the geometric domain over which the tool profile is modeled. Subsequent to edge identification, the edge has been modeled by parametric quadratics. The application of four geometrically-relevant, contour-based parameters derived from the best parabolic fit to the cutting edge in characterizing both symmetric and asymmetric honed edges is also demonstrated.

These parameters serve to reconstruct the cutting edge geometry for numerical analyses of cutting processes, and enable the specification of tool edge geometries that are tailored to optimize the cutting response in the manufacture of high-value components.

References

- [1] P. Albrecht, New developments in the theory of metal cutting process, Part 1: The ploughing process in metal cutting, *Journal of Engineering for Industry* 82 (1960) 348–357.
- [2] R.J. Schimmel, J. Manjunathaiah, W.J. Endres, Edge radius variability and force measurement considerations, *Journal of Manufacturing Science and Engineering* 122 (2000) 590–594.
- [3] B. Denkena, A. Lucas, E. Bassett, Effects of the cutting edge micro-geometry on tool wear and its thermo mechanical load, *CIRP Annals-Manufacturing Technology* 60 (2011) 73–76.
- [4] J. Rech et al., Influence of cutting edge radius on the wear resistance of PM-HSS milling inserts, *Wear* 259 (2005) 1168-1176
- [5] T.H.C. Childs et al., Surface finishes from turning and facing with round nosed tools, *CIRP Annals-Manufacturing Technology* 57 (2008) 89–92.
- [6] M.A. Nasr, E. Ng, M.A. Elbestawi, Modelling the effects of tool-edge radius on residual stresses when orthogonal cutting AISI 316L, *International Journal of Machine Tools and Manufacture* 47 (2007) 401–411.

-
- [7] D. Biermann, A. Baschin, Influence of cutting edge geometry and cutting edge radius on the stability of micromilling processes, *Production Engineering* 3 (2009) 375–380.
- [8] W.J. Endres, R.K. Kountanya, The effects of corner radius and edge radius on tool flank wear, *Journal of Manufacturing Processes* 4 (2002) 89–96.
- [9] B. Denkena, L. Len-Garca, E. Bassett, Preparation of designed cutting edge microgeometries by simultaneous 5-axes brushing, *Proceedings of the 3rd International Conference on Manufacturing Engineering* (2008).
- [10] B. Karpuschewski, V.S. Byelyayev, O. Maiboroda, Magneto-abrasive machining for the mechanical preparation of high-speed steel twist drills, *CIRP Annals - Manufacturing Technology* 58 (2009) 295–298.
- [11] J.C. Aurich, M. Zimmermann, L. Leitz, The preparation of cutting edges using a marking laser, *Production Engineering* 5 (2010) 17–24.
- [12] N.Z. Yussefian, P. Koshy, S. Buchholz, F. Klocke, Electro-erosion edge honing of cutting tools, *CIRP Annals - Manufacturing Technology* 59 (2010) 215–218.
- [13] B. Denkena, Report on the cooperative work on cutting edge geometry, International Academy for Production Engineering (CIRP), August 2008.
- [14] C.J.C. Rodriguez, Cutting edge preparation of precision tools by applying microabrasive jet machining and brushing, Dissertation (2009) Kassel University.

-
- [15] B. Wyen, W. Knapp, K. Wegener, A new method for the characterisation of rounded cutting edges, *International Journal of Advanced Manufacturing Technology* 59 (2012) 899–914.
- [16] L. Piegl, W. Tiller, *The NURBS book*, Springer Verlag, Berlin (1997).
- [17] H. Schwetlick, T. Schutze, Least squares approximation by splines with free knots, *BIT Numerical Mathematics* 35 (1995) 1–3.
- [18] T.W. Sederberg, D.C. Anderson, Implicit representation of parametric curves and surfaces, *Computer Vision, Graphics and Image Processing* 28 (1984) 72–84.

Chapter 6

Numerical Simulation of Electro-Erosion Edge Honing

6.1 Introduction

Simulation of the EDM (like any other process) can provide an enhanced insight into the process, it can further facilitate the prediction of process behavior and the geometry of the machined workpiece under different parameters. In spite of its complexity, there are several fundamental principles governing the EDM which facilitate the simulation of its behaviors. In EDM, electrical sparks which form the very basic units of material removal mechanism, occur in millionth of second ($0.05\text{-}1000\ \mu\text{s}$), removing micro scale amount of material ($10^{-6} - 10^{-4}\ \text{mm}^3$) [43] from both tool electrode and the workpiece. The ratio of material removed from tool electrode and workpiece is wear ratio and the amount of material removed per single spark is called crater volume. Wear ratio and crater size depend on the tool/workpiece material and geometry as

well as polarity and pulse parameters. They remain almost constant per discharge through the EDM process. There is also a micro-scale gap between the tool electrode and the workpiece that is filled with dielectric fluid. This gap provides the electrical resistance to be potentially overwhelmed by electrical sparks following the dielectric ionization. Gap size which depends on open circuit voltage and the material of dielectric fluid, is constantly oscillating about an average value in a servo-controlled range.

Based on the above mentioned principles there have been a few studies on the geometric simulation of EDM process. Yu et al. [78] predicted the longitudinal wear length of simple-shaped tool electrodes by a uniform one-dimensional wear model. Tricarico et al. [77] developed a die sinking EDM simulation in which discrete nodes on tool electrode and workpiece surface were relocated iteratively with respect to a layer thickness function. This function was derived by considering the relationship between material removal rate and electrode wear with gap width. Kunieda et al. [60] developed a numerical simulation which modeled the removal on both electrode and workpiece considering the gap width, crater size and debris particle concentration in the gap. This method which was only applicable to flat surfaces was later enhanced [79] to be applicable to large curvatures by including the effect of curvature difference between the electrode and workpiece at curvilinear profiles. The crater shape was assumed to be of cubic shape by considering one mesh area to be equivalent to the crater size. Zhao et al. [80] employed a mesh modeling of workpiece ignoring the material removal in the tool electrode. They considered the crater geometry to be of conic shape as opposed to the previous models which considered it to be cubic. For geometric prediction of micro-EDM drilling, Jeong and Min [81] used a mesh modeling of both workpiece and tool electrode. The crater geometry was considered to be a circular section. The effect of surface

condition on material removal was also incorporated by assuming that removal per spark is constrained by surface topography. It was further assumed that depth to diameter ratio of the electrode and workpiece craters are equal. This model was then applied to micro-EDM drilled holes showing maximum error at the corners.

Electro-erosion edge honing [82] relies on localized wear on high curvature surfaces during the sink EDM process. This phenomenon is exploited to round off the sharp edges of cutting tools used as tool electrodes while ED-machining of an appropriate counterface. In this regard, the simulation of EE-honing requires a modeling technique that can simulate removal on both tool electrode and workpiece. It should further be capable of modeling the elevated wear at high curvatures in micro-scale. This is only possible by a modeling technique that is based on the true crater geometry in such a way that a realistic modeling of overlapping craters is facilitated. In this context, this section details an innovative simulation of material removal during the sink EDM process which is capable of predicting the geometry of EE-honed cutting edges. Such simulation will provide a better understanding of EE-honing process behaviour and characteristics. It can be used for off-time investigation of the effect of various parameters such as initial edge geometry, tool angle, foil thickness and gap size on the geometry of prepared edges.

6.2 Simulation Methodology

The numerical simulation considers the cutting edge and the counterface to be two vectors of equally spaced nodes. Counterface is a foil with a known thickness. Cutting edge is modeled as a wedge with an initial edge radius. The algorithm is based on geometrical (tool angle, foil thickness), process (gap size,

crater size) and programming (simulation duration, node density) parameters. There are three major assumptions in this algorithm:

- Energy per spark and the removed material per spark remain constant during the EDM process
- Crater size on tool electrode and workpiece and gap width (s) are known
- Spark occurs at the shortest path between the tool electrode and the counterface

In consideration of aforementioned assumptions it should be noted that crater size and gap width are experimentally measured and employed as calibration parameters for the simulation. Gap width depends on open circuit voltage and the material of dielectric both of which are fixed in the EE-honing process. In addition to the shortest path criterion, spark location is also a function of debris diameter and debris concentration [83]. However, the volume of material removed during the EE-honing process is very small. This results in minimum contamination of the machining gap which in turn dominates the effect of shortest path on spark location as compared to debris diameter and concentration.

EDM simulator is consisted of different modules each performing a separate task. A brief explanation of how the algorithm works and the tasks of these modules follow.

Electrode Feed Module

In EDM process a constant gap between electrode and workpiece is controlled and adjusted by a servo mechanism [77]. In practice gap is usually controlled indirectly by mean working voltage which is compared with a servo

reference voltage. In this simulation gap is controlled directly by the distance of closest points between electrode and workpiece in the same manner. The tool electrode feeds towards the counterface until the shortest distance to the counterface surface is less than the gap size (s). Then the spark location search module identifies the spark location. During the EDM process, tool electrode feed continues until the shortest distance of the electrode and counterface is less than a threshold value ($0.8s \mu\text{m}$). At this point, the tool retracts for a random value in $[0 \ 0.2s]$ range from where it continues to feed in. This back and forth movement simulates the servo controlled feed of the tool electrode to maintain a constant gap in an actual EDM process. It further provides the required randomness to the EDM process simulation.

Spark Location Search Module

Spark location search module identifies the range of potential nodes that the spark might occur with respect to gap size. The identification of potential spark locations optimizes the search algorithm. A pair of nodes with minimum distance on tool electrode and the counterface defines both the spark location and its direction. Once the spark location is known on the tool and the counterface, material removal is simulated by material removal module.

Material Removal Module

Experimental observations have shown spark crater shape to be spherical [84]. The cross section of a crater geometry is shown in Fig. 6.1. As can be seen it consists of a circular section and two small rims at both ends. However, the area of these rims is quite negligible compared to the area of the circular section. Therefore, a circular section accounts for the spark crater geometry in this simulation with the maximum depth at the sparking node which physically

represents the center of arc plasma. This is a valid assumption since arc plasma temperature is maximum at the center [85].

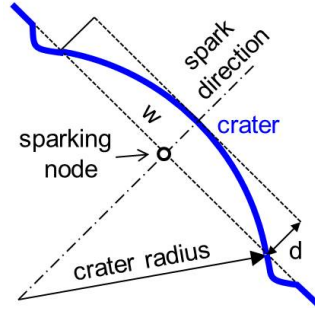


Figure 6.1: Circular crater geometry in the direction of spark.

This circular section is in the direction of spark into the material with the sparking node being on its axis of symmetry. If the crater width and depth are w and d , respectively, the crater radius can be computed:

$$R = \frac{w^2 + 4d^2}{8d} \quad (6.1)$$

Having the radius of crater and the direction of spark, the center point coordinates of the circular section can be computed and the equation of the circle can be derived. In order to simulate the crater geometry, the simulation is developed so that multi-nodes are assigned to a single crater. Once the equation of the circular section is known, with reference to the sparking node, the neighboring nodes within the crater region will be examined, Fig. 6.2. If they fall within the crater circular section, their y coordinate will be updated to correspond to crater shape. Fig. 6.2 illustrates such removal on both the tool electrode and the counterface material. As can be seen, the distance between nodes on electrode is different from that of workpiece nodes. This distance is determined with respect to the crater width on tool electrode and workpiece such that same number of nodes cover a horizontally positioned crater.

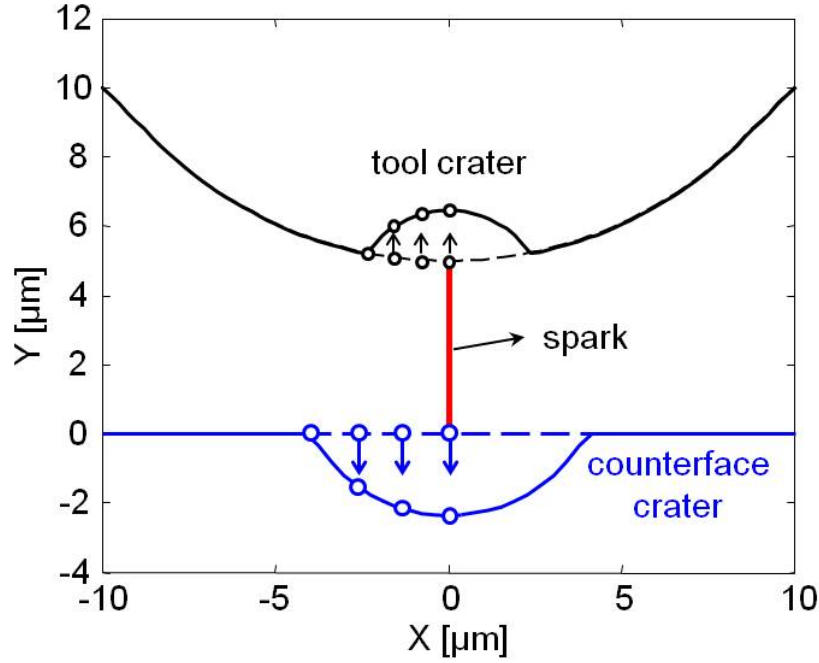


Figure 6.2: Simulated removal mechanism per spark.

The material removal modeling explained overwhelms a major challenge for EDM simulation which is the modeling of overlapping craters. Fig. 6.3a shows overlapping craters simulated with such a modeling strategy.

As can be seen in Fig. 6.3a, the amount of material removed per spark is constrained by the surface topography of the electrode and/or workpiece. For instance, the amount of material removed by second discharge is much smaller than the amount of material removed by the first one which itself is smaller than the material removed by the single spark test on a flat surface being the reference crater area:

$$A_r = R^2 \cos^{-1}\left(\frac{R-d}{R}\right) - (R-d)\sqrt{2Rd-d^2} \quad (6.2)$$

This is indeed not true, since material is removed with respect to spark energy and the effect of surface topography should be compensated. To overcome this limitation the amount of material removed per spark is calculated on both electrode and workpiece if this amount is smaller than the reference crater area of eqn. (6.2) crater width and depth are incremented as follows:

$$w = w + 0.01w$$

$$d = d + 0.01d$$
(6.3)

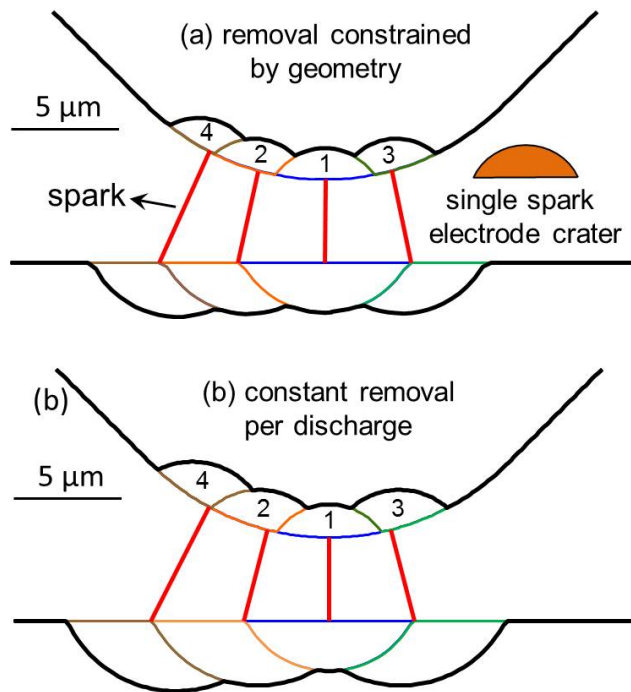


Figure 6.3: Modeling of overlapping craters (a) Constrained by geometry (b) Constant removal per spark.

Removal is then performed by new crater dimensions. This procedure is repeated until the amount of material removed corresponds to the reference crater area. Such material removal mechanism is shown in Fig. 6.3b.

6.3 EE-honing Process Investigations

Prior to experimental verification of the numerical simulation, it is possible to perform qualitative investigation of the process to get a better insight of the EE-honing process.

6.3.1 Electrode Wear at Sharp Edges

The key idea of the EE-honing is based on the fact that in sink EDM process sharp edges of tool electrodes quickly round-off as a result of localized electrode wear at the corners. The geometric explanation for this phenomenon is that workpiece area facing a unit electrode area is larger than one at the corners. This results in occurrence of higher number of sparks at sharp edges and removes more material at these positions [45], Fig. 1.22.

The localized wear at electrode corner, is hence the fundamental principle of EE-honing process. A successful simulation of EE-honing should be able to model this effect. This was investigated by the numerical simulation using the definition of discharge density. Discharge density is the total number of sparks per unit area (or length in 2-D simulation) of the tool electrode. Fig. 6.4 illustrates discharge density along the cutting edge subsequent to the EE-honing process.

As can be seen in Fig. 6.4, while discharge density is almost constant at sections of linear geometry, it is elevated at the tip of the tool electrode. This confirms the occurrence of higher number of sparks at sharp electrode corners. Fig. 6.4 also designates increasing discharge density at parts of the edge which are still under process.

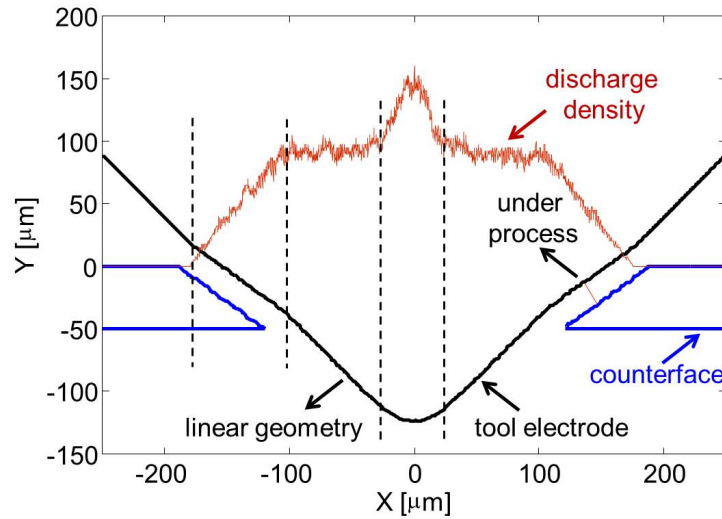


Figure 6.4: Discharge density along the electrode length.

6.3.2 Effect of Wear Ratio

Wear ratio is the ratio of the volumetric amount of material removed from electrode to that of the workpiece. EE-honing process is based on localized wear at sharp edges of the tool electrode. Therefore, it is evident that wear ratio should dominantly affect the final worn edge geometry. This was experimentally verified. Fig. 6.5 illustrates edge 3D surface model along with a cross section profile obtained from experimental EE-honing tests conducted under different wear ratio values. By increasing wear ratio, the shape of the wear pattern gradually changes from dome-shaped to circular and further to a flat profile.

To investigate the shape generation in EE-honing, simulation was implemented for a wide range of wear ratios. This was done by fixing the electrode crater size while changing the size of counterface crater to obtain the desired wear ratio. Typical simulated edge geometries are illustrated in Fig. 6.6a.

The reason for this is deducible from Fig. 6.6b which designates the angular

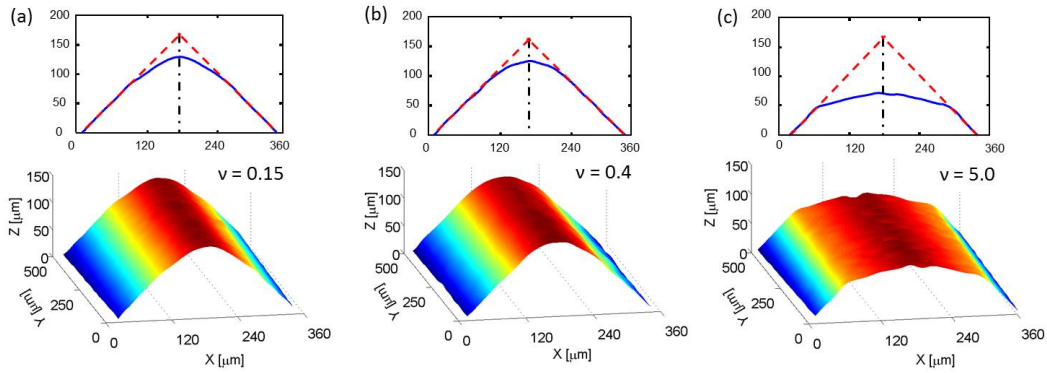


Figure 6.5: Cutting edge geometry for (a) 0.15 (b) 0.4 (c) 5 wear ratios.

range that the spark sweeps during the EE-honing process. It is evident that to circularly hone an edge of a 90° wedge (like that of Fig. 6.5), spark angular sweeping range should fall within $45\text{-}135^\circ$. For small wear ratio of 0.1, spark travels a wider angular range far beyond what is required to circularly hone the edge. This results in removal from the rake and flank lines and thereby generates a dome-shaped geometry. For a perfectly honed edge ($\nu = 0.5$), spark travels on an annular path exactly within the desired angular boundary required to generate a hone on a 90° wedge ($45\text{-}135^\circ$). For a flat edge geometry however, the spark moves rather linearly in a limited angular span resulting in

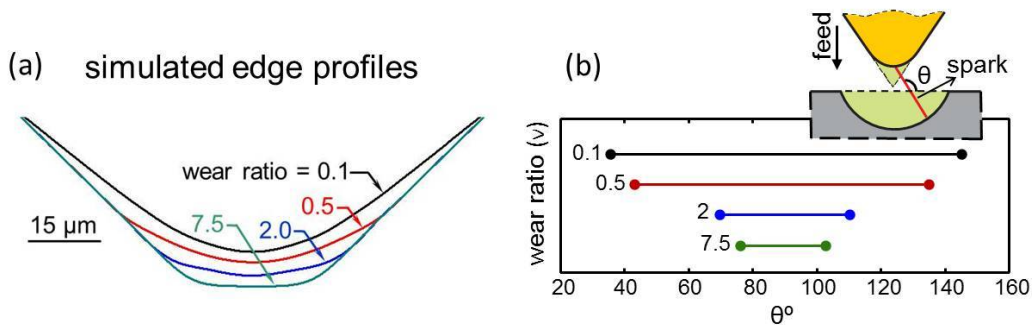


Figure 6.6: (a) Simulated effect of wear ratio on edge geometry. (b) Effect of wear ratio on spark angular sweeping range

a flat (chamfer) edge geometry. With high wear ratio the amount of material removed from tool is considerably higher as compared to that removed from counterface, therefore the edge conforms to the flat shape of counterface. The comparison of the simulation and experimental results confirms the validity of the simulation predictions and further confirm the existence of a threshold wear ratio value for the generation of circular edge wear pattern.

6.3.3 Effect of Foil Counterfaces

While EE-honing edge preparation, it was observed that the cutting edge radius is at its maximum exactly before the edge tip exits the foil counterface, Fig. 6.7a. This was seen to be related to removal of the two lateral foil segments that continue to remove material from sides of the tool tip and thereby reduce its radius (Fig. 6.7b). The effect of lateral removal of foil counterface continues on the rake and clearance faces as long as the machining continues generating two parallel lines on the processed faces (Fig. 6.7c).

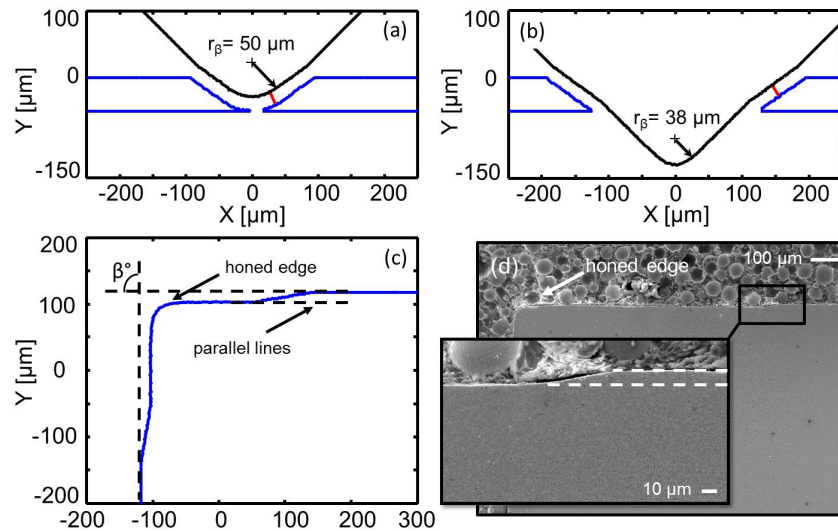


Figure 6.7: The effect of foil counterfaces.

It was desired to investigate if real experimental tests exhibit such maximum edge radius value at the tool tip exit. However, it is practically impossible to stop the honing process at the exact position where the edge exits the foil. Therefore, physical sections of the experimentally prepared edges were closely examined to find any traces of such effect on the rake and clearance faces. Fig. 6.7d illustrates the same two parallel lines on the rake and clearance faces as simulated by the algorithm in Fig. 6.7c and thereby confirms the existence of such foil counterface effect on edge preparation.

The foil effect depends on the counterface foil thickness and does not alter the macro-geometry of the cutting edge as the tool angle (β) is unaffected. Its position can be placed far enough from the cutting edge by increasing the processing time of the EE-honing process. However, one benefit of such microgeometric feature might be related to its potential functionality as a micro size chip breaker.

6.4 Experimental Verification

6.4.1 Required Data for the Simulation

Table 6.2 illustrates the baseline EE-honing process parameters. Required data for EE-honing simulation are measured for these parameters while EDM-machining of an aluminum counterface with carbide electrodes. Wear ratio was measured to be 0.4 by careful electrode and counterface weight measurements before and after the EDM process. Gap size was measured using the 3D geometric models of both the electrode and a thick counterface subsequent to the EDM process. Considering a curvilinear profile, the difference between the curvature radius of electrode and workpiece which designates the off-set

Table 6.2: Baseline EE-honing parameters

Parameter	Value
Pulse duration (μs)	0.4
Pulse off-time(μs)	1.12
Gap voltage (V)	50
Current (I)	1.2
Polarity	+

distance of two geometries corresponds to the gap size. It was measured to be approximately $15 \mu m$. Tool wedge angle was 90° in all the simulations which corresponds to the wedge angle of the industrial SNE inserts on which all the experiments were performed. Cutting edge was considered to have an initial edge radius of $5 \mu m$ which is the average edge radius of unprepared inserts.

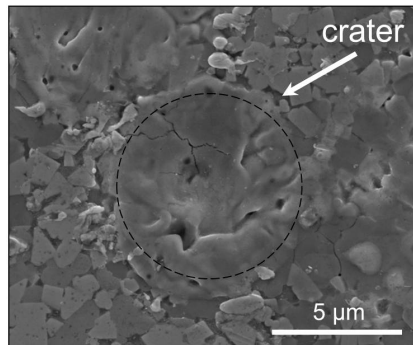


Figure 6.8: SEM micrographs of spark craters on carbide surface.

Single spark tests under the baseline EE-honing parameters were performed to obtain the crater geometry. In order to facilitate the crater shape investigations, one carbide insert was mounted in epoxy resin and polished with sequentially finer sand papers and cloths. The mounted insert was connected to a metallic base with a conductive paste to enable the discharge in EDM process. Single spark tests were performed on this polished carbide surface. Aluminum foils had a finely polished surface and required no preparation. Crater geometry was then investigated using the SEM, Fig. 6.8. Crater width

was measured from the micrographs to be approximately $8.2 \mu\text{m}$ for carbide tool and $14 \mu\text{m}$ for aluminum. Crater depth was measured to be $1.7 \mu\text{m}$ for carbide tool and $2.3 \mu\text{m}$ for aluminum using a high resolution optical microscope.

6.4.2 Symmetric Edge Honing

Electro-erosion edge honing simulation was implemented to investigate the effect of foil thickness on cutting edge radius. Simulated cutting edge profiles were investigated and the cutting edge radius values prepared by different foil thicknesses were computed. Sharp unprepared SNE inserts were symmetrically honed under the baseline EDM parameters. Aluminum foil thickness varied from 25 to $100 \mu\text{m}$. Subsequent to the EDM process edge radius values were measured by the methodology detailed in Chapter 2. Simulation and experimental results are shown in Fig. 6.9.

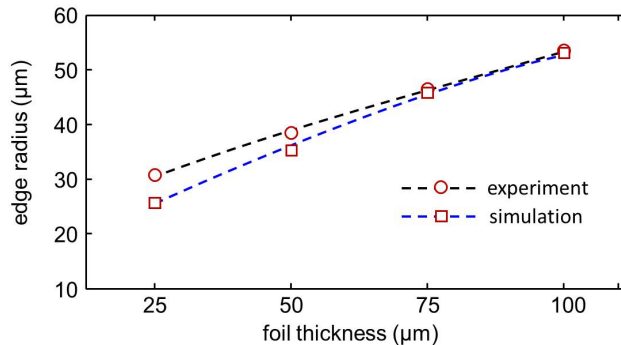


Figure 6.9: Simulated and experimental edge radius values for different counterface thicknesses.

As can be seen, the simulation underestimates the edge radius values with the maximum error of 14% related to the smallest edge radius ($30 \mu\text{m}$). The error decreases substantially for higher processing times. For foil thickness of

100 μm which generated an edge radius of 53 μm error reduces to as low as 1 %. This is due to the fact that for larger edge radius values the initial condition of the unprepared inserts becomes less dominant. This initial geometry of unprepared inserts which is extensively variable and accompanied with edge defects like chippings and flashes has been considered to be equivalent to an initial edge radius of 5 μm in the simulation.

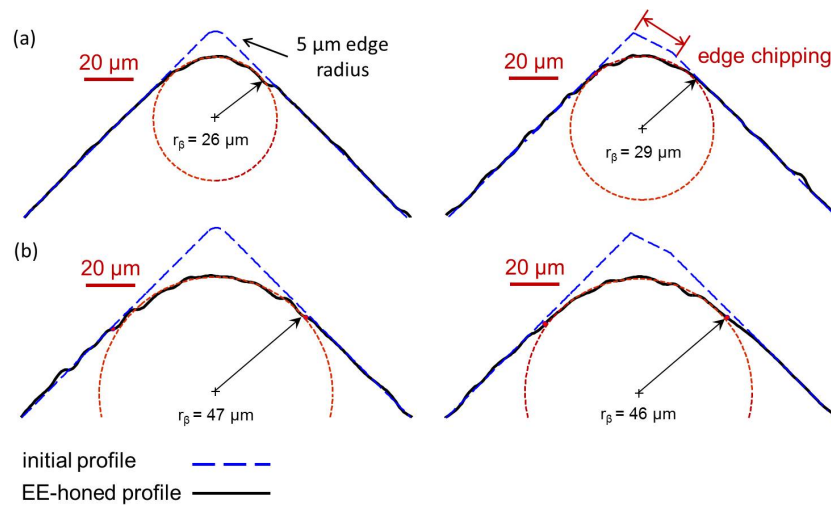


Figure 6.10: Effect of initial edge defects on final honed edge geometry.

In order to further investigate the effect of edge defects, two profiles one with perfect initial edge radius of 5 μm and another with a small edge chipping of 20 μm are numerically processed under the same conditions, Fig. 6.10a. As can be seen, although edge chipping is removed completely subsequent to the honing process the final profiles are quite different. The edge radius of the imperfect edge ($r_{\beta} = 29\mu\text{m}$) is increased by more than 11% as compared to the initially round one ($r_{\beta} = 26\mu\text{m}$) which signifies the significant influence of initial edge condition on final geometry of the prepared cutting edge. This initial geometric variation becomes less dominant when the edge is processed more. This is deducible from Fig. 6.10b.

6.4.3 Asymmetric Edge Preparation

The potential capability of the EE-honing process to generate asymmetric cutting edges was briefly explained in Chapter 4. By rotating the edge about its axis of symmetry (Z) asymmetric wear pattern on the tool electrode edge is expected, Fig. 6.11.

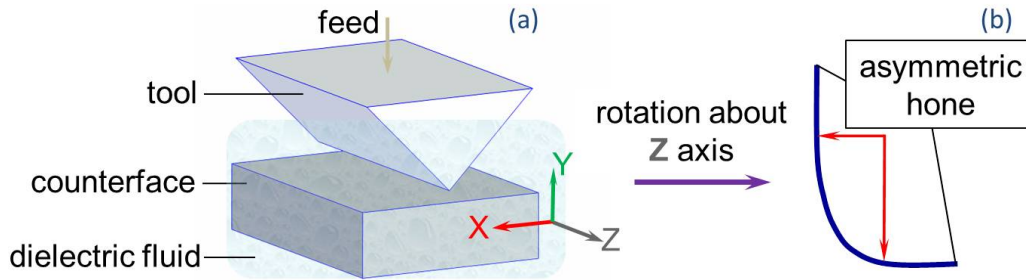


Figure 6.11: Preparation of asymmetric cutting edge.

EE-honing numerical simulation was implemented to study the effect of asymmetric cutting edge engagement for rotation angle of 20° . Experimental EE-honing tests were also performed under the same kinematic configuration. Fig. 6.12 presents the simulated and experimental cutting edge profiles subsequent to the EE-honing process for two counterface thickness values of $50 \mu\text{m}$ and $100 \mu\text{m}$.

Characterization parameters for both profiles are listed in table 6.3 using the asymmetric cutting edge characterization parameters detailed in chapter 5. These parameters are shown in Fig. 6.13. S_a and r_a are the distance of cutting edge apex from the axis of symmetry and its curvature radius, respectively. S_f and S_r are the distance of edge separation points on the flank and rake faces from the axis of symmetry. As can be seen, simulation closely models the form of the cutting edge for both cases. However variation of parameters is higher for the smaller edge as compared to the more processed one. The

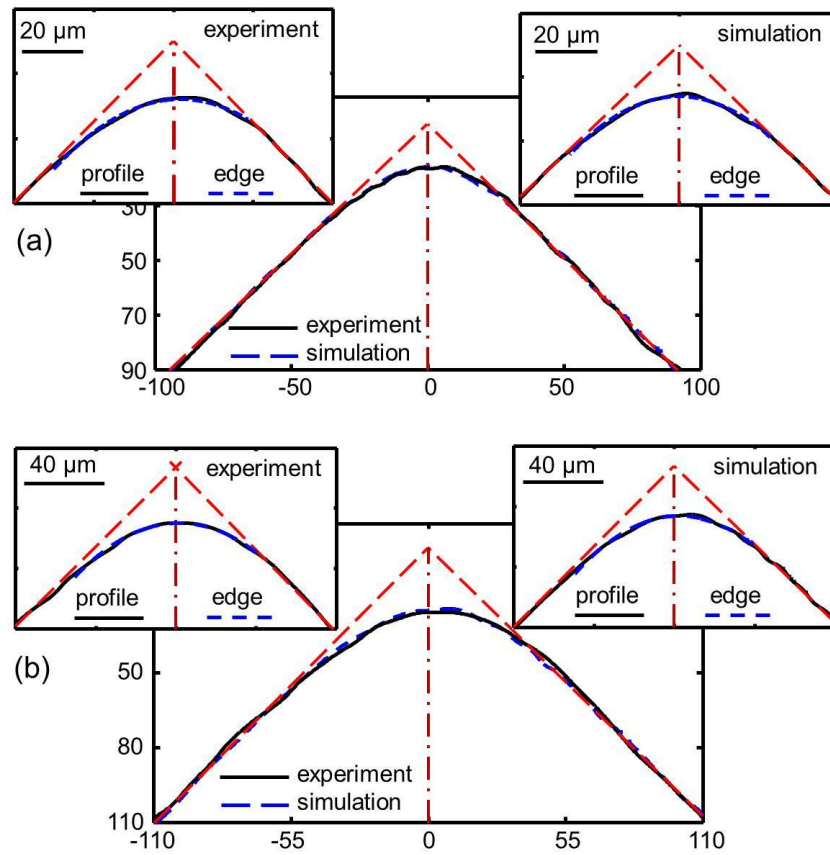


Figure 6.12: Asymmetric edge preparation for rotation angle of 20° for foil thickness of (a) $50 \mu\text{m}$ (b) $100 \mu\text{m}$.

influence of the initial edge condition on the prepared geometry was elaborated in the previous section. This effect is more significant for asymmetric edge preparation since it is the form of the edge that is of interest as opposed to its overall curvature (cutting edge radius). As can be seen, although the predicted asymmetric geometry is close to the experimentally created one for smaller edge that is prepared by a foil of $50 \mu\text{m}$, there is a noticeable difference in S_r . This difference is much smaller for an asymmetric edge prepared by a foil of $100 \mu\text{m}$.

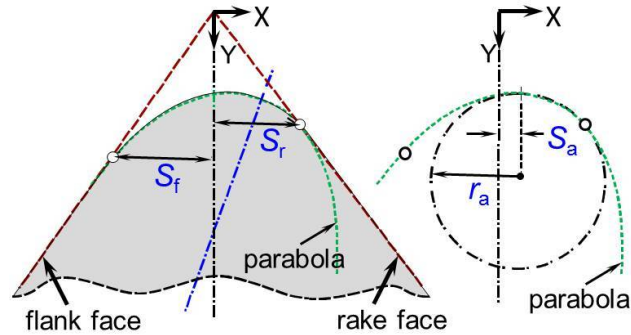


Figure 6.13: Asymmetric cutting edge characterization parameters.

Table 6.3: Asymmetric edge characterization parameters

Parameter	Foil Thickness(μm)	$S_a(\mu\text{m})$	$r_a(\mu\text{m})$	$S_f(\mu\text{m})$	$S_r(\mu\text{m})$
Experimental	50	2	36	38	23
Simulation	50	0	32	35	29
Experimental	100	2	51	50	39
Simulation	100	2	47	50	38

6.5 Conclusions

The numerical simulation of EE-honing process was detailed in this chapter. The modeling of localized wear at electrode sharp edges was facilitated by considering the true crater shape on both the tool electrode and counterface along with a realistic modeling of the overlapping craters on curvilinear profiles. This in turn enabled the geometric prediction of the EE-honed cutting edges under different conditions. Numerical simulation predicted the edge radius value with maximum error of 14% for edge radius of $30 \mu\text{m}$. This error substantially decreased for higher radius values as for the edge of $53 \mu\text{m}$ it was less than 1%. It was shown that this error is mostly related to the initial geometry of the cutting tools which becomes less dominant as the processing

time increases. Numerical simulation also predicted the geometry of asymmetrically prepared cutting edges. For a rotation angle of 20° asymmetric profile was predicted with minimal error. These results verify the validity of the numerical simulation. The simulation developed can therefore be employed for the investigation of different influential parameters on the geometry of cutting edges prepared by EE-honing process.

Chapter 7

Conclusions and Future Work

In this chapter a summary of the achievements that have been accomplished during the course of this PhD research is presented. This is followed by a proposal of ideas and alternatives that can potentially enhance the performance and/or expand the application envelope of the process developed in this research.

7.1 Conclusions

The significant effect of the geometry of cutting edge on almost every machining process response, detailed in Sec 1.2, has spurred the development of several novel edge preparation techniques in the recent years. In line with these attempts and based on an innovative idea, this PhD research project aimed to develop and present the proof-of-concept of a novel edge preparation technique called electro-erosion edge honing. EE-honing takes advantage of the inevitable and unfavorable localized wear at the sharp corners of tool electrode in a sink EDM process. Sharp unprepared cutting edges used as

electrodes are eroded into a desired geometry while ED-machining of an appropriate counterface. In addition to the preparation of cutting edge with EE-honing, a novel method for geometric characterization of the cutting edge is also proposed. A summary of the results attained in this thesis research follows:

The process development of electro erosion edge honing was detailed in Chapter 3. High speed steel inserts of the simplest geometry were honed while ED machining of a flat plate counterface. The significant influence of electrode to counterface wear ratio on the geometry of prepared edges was demonstrated which led to the identification of a threshold wear ratio that generates the desired circular geometry. Through experimental wear ratio measurements, aluminum with positive polarity was shown to provide the threshold wear ratio and thereby capable of honing sharp unprepared HSS tools. EE-honed tools were then evaluated in terms of their geometric consistency and tool performance. A cutting edge measurement methodology based on optical microscopy was developed for geometric evaluation of the prepared inserts. Cutting edge radius variation was shown to be less than 5% along the cutting edge and between inserts prepared under the same condition. Experimental cutting tests revealed the four-fold enhancement of the life of EE-honed tools as compared to sharp unprepared ones.

The application envelope of EE-honing process was then expanded to include complex geometry cutting tools as well as to prepare carbide tools being the most common cutting tool material in metal cutting industry. To ensure the uniform engagement of the entire length of the cutting edge regardless of the macrogeometric complexity, the innovative idea of using foil counterfaces, as opposed to the thick plate previously employed, was applied. Taking advantage of this idea, cutting tools having macrogeometric complexities such

as curvilinear edges, nose radius and chip breakers were prepared. Electro-discharge machining of carbide tools brought about a number of challenges, a major one being the difference in electro-thermal properties of the carbide matrix elements. The systematic methodology to identify EDM parameters that yield the most stable machining process while preserving surface integrity was detailed in Chapter 4. The EE-honing process was then evaluated in terms of process duration, geometric repeatability and tool life tests. Preparation time as low as 1.5 s/mm was achieved. Edge radius variation was shown to correspond to only 13% along the complex macrogeometric cutting edge as well as between inserts that were similarly prepared. As the final criterion, EE-honed inserts achieved the same life of brush-honed ones of the same radii.

Symmetric circular cutting edge geometry was generated on sharp unprepared edges of cutting tools during the course of developing the EE-honing process in chapters 3 and 4. However, the evolution of advanced edge preparation techniques resulted in the creation of engineered cutting edge microgeometries in the recent years most of which could not be represented by a single edge radius value. Therefore, an innovative application of parametric quadratics to model and characterize the cutting edge was developed and detailed in chapter 5. Free-knot B-spline curves were first applied to separate the cutting edge from the rake and flank lines. This method was shown to be robust against edge profile point uncertainty and also the distance from the edge tip over which the edge profile is considered for modeling. Once the cutting edge is identified, a set of four parameters derived from the quadratic parametric equation of the cutting edge are used to characterize symmetric and asymmetric edges. This set of parameters is contour-based, comprehensible and influential on machining process behavior.

Finally, a numerical simulation of the EE-honing process was developed to

provide a deeper insight into the process behaviour. True crater geometry and a realistic modeling of overlapping craters on curvilinear profiles enabled the modeling of localized electrode wear at sharp electrode corners. In addition, simulation facilitated the explanation of the effect of wear ratio and foil counterface on EE-honing process. Finally, the developed numerical simulation was verified by experimental EE-honing tests for different foil thickness values for both symmetric and asymmetric cutting edge preparation. It was shown that as the processing time increases, the variation of the simulated profile to the actual edge profile decreases. This was shown to be related to the initial condition of unpreprad cutting edges.

7.2 Future Work

In this thesis, the proof-of-concept of electro-erosion edge honing was presented. Even though it was shown that EE-honed inserts achieve the same tool life of brush-honed ones with same radii, there are still several potential ways to further enhance the performance of this process.

EE-honing process was applied to cutting tools with a single set of baseline parameters which were systematically identified. Alternatively progressive decrease of pulse energy could be employed during the roughing, semi-finishing and finishing processes to acquire better surface integrity. To enhance the surface integrity of the prepared tools, application of secondary processes such as thermal annealing [64] and finish micro-blasting [71] are also advisable subsequent to the EE-honing process. EE-honing process parameters can be further optimized by adopting strategies such as pulse shaping [69]. Moreover, it would be of interest to investigate the use of dielectric fluid mixed with nanopowders as it is advised [67] to increase the surface integrity without affecting

the removal rate. The performance evaluation of EE-honed tools subsequent to vapor deposited coatings [63] is also of special interest.

In addition to the prospective improvements that this process can adopt by the above mentioned approaches, there are several application alternatives which can get EE-honing to its full potential. One of them is devising ways to prepare variable edge radius along the cutting edge. In these tools, the cutting edge radius increases along the nose section of the cutting edge with respect to the increase of undeformed chip thickness. Such preparation is particularly important in applications where undeformed chip thickness is small compared to edge radius (e.g. hard turning and micro-machining).

Electro-erosion edge honing is based on electrical discharge machining. This process has been applied on carbide cutting tools being a metal matrix composite of tungsten carbide (WC) grains (as well as TiC and TaC for some grades) in a cobalt binder [86]. Polycrystalline diamond (PCD) tools consist of nonconductive diamond grains in a metallic cobalt binder. This renders the super hard PCD tools electro-discharge machinable. Therefore, EE-honing process can be applied to hone the cutting edge of PCD tools based on the same principles. This would be particularly important since EDM, along with grinding, are the major processes to cut PCD tools into the required shape [87], therefore EE-honing process can be integrated to the PCD tool manufacturing process. While EE-honing PCD tools a major challenge would involve process destabilization due to the dislodging of nonconductive diamond grains. Last but not the least, techniques have been developed that facilitate the ED-machining of electrically non-conductive materials [88]. Employment of such techniques can enable the EE-honing process to prepare ceramic cutting tools.

References

- [1] I. Time, Resistance of metals and wood to cutting (in Russian), *Dermacow Press* 1870, House St. Petersburg, Russia.
- [2] H. Treska, Mmoires Sur le Rabotage des Mtaux, *Bulletin de la Scite dE-couragement pour lIndustrie Nationale*, 15 (1873), 585–685.
- [3] E. M. Merchant, Mechanics of the metal cutting process : I orthogonal cutting and the type 2 chip, *Journal of Applied Physics*, 16 (1945), 267–275.
- [4] M. Masuko, Fundamental researches on the metal cutting. A new analysis of cutting force. *Transactions of the Society of Mechanical Engineers (Japan)* 19 (1953), 32–39.
- [5] P. Albrecht, New developments in the theory of metal cutting process, Part 1: The ploughing process in metal cutting, *Journal of Engineering for Industry* 82 (1960), 348–357.
- [6] W.R. Shaffer, Cutting tool edge preparation, *Technical Paper - Society of Manufacturing Engineers*, 1999, 1–8.
- [7] E.H. Lee, B.W. Shaffer, The theory of plasticity applied to a problem of machining, *Journal of Applied Mechanics* 73 (1951), 405-413.

-
- [8] P.L.B. Oxley, The Mechanics of Machining: An Analytical Approach to Assessing Machinability. *Ellis Horwood Limited*, Chichester, 1989.
- [9] C. J. C. Rodriguez, Cutting edge preparation of precision tools by applying microabrasive jet machining and brushing, Dissertation (2009), Kassel University.
- [10] K. Nakayama, K. Tamura, Size effect in metal cutting force. *Journal of Engineering for Industry* 90 (1968), 119-126.
- [11] D. Dornfeld, S. Min, Y. Takeuchi, Recent Advances in Mechanical Micro-machining, *CIRP Annals - Manufacturing Technology* 55 (2006), 745-768.
- [12] N. Fang, Slip-line modeling of machining with a rounded-edge toolPart I: new model and theory *Journal of the Mechanics and Physics of Solids*, *Journal of the Mechanics and Physics of Solids* 51 (2003), 715-742.
- [13] J. Rech, Y. C. Yen, M. J. Schaff, H. Hamdi, T. Altan, K. D. Bouzakis, Influence of cutting edge radius on the wear resistance of PM-HSS milling inserts, *Wear* 259 (2005), 1168–1176.
- [14] R. J. Schimmel, W. J. Endres, R. Stevenson, Application of an Internally Consistent Material Model to Determine the Effect of Tool Edge Geometry in Orthogonal Machining, *Journal of Manufacturing Science and Engineering* 124 (2002), 536–543.
- [15] N. Fang, Slip-line modeling of machining with a rounded-edge toolPart II: analysis of the size effect and the shear strain-rate, *Journal of the Mechanics and Physics of Solids* 51 (2003), 743-762.

- [16] R. T. Coelho, L. R. Silva, A. Braghini, A. A. Bezerra, Some effects of cutting edge preparation and geometric modifications when turning INCONEL 718TM at high cutting speeds, *Journal of Materials Processing Technology* 148 (2004), 147–153.
- [17] M. N. A. Nasr, E. G. Ng, M. A. Elbestawi, Modeling the effects of tool-edge radius on residual stresses when orthogonal cutting AISI 316L, *International Journal of Machine Tools & Manufacture* 47 (2007), 401–411.
- [18] K. D. Bouzakis, N. Michailidis, G. Skordaris, S. Kombogiannis, S. Hadjiyiannis, K. Efstathiou, G. Erkens, S. Rambadt, I. Wirth, Effect of the Cutting Edge Radius and Its Manufacturing Procedure on the Milling Performance of PVD Coated Cemented Carbide Inserts. *CIRP Annals-Manufacturing Technology* 51 (2002), 61-64.
- [19] R. M'Saoubi, H. Chandrasekaran, Investigation of the effects of tool-microgeometry and coating on tool temperature during orthogonal turning of quenched and tempered steel, *International Journal of Machine Tools & Manufacture* 44 (2004), 213–224.
- [20] Y. C. Yen, A. Jain, T. Altan, A Finite Element Analysis of Orthogonal Machining Using Different Tool Edge Geometries. *Journal of Materials Processing Technology* 146 (2004), 72-81.
- [21] B. Denkena , A. Lucas, E. Bassett, Effects of the cutting edge micro-geometry on tool wear and its thermomechanical load, *CIRP Annals - Manufacturing Technology* 60 (2011), 73-76.
- [22] B. Denkena, J. Kohler, M. S. Mengesha, Influence of the cutting edge rounding on the chip formation process: Part 1. Investigation of material

- flow, process forces, and cutting temperature, *Production Engineering* (2012) DOI: 10.1007/s11740-012-0366-x.
- [23] J. Rech, Cutting Edge Preparation and Surface Issues, *HSS Forum's International Conference " Smart solutions for metal cutting "*, Aachen, 2005.
- [24] E. Bassett, J. Kohler, B. Denkena, On the honed cutting edge and its side effects during orthogonal turning operations of AISI1045 with coated WC-Co inserts, *CIRP Journal of Manufacturing Science and Technology* 5 (2012), 108–126.
- [25] W.J.Endres, R.K. Kountanya. The effects of corner radius and edge radius on tool flank wear. *Journal of Manufacturing Processes* 4 (2002), 89–96.
- [26] R.J. Schimmel, J. Manjunathaiah, W.J. Endres, Edge radius variability and force measurement considerations, *Journal of Manufacturing Science and Engineering* 122 (2000), 590–594.
- [27] M. W. Chastagner, A. J. Shih, Abrasive Jet Machining for Edge Generation, *Transactions of NAMRI/SME* 35 (2007), 359–366
- [28] D. M. Kennedy, J. Vahey, D. Hanney, Micro shot blasting of machine tools for improving surface finish and reducing cutting forces in manufacturing, *Materials and Design* 26 (2005), 203–208.
- [29] N. P. Mahalik, *Micro-manufacturing and Nanotechnology handbook*, Berlin- New York : Springer, 2006.
- [30] J. Rech, Influence of cutting edge preparation on the wear resistance in high speed dry gear hobbing, *Wear* 261 (2006), 505-512.

- [31] D. Biermann, I. Terwey, Cutting edge preparation to improve drilling tools for HPC processes, *CIRP Journal of Manufacturing Science and Technology* 1 (2008), 76-80.
- [32] K. A. Gogaev, V. V. Nepomnyashchii, T. V. Mosina, I. P. Neshpor, and M. Leonowicz, Special Features of the Magnetic Abrasive Machining, *Refractories and Industrial Ceramics* 47 (2006), 492-494.
- [33] F.Y. Cheung, Z.F. Zhou, A. Geddam, K.Y. Li, Cutting edge preparation using magnetic polishing and its influence on the performance of high-speed steel drills, *Journal of Materials Processing Technology* 208 (2008), 196-204.
- [34] B. Karpuschewski, O. Byelyayeva, V.S. Maiboroda, Magneto-abrasive machining for the mechanical preparation of high-speed steel twist drills, *CIRP Annals - Manufacturing Technology* 58 (2009), 295-298.
- [35] J. C. Aurich, M. Zimmermann, L. Leitz, The preparation of cutting edges using a marking laser. *Production Engineering* 5 (2011), 17-24.
- [36] B. Denkena, L. Leon-Garcia, E. Bassett,. Preparation of designed cutting edge microgeometries by simultaneous 5-axes brushing, *In: Proceedings of 3rd International Conference on Manufacturing Engineering*, Greece (2008), 117-123.
- [37] B. Wyen, W. Knapp, K. Wegener, A new method for the characterisation of rounded cutting edges, *International Journal of Advanced Manufacturing Technology* 59 (2012), 899-914.

- [38] B. Bojorquez, R. T. Marloth and O. S. Es-Said, Formation of a crater in the workpiece on an electrical discharge machine, *Engineering Failure Analysis* 9/1 (2002), 93–97.
- [39] W. Natsu, S. Ojima, T. Kobayashi, M. Kunieda, Temperature Distribution Measurement in EDM Arc Plasma Using Spectroscopy, *SME International Journal Series C* 47 (2004), 384–390.
- [40] S. Singh, S. Maheshwari, P. C. Pandey, Some investigations into the electric discharge machining of hardened tool steel using different electrode materials, *Journal of Materials Processing Technology*, 149 (2004), 272–277.
- [41] E. C. Jameson, Electrical Discharge Machining, *Society of Manufacturing*, Dearborn Michigan, 2001, p. 87.
- [42] Y. S. Wong, M. Rahman, M. P. Jahan, A study on the fine-finish die-sinking micro-EDM of tungsten carbide using different electrode materials, *Journal of Materials Processing Technology*, (209) 2009, 3956–3967.
- [43] S. Kalpajian, S.R. Schmid, Material removal processes: abrasive, chemical, electrical and high-energy beam in: Manufacturing Processes for Engineering Materials, *Prentice Hall* 2003, New Jersey, p. 541.
- [44] N. Mohri, M. Suzuki, M. Furuya; N. Saito, Electrode Wear Process in Electrical Discharge Machining, *Annals of the CIRP*, 44 (1995), 165–168.
- [45] M. Kuniedaa, Y. Kanekob, W. Natsu, Reverse Simulation of Sinking EDM Applicable to Large Curvatures, *Precision Engineering*, 36 (2012), 238–243.

- [46] J. R. Crookall, R. J. Fereday, An Experimental Determination of the Degeneration of Tool-Electrode Shape in Electro-Discharge Machining. *Microtecnica*, 17 (1973), 197-200.
- [47] K. H. Ho, S. T. Newman, State of the art electrical discharge machining (EDM), *International Journal of Machine Tools and Manufacture* 43 (2003), 1287–1300.
- [48] H. Ramasawmy, L. Blunt, Effect of EDM process parameters on 3D surface topography, *Journal of Material Processing Technology*, 148 (2004), 155–164.
- [49] B. Lauwers, J. P. Kruth, W. Eeraerts, Wear Behavior and Tool Life of Wire EDM-ed and Ground Carbide Punches, *CIRP Annals- Manufacturing Technology* 54(1) (2005), 163-166.
- [50] P. Echlin, Low-temperature microscopy and analysis, *Springer* 1992, New York.
- [51] Y. N. Picard, D. P. Adams, M. J. Vasile, and M. B. Ritchey, Focused ion beam-shaped microtools for ultra-precision machining of cylindrical components, *Precision Engineering* 27 (2003), 59–69.
- [52] X. P. Li, M. Rahman, K. Liu, K. S. Neo, and C. C. Chan, Nano-precision measurement of diamond tool edge radius for wafer fabrication, *Journal of Materials Processing Technology* 140 (2003), 358–362.
- [53] A. Weckenmann, V. P. Radhakrishnan, S. Schmitz, Fringe Projection Method for Measuring Geometry and Wear of Cutting Tool Inserts, *Proceedings of ASPE, 14th Annual Meeting, Monterey, USA 1999*, 473-476.

- [54] F. Klocke, A. Kuchle, Manufacturing Processes 1: Cutting, *Springer* 2011, Berlin.
- [55] W. Tiller, L. Piegl, The NURBS Book, *Springer* 1997, New York.
- [56] I. Ksa, A circle fitting procedure and its error analysis, *IEEE. Transactions on instrumentation and measurement* IM-25 (1976), 8-14.
- [57] F. Klocke, H. Kratz, Advanced Tool Edge Geometry for High Precision Hard Turning. *CIRP Annals- Manufacturing Technology* 54 (2005), 47-50.
- [58] L. K. Gillespie, Deburring and Edge Finishing Handbook, *Society of Manufacturing Engineers* 1999, Dearborn.
- [59] Y. Y. Tsai, T. Masuzawa, An index to evaluate the wear resistance of the electrode in micro-EDM, *Journal of Materials Processing Technology* (149) 2004, 304–309.
- [60] M. Kunieda, W. Kowaguchi, T. Takita, Reverse simulation of die-sinking EDM, *CIRP Annals- Manufacturing Technology* 48 (1999), 115–118.
- [61] E. J. A. Armarego, R. H. Brown, The Machining of Metals, *Prentice Hall* 1969, Englewood Cliffs.
- [62] K. Bonny, P. De Baets, W. Ost, S. Huang, J. Vleugels, W. Liu, B. Lauwers. Influence of electrical discharge machining on the reciprocating sliding friction and wear response of WC-Co cemented carbides. *International Journal of Refractory Metals & Hard Materials* 27 (2009), 350–359.
- [63] B. Casas, A. Lousa, J. Caldern, M. Anglada, J. Esteve, L. Llanes. Mechanical strength improvement of electrical discharge machined cemented

- carbides through PVD (TiN, TiAlN) coatings. *Thin Solid Films* 447–448 (2004), 258–263.
- [64] B. Casas, Y. Torres, L. Llanes, Fracture and fatigue behavior of electrical discharge machined cemented carbides. *International Journal of Refractory Metals & Hard Materials* 24 (2006), 162–167.
- [65] B. Casas, U. Wiklund, S. Hogmark, L. Llanes,. Adhesion and abrasive wear resistance of TiN deposited on electrical discharge machined WC-Co cemented carbides. *Wear* 265 (2008), 490–496.
- [66] B. Denkena, L. de Leon, E. Bassett, M. Rehe, Cutting edge preparation by means of abrasive brushing. *Key Engineering Materials* 438 (2010), 1–7.
- [67] M. P. Jahan, R. Rahman, Y. S. Wong. Modeling and experimental investigation on the effect of nanopowder mixed dielectrics in fine-finish micro-EDM of tungsten carbide. *Journal of Engineering Manufacture* 224 (2010), 1725–1739.
- [68] M.P. Jahan, M. Rahman, Y. S. Wong. A review on the conventional and micro-electrodischarge machining of tungsten carbide. *International Journal of Machine Tools and Manufacture* 51 (2011), 837–858.
- [69] H. Jühr, H. P. Schulze, G. Wollenberg, K. Kunanz, Improved cemented carbide properties after wire-EDM by pulse shaping. *Journal of Materials Processing Technology* 149 (2004), 178–183.

- [70] Y. C. Lin, L. R. Hwang, C. H. Cheng, P. L. Su. Effects of electrical discharge energy on machining performance and bending strength of cemented tungsten carbides. *Journal of Materials Processing Technology* 206 (2008), 491–499.
- [71] J. Qu, A.J. Shih, R.O. Scattergood, J. Luo, Abrasive micro-blasting to improve surface integrity of electrical discharge machined WC-Co composite. *Journal of Materials Processing Technology* 166 (2005), 440–448.
- [72] T.H.C. Childs, K. Sekiya, R. Tezuka, Y. Yamane, D. Dornfeld, D.-E. Lee, S. Min, P.K. Wright, Surface finishes from turning and facing with round nosed tools, *CIRP Annals-Manufacturing Technology* 57 (2008), 89–92.
- [73] D. Biermann, A. Baschin, Influence of cutting edge geometry and cutting edge radius on the stability of micromilling processes, *Production Engineering* 3 (2009), 375–380.
- [74] B. Denkena, Report on the cooperative work on cutting edge geometry, *International Academy for Production Engineering (CIRP)*, August 2008.
- [75] H. Schwetlick, T. Schutze, Least squares approximation by splines with free knots, *BIT Numerical Mathematics* 35 (1995), 1–3.
- [76] T.W. Sederberg, D.C. Anderson, Implicit representation of parametric curves and surfaces, *Computer Vision, Graphics and Image Processing* 28 (1984), 72–84.
- [77] C. Tricarico, R. Delpretti, D. F. Dauw, Geometrical simulation of the EDM die-sinking process, *Annals of the CIRP- Manufacturing Technology* 37 (1988), 191-196.

- [78] Z.Y. Yu, J. Kozak, K.P. Rajurkar, Modelling and simulation of Micro-EDM Process, *Annals of the CIRP- Manufacturing Technology* 52 (2003), 143-146.
- [79] M. Kunieda, Y. Kaneko, W. Natsu, Reverse Simulation of Sinking EDM Applicable to Large Curvatures, *Precision Engineering* 36 (2012), 238-243.
- [80] Y. Zhao, X. Zhang, X. Liu, K. Yamazaki, Geometric modeling of the linear motor driven electrical discharge machining (EDM) die-sinking process, *International Journal of Machine Tools & Manufacture* 44 (2004), 1-9.
- [81] Y. H. Jeong, B. K. Min, Geometry prediction of EDM-drilled holes and tool electrode shapes of micro-EDM process using simulation, *International Journal of Machine Tools & Manufacture* 47 (2007), 1817-1826.
- [82] N.Z. Yussefian, P. Koshy, S. Buchholz, F. Klocke, Electro-erosion edge honing of cutting tools, *CIRP Annals - Manufacturing Technology* 59 (2010), 215-218.
- [83] Kenji Morimoto, Masanori Kunieda, Sinking EDM simulation by determining discharge locations based on discharge delay time, *CIRP Annals - Manufacturing Technology* 58 (2009) , 221-224.
- [84] S. Heo, Y. H. Jeong, B. Min, S. J. Lee, Virtual EDM simulator: Three-dimensional geometric simulation of micro-EDM milling processes, *International Journal of Machine Tools & Manufacture* 49 (2009), 1029-1034.
- [85] A. Kojima, W. Natsu, M. Kunieda, Spectroscopic measurement of arc plasma diameter in EDM, *CIRP Annals - Manufacturing Technology* 57 (2008), 203-207.

- [86] G. Tlustý, Manufacturing Process and Equipment, *Prentice Hall* 1999, Upper Saddle River.
- [87] J. R. Davis, Tool Materials Asm Specialty Handbook, *ASM International* 1995, Materials Park, Ohio.
- [88] T. Tani, Y. Fukuzawa, N. Mohri, N. Saito, M. Okada, Machining phenomena in WEDM of insulating ceramics, *Journal of Materials Processing Technology* 149 (2004), 124-128.